Doctoral Dissertation
博士論文

Chirality Generation under Strong Electromagnetic Fields and the Schwinger Mechanism
(強電磁場中でのカイラリティ生成とシュウィンガー機構に関する研究)

A Dissertation Submitted for the Degree of Doctor of Philosophy
December 2019
令和元年12月博士（理学）申請

Department of Physics, Graduate School of Science,
The University of Tokyo
東京大学大学院理学系研究科物理専攻

Patrick Arthur Copinger
カピンガー　パトリック　アーサー

Abstract

The axial Ward identity and its dependence on the Schwinger mechanism are examined in parity breaking homogeneous background fields. The importance of vacuum asymptotic states on the nature of observables under the vacuum unstable Schwinger mechanism is elucidated. We find expectation values found under scattering matrix element in-out vacuum states are consistent with those under an equilibrated Euclidean metric. Whereas expectation values found under in-in vacuum states predict an out-of-equilibrium scenario, which agrees with a heuristic picture of chirality generation under the Schwinger mechanism–clarifying key issues on the mechanism's contributions to the axial Ward identity. In-out expectation values associated with the chiral anomaly thought sourced by the Schwinger mechanism, and anomaly related phenomena such as the chiral magnetic effect, are found to vanish. However, in-in expectation values possess an exponentially suppressed quadratic mass term consistent with Schwinger pair production. The absence of the chiral anomaly in an equilibrated Euclidean setting whereas its manifestation out-of-equilibrium motivates a new understanding of the anomaly and its dependence on a vacuum instability. Calculations are performed using worldline methods, and in-out and in-in observables are one-loop exact.

Applications to the axial Ward identity and chiral magnetic effect are also explored with in-out and in-in vacuum state expectation values. These include chiral density fluctuations as well as the chiral condensate. Real-time chiral density fluctuations, similar to the cases of the axial Ward identity and chiral magnetic effect, and in contrast to the equilibrated case, were found to possess linear time dependence and also had a characteristic exponential suppression due to the Schwinger mechanism. The chiral condensate was found to melt for the large electric field, small mass case, prompting a new outlook for magnetic catalysis and a dynamically generated mass.

Acknowledgements

There are many to whom I am sincerely indebted to in the production of my thesis and research therein, however, first and foremost I want to acknowledge a debt of gratitude to my adviser Prof. Kenji Fukushima. Without his guidance and physical insight, this work would not be possible. Prof. Fukushima has shared a breath and depth of physics knowledge with which proved indispensable at pivotal times in research. Furthermore, he has remarkably contagious enthusiasm for physics; his passion has forged my development as a physicist here and will serve as an exemplary force in the shaping of the rest of my career.

I would also be remiss for not acknowledging my colleague and friend Shi Pu. We have fought alongside through some of the most challenging problems. Shi Pu, too, has offered supportive guidance and I don't believe I could have accomplished what I had without him. He has demonstrated through example the merits of hard work and a commitment to excellence in research.

Of course, none of this would have been possible without the undying support of my wife Ayano Copinger. Her compassion during the most trying of times–of which there were a few–have kept me motivated and undistracted. And her support during the most uncertain of times have given me purpose. Indeed, I can never repay the sacrifices Ayano has made for me.

I would also like to thank my fellow members of the Hadron Physics Theory Group throughout my graduate studies. During my early graduate studies I had many informative discussions with Sanjin Benić about physics and mathematics. Later he offered many pointed questions regarding this thesis; all of which added to its quality. I have benefited from numerous conversations with Pablo Morales as well. He too shares an opaque enthusiasm for physics, and our talks on the Schwinger mechanism and the chiral magnetic effect were frequent and helpful. Also related discussions on chiral phenomena and the Casimir force with Zebin Qui really likewise helpful. The whole of the group, however, has been immensely constructive towards the development of this work and my education.

Discussions with experts in the field have also contributed greatly. Francois Gelis offered calculation advice in inhomogeneous fields along with how to properly treat backreaction effects. Also members of the Yukawa Institute for Theoretical Physics Nuclear Theory Group including Koichi Hattori and Di-Lun Yang helped with several aspects of the direction of research through informative questions.

I would also supremely remissent in not acknowledging the support of my family and friends. My mother and father have given unrelenting support both emotional and financial in my journey in physics. I have fond childhood memories of my father telling stories of Feynman, Einstein, and other physicists. These impressions have lived with me and shaped my decision to pursue theoretical physics. Interactions with good friends and enjoying the many sights and experiences of Japan have helped me unwind and were enriching.

Lastly, I would like to thank the University of Tokyo Graduate School of Science and the International Liaison Office whose Scholarship for International Students has made this research and my studies possible.

Contents

List of Figures

Chapter 1

Introduction

1.1 Motivation and Outstanding Issues

An anomaly is said to be present when a symmetry realized at the classical level is broken at the quantum level. This phenomenon is ever-present in relativistic fermionic systems for a chiral symmetry. At first glance theories with massless fermions seem to possess a chiral symmetry–allowing a break-up into left and right-handed parts. However, due to quantum effects [1] the chiral anomaly resides and no such break-up is possible. The breaking of the chiral symmetry has impacted all realms of physics, and it is notably responsible for giving rise to the bulk of the visible mass in the universe [2, 3]. It is, therefore, an essential task to directly observe the chiral anomaly, and an important manifestation of the anomaly that may help achieve the task is the chiral magnetic effect.

The chiral magnetic effect (CME) arises as an electromagnetic current when a net chirality is present in conjunction with a magnetic field [4]. See Fig. 1.1. In the left diagram of Fig. 1.1 the chiral anomaly is represented in a topologically non-trivial quantum chromodynamic background as causing a net chirality difference. Here massless particles are assumed, therefore particle chirality and helicity are similar. However, according to our conventions–see also Ref. [4]–anti-particles possess an opposite chirality to their helicity. This amounts to a measure of chirality difference as being the number of particles plus anti-particles with right minus left-handed helicity. And a right (left)-handed helicity is indicted with an alignment (anti-alignment) of momentum and spin vectors. In the right diagram, if one were to examine the same scenario as in the left diagram but with an added strong magnetic field, one could see an electromagnetic current develop along the direction of the magnetic field; this is the CME. This phenomenon is due to the magnetic field projecting the particles' spins in the direction of the magnetic field, or rather ensuring that only the lowest Landau level is occupied.

The electromagnetic current associated with the CME was thought to be observed in a Dirac semimetal [5]. Indeed, in 2D and 3D condensed matter analog systems such as Weyl and Dirac semimetals, fermionic relativistic dispersion relations are producible [6–9]. However, the CME has yet to be observed in quantum chromodynamics (QCD). Even so, a distinct feature of the CME, a strong magnetic field, is present in off-central heavy-ion collisions where it is thought the CME may be observable. For a particle beam collision in which the two beams are offset (a non-central collision) a transient strong magnetic field is thought to form perpen-

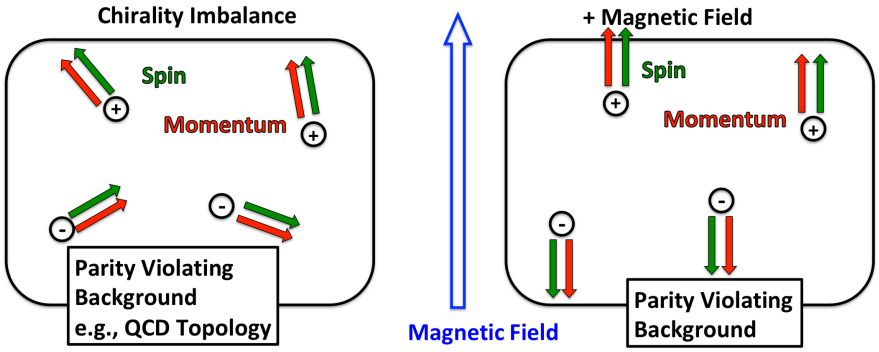

Figure 1.1: Anomaly and CME diagrams. (Left) The chiral anomaly relates a non-conservation of chirality due to a parity violating field; e.g., the field depicted here could come from a quantum chromodynamic (QCD) topology. Green (red) arrows depict the vector of spin (kinetic momentum), and here a particle (anti-particle) is represented with a positive (negative) sign. The diagram shows a net chirality difference of $\Delta N_5 = 4$. (Right) Consider the same setup as in the left figure however with a background electromagnetic magnetic field applied. Here owing to the net chirality difference caused by the anomaly, and the magnetic field polarizing the particles' spins, an electromagnetic current along the direction of the magnetic field will be generated, and this is the chiral magnetic effect.

dicular to the reaction plane. In fact, the magnetic field in heavy-ion collisions is the strongest known terrestrial one, thought to reach magnitudes of $eB \sim m_\pi^2$, for the mass of the pion [10]. Even so, identifying the CME in colliders is a challenging task, and to this end, there are outstanding theoretical issues in need of clarification:

1. The finite generation of a chirality imbalance is an essential feature of the CME. Many studies rely on an artificial insertion of a net chirality by hand. For example, it is common practice to introduce a chiral chemical potential to a system under a magnetic field to produce the CME. While this practice is a useful theoretical construct, there are many applications in which this treatment is not just, we will elaborate later in the thesis. One such example is provided by highly un-equilibrated systems, such as in heavy-ion collision experiments.

2. How do the CME and related anomaly applications behave in and out-of-equilibrium? And, how could one characterize such observables in and out-of-equilibrium? This problem is transparent in heavy-ion collisions where just after the collision a dense gluonic state called the glasma [11, 12] forms and is thought to give rise to parity-violating flux tube configurations that may predict the CME [13]. However, this formation by its transient nature is highly un-equilibrated, necessitating an out-of-equilibrium description of the CME in colliders.

3. Last, how does a fermion mass affect the CME and anomaly? In the absence of mass the helicity and chirality are indistinguishable (as is common in high energy applications–and which has even prompted a redefinition in chemistry [14]). Yet, in many high energy applications, a mass is frequently

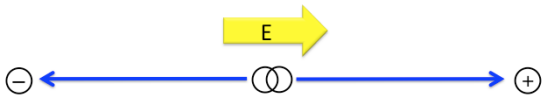

Figure 1.2: Cartoon of Schwinger mechanism process from intuitive perspective. Pairs of particles tunnel from the vacuum and are accelerated in the direction of the electric field with strength E. Consider a virtual pair, depicted above as two overlapping circles. Then from a classical analogy, if one were to apply a strong enough electric field, imparting work to the pair, a particle anti-particle pair may be produced. Here, the blue lines represent the direction of momentum.

dismissed. This dismissal, we will argue, is however not suitable–particularly for anomalous physics applications.

1.2 Anticipations

How might one furnish a net chirality and explore the effects of a fermion mass? The Schwinger mechanism is thought to provide an answer [13]. In the presence of a strong background electric field, the quantum field theory (QFT) vacuum is unstable against the spontaneous creation of particle anti-particle pairs in what is known as the Schwinger mechanism [15]. See Fig. 1.2 for a cartoon, where we have made use of a classical analogy: an electric field separating a virtual particle anti-particle pair (representative of the vacuum). The background electric field, it is thought, makes possible tunneling from the vacuum allowing the production of a particle (excitation) and anti-particle (hole). The QCD analog, namely chromo-electric flux tube breaking, is also thought to exist in heavy-ion collisions leading to hadronization [16].

From the Schwinger mechanism, then, how might one anticipate an anomalous generation of chirality? This is made possible through a strong magnetic field–parallel to the electric field so that the background be parity violating. Then, as foreshadowed earlier, the strong magnetic field will polarize the produced particle anti-particle's spins, yielding a net chirality [13]; see Fig. 1.3 for a cartoon of the Schwinger mechanism process with a magnetic field. Again we make use here of a classical picture of a virtual particle anti-particle pair being separated with an electric field; also note that since a magnetic field cannot impart work, no Schwinger pair production is permissible solely from a magnetic field. Here in addition to blue lines depicting momentum, the spin vector is shown with red lines.

One should expect to see a net chirality difference due to the Schwinger mechanism in parallel fields, and an unambiguous means of accessing a chirality indifference is provided through the axial Ward identity [17, 18]. The axial Ward identity famously predicts the non-conservation of chiral charge density not only due to quantum effects, (in essence the chiral anomaly), but also explicitly due to a mass through the pseudoscalar condensate. Then to quantify the above picture of chirality generation one ought to calculate an expectation value of the axial Ward identity. The problem is–we will show–using traditional QFT calculation methods lead to such observables surprisingly vanishing. Most prominent, we find is a vanishing of the divergence of the chiral current, in other words, no anomaly. And chirality would

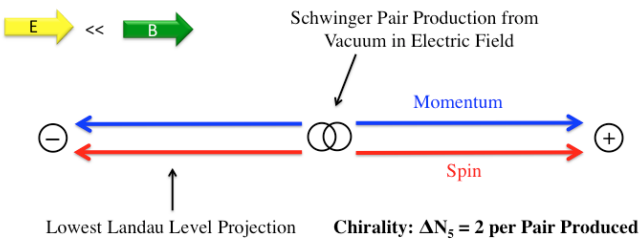

Figure 1.3: Cartoon of Schwinger mechanism process from an intuitive perspective with the inclusion of a strong parallel magnetic field with strength B. Pairs of particles are created from vacuum and are accelerated in the direction of the electric field, as shown in Fig. 1.2. Overlapping circles are depictive of a virtual particle anti-particle pair. Blue (red) lines represent momentum (spin) vectors. Due to a parallel strong magnetic field, particle anti-particle pairs will have their spins polarized in the direction of the magnetic field–setting up a net chirality; here given by $\Delta N_5 = 2$, c.f., Fig. 1.1. Alternatively, only the lowest Landau level will be occupied. Note that while here the $E \ll B$ condition–for later convenience–has been given, our final calculations do not rely on such an approximation.

be conserved! Yet this picture is at odds with the heuristically motivated scenario just described. Then in addition to the issues raised above, one must ask: Why do expectation values of the CME and axial Ward identity using traditional QFT methods not coincide with our heuristic picture of Schwinger pair production? Or rather, why do they seem to vanish?

1.3 Issue Resolutions

The resolution to these issues we find is a clear identification of vacuum states [19]. Depending on whether one uses in-in or in-out vacuum states, the expectation values differ markedly and predict different physical scenarios.

Traditional QFT methods involve the usage of an in-out matrix element expectation value. This scenario we argue represents a Euclidean observable in equilibrium. However, the Schwinger mechanism is inherently an out-of-equilibrium process; therefore expectation values derived using an in-out matrix element we argue simply do not give rise to any produced pairs–and this outcome is similar to what one would measure for a Euclidean observable in equilibrium. What is more here are the implications for anomalous physics: We find that the anomaly, as well as the CME, do not exist in equilibrium. This has profound implications both for theories built on anomalous physics and for their experimental detection.

On the other hand, we find–as anticipated above–the anomaly and CME do exist out-of-equilibrium and such observables are furnished using in-in vacuum expectation values. Indeed, we find a characteristic mass dependence indicative of the Schwinger mechanism for the real-time out-of-equilibrium case. The mass dependence associated with the Schwinger mechanism is highly suppressed, however, and then we expect the chirality generation brought on by parity-violating backgrounds, too, to be highly suppressed. This, as well, has deep implications for theories built on the anomaly, such as theories of baryogenesis driven by a parity-violating inflation [20]). This also has implications for the measurement of the CME in heavy-ion

collisions as well–where now one would expect an approximately similar exponential suppression with small quark masses and chromo-electric field strengths.

With a new perspective on the physics of the anomaly in hand, we also address important extensions to the study of anomalous physics. These are the chiral condensate and fluctuations in chirality.

The breaking of the chiral symmetry can be characterized by a non-vanishing chiral condensate in QCD, analogous to cooper pairs in a superconductor. However, it then begs the question: how else may one drive a non-vanishing chiral condensate? The answer is with a magnetic field. Much like temperature and density, one may make use of a background magnetic field as a tunable parameter for a theory. The enhancement of the chiral condensate, or a dynamically driven mass, in a magnetic field is referred to as magnetic catalysis [21–23]. However, while it is well understood how the chiral condensate behaves under a magnetic field, how it does so under an electric field–or rather parallel electric and magnetic field–is unknown. We find an electric field serves to diminish the condensate and, in fact, for the emergence of Schwinger pairs can even negate the chiral condensate all together. This "melting" of the chiral condensate in an electric field could play an important role in conjunction with chiral symmetry breaking in QCD.

In the formation of flux tubes, even though we argued to give rise to a net chirality through the Schwinger mechanism, the global chirality ought to be zero, however locally this is not thought to be the case [24, 25]. One way one might measure a local chirality violation is through fluctuations in chirality. Therefore it is an important task to calculate, using our in-out and in-in formalisms, chiral fluctuations. We found as expected there is a non-zero value for either case. However, for the out-of-equilibrium case using an in-in setup, we moreover found an exponential quadratic mass suppression associated with the Schwinger mechanism and linear time dependence. Before embarking on a more through explanations let us outline the thesis as a whole while also introducing our notations.

1.4 Notations and Outline

We have offered a cursory look at a chirality production via the Schwinger mechanism above, however to capture a more complete understanding of the physics to come let us explain the backgrounds of the CME and Schwinger mechanism, as well as related phenomena in Ch. 2. Then we cover relevant methods in Ch. 3, where we introduce past results on the enhancement of the Schwinger mechanism in inhomogeneous fields. The main contents of the thesis begin in Ch. 4, where we outline the importance of vacuum states, from which we can then find propagators and Green's functions using both a standard in-out, Sec. 4.2, representation as well as an in-in representation in Sec. 4.3. And the differences between both observables are discussed in Sec. 4.4. The primary observables related to chirality are calculated and discussed in Ch. 5; this includes the pseudoscalar, Sec. 5.1, and chiral density, Sec. 5.2, examined both in and out-of-equilibrium or rather in Euclidean equilibrium and real-time. Then applications to the axial Ward identity including the chiral magnetic effect, Ch. 6, and chiral density fluctuations, Ch. 7, are introduced and sought in and out-of-equilibrium as well. Last, we look at the chiral condensate too for both for in-out and in-in vacuum states in Ch. 8. The conclusions are finally presented in Ch. 9.

Throughout the thesis the following notations are adopted: A metric $g = \mathrm{diag}(+,-,-,-)$ is used, and wherever appropriate a condensed notation for contraction of Lorentz indicies is used, i.e. $A_\mu B^\mu =: AB$. Covariant derivatives are $D_\mu = \partial_\mu + ieA_\mu$. We also use units such that $c = \hbar = 1$. And we use a Weyl representation for the gamma matrices:

$$\gamma^0 = \begin{pmatrix} & I_2 \\ I_2 & \end{pmatrix}, \quad \gamma^i = \begin{pmatrix} & \vec{\sigma} \\ -\vec{\sigma} & \end{pmatrix}, \quad \gamma_5 = \begin{pmatrix} -I_2 & \\ & I_2 \end{pmatrix}. \tag{1.1}$$

$\vec{\sigma}$ are the usual Pauli matrices. And the spin tensor is $\sigma_{\mu\nu} = \frac{i}{2}[\gamma_\mu, \gamma_\nu]$. Point split observables are understood using a half point definition for Heaviside functions, i.e. $\theta(x \to 0) = 1/2$.

In contrast to the above, in Sec. 3.3 a Euclidean metric is used. There we have $g = \delta = (+,+,+,+)$. The magnetic and electric fields are defined from their Minkowski equivalent such that $F_{ij} = \epsilon_{ijk}B_k$ and $F_{4i} = -iE_i$ with both B and E real functions. Therefore F_{4i} is given as a purely imaginary function for Minkowski real fields, but is given as a purely real function for Euclidean real fields. And for the gamma matrices a Euclidean Weyl representation is used:

$$\gamma_E^i = \begin{pmatrix} & -i\vec{\sigma} \\ i\vec{\sigma} & \end{pmatrix}, \quad \gamma_E^4 = \begin{pmatrix} & I_2 \\ I_2 & \end{pmatrix}. \tag{1.2}$$

for $i = 1-3$; all γ_E^μ are Hermitian.

Chapter 2

Background

2.1 Chiral Anomaly

To gain a better perspective of the CME, (an electromagnetic current in the direction of a magnetic field driven by a chirality imbalance), let us first touch on some aspects of the anomaly. The importance of anomalies in the analysis of quantum theories can hardly be understated. An anomaly can be responsible for constraints on conserved currents, symmetries of the theory both global and gauged, and the spectrums of the theory. An instance of the anomaly most clearly demonstrated through experiment is provided by the decay of a neutral pion, a pseudoscalar, into two photons, of which the underlying broken chiral symmetry makes up the basis of this thesis.

The QCD Lagrangian possesses not only a color $SU(3)$ gauged symmetry but also a $SU(2)_L \times SU(2)_R$ chiral symmetry in the massless limit, (a good approximation for up and down quarks). The neutral pion is one of the Goldstone bosons associated with the spontaneous breaking of a chiral symmetry brought on by the formation of a dynamically driven condensate[2, 3]. And the neutral pion is a psuedoscalar whose decay into photons created unrest as classically the transition was forbidden. The loop diagram associated with the neutral pion decay can be formulated in terms of a background pseudoscalar calculation whose classical expectation values predicts

$$\partial_\mu \langle \Omega | \, \bar{\psi} \gamma^\mu \gamma_5 \psi \, | \Omega \rangle = 0 \, . \tag{2.1}$$

The vacuum states are not arbitrary, or generally equivalent, we will argue in the coming pages. However, for the purposes here why this expectation value takes on a nonzero value underscores the significance of the anomaly. The calculation of the decay rate was first achieved at the diagrammatic level [17], yet Schwinger first presented the calculation in a manifestly gauge invariant way through his proper time formalism[15][1]. Including quantum effects yields the famous axial Ward identity[2] which predicts a one-loop exact quantity associated with a broken chiral symmetry and the non-conservation of chirality:

$$\partial_\mu \langle \Omega | \, \bar{\psi} \gamma^\mu \gamma_5 \psi \, | \Omega \rangle = -\frac{e^2}{(4\pi)^2} \epsilon_{\mu\nu\alpha\beta} F^{\mu\nu} F^{\alpha\beta} \, . \tag{2.2}$$

[1] Please see the discussion in Section 2.3.2

[2] Again, here a discussion of appropriate vacuum states here markedly augments this expectation value. However, independent of vacuum states, the axial Ward identity at the operator level is exact.

That the two, Eq. (2.1) and Eq. (2.2), differ highlights the fact that classical and quantum prescriptions differ and an anomaly is present.

A more modern treatment of the calculation of the anomaly is provided by Fujikawa [1] through an analysis of the path integral measure under chiral rotations. There $U(1)_A$ axial rotations, while at the Lagrangian level for massless fermions reproduce Eq. (2.1) and a conserved chiral current, when incorporated in the path integral measure, associated with quantum effects, shows chiral nonconservation, Eq. (2.2). Besides the simplicity of the calculation and it's robustness, one may infer a host of anomalies which must cancel for a symmetry to be a symmetry in a QFT.

For example, for the $SU(3)_C \times SU(2)_W \times U(1)_Y$ color, weak, and hypercharge symmetry of the standard model, (mixed) anomaly cancellation requires that the electron and proton charges be equivalent. In turn, one may also find that while the baryon number and lepton number are separately anomalous, the baryon minus lepton number is not. And this with Sakharov's conditions [26], permit matter-antimatter asymmetry, or baryogenesis, in the universe. However, the amount of matter-antimatter asymmetry permissible by the standard model and what is observed in the universe remains a mystery.

Let us characterize the anomaly and we will soon find the CME through a topological term. A Lorentz invariant topological term is permissible in the QCD Lagrangian which violates both $\mathcal{P}$ (parity) and $\mathcal{CP}$ (charge-parity):

$$\frac{\theta}{32\pi}\epsilon_{\mu\nu\alpha\beta}G^{\mu\nu a}G^{\alpha\beta a}\,. \tag{2.3}$$

a sums over the group, $SU(3)_C$, generators for the gluon fields, with G being the field strength. However, experimentally this topological term is found to vanish; specifically according to neutron dipole experiments, an electric dipole moment restriction as low as $|d_n| < 2.9\times10^{-26}\ e$ cm was found in Ref. [27]. There $\mathcal{CP}$ violating electroweak contributions have been included. In spite of this, there is no compelling theoretical reason why such a topological term should be absent. This great mystery is one of the last problems of the standard model and is coined the "strong $\mathcal{CP}$ problem."

For highly equilibrated scenarios such as for a neutron electric dipole measurement, it is reasonable to expect no topological effect. Yet, if such a term is permissible then it is a reasonable question to ask would such a term vanish for all cases even those which are highly out-of-equilibrium. This is believed to be the case for a quark-gluon plasma (QGP); there the topological angle may differ at different space-time points [28]. This phenomenon is also predicted to take place in sphaleron transitions, which are instanton-like thermal transitions between different vacua–these are thought to elicit baryogenesis for electroweak interactions. Therefore we find that the topological θ term in Eq. (2.3) may not only represent a constant but may, in fact, depend on space-time, as for an axion-like term. A ramification of which permits a topologically dependent (chromo)electromagnetic current called the chiral magnetic effect.

2.1.1 Chiral Magnetic Effect

We may find a space-time dependent θ term clearly through Fujikawa's path integral measure method [1]. Performing a $U_A(1)$ space-time dependent axial transformation[3] in the Lagrangian one would find the addition of a topological term [29], Eq. (2.3), only with $\theta \to \theta(x)$. With a space-time dependent θ one can perform an integration by parts in the topological term to find a term which couples a pseudo-vector to the (chromo)electromagnetic gauge. Then, the classical equations of motion for the gauge field are modified to find a correction to the three-dimensional (chromo)electromagnetic current, called the chiral magnetic effect (CME):

$$j_\mu = -\frac{e^2}{4\pi^2}\mu_5 \epsilon_{0\mu\alpha\beta} F^{\alpha\beta}\,, \tag{2.4}$$

$$\mu_5 \coloneqq \partial_0 \theta\,. \tag{2.5}$$

μ_5 is the chiral chemical potential. Also, here we have depicted the Abelian case for uniformity with later results; the CME is non-vanishing for the non-Abelian case as well. j_μ is the electromagnetic current.

One may intuitively understand the CME as a polarization of the net chirality by an external magnetic field brought on by the topological structure, which sets up an electromagnetic current in the direction of the magnetic field. A diagrammatic example of the CME phenomenon was shown in Fig. 1.1.

One may also envision the CME as originating from the Dirac sea and anomaly [28]; here we consider massless fermions. Due to a conserved chirality owing to massless fermions the Fermi levels for both left and right-handed particles will be distinct and separate. Then let us consider what happens when an external parallel electric and magnetic field is turned on. The electric field will set up a longitudinal force, aligning (opposing) the anti-fermions (fermions) in the direction of the electric field and in turn projecting the fermions' momentum. Likewise, the magnetic field will align the spins' of the fermions. Therefore, the combination of the electric and magnetic fields will set up a net chirality and moreover the CME will be born from the net current projected along the direction of the magnetic field. Actually, the basis of this Dirac sea explanation underlies the Schwinger mechanism to be discussed below. The net chirality increase is characterized through an increase in the Fermi momentum from the electric field, and also from the magnetic field an increase in the density of the Landau levels in the transverse direction,

$$\frac{d^4 N_R}{dT dV} = \frac{e^2}{4\pi^2} EB\,. \tag{2.6}$$

Here N_R is the number of right-handed fermions for a given volume, V, and time, T [28]. We may also do the same for the left-handed fermions and then we can find that the total chirality change is given by

$$\frac{d^4 (N_R - N_L)}{dT dV} = \frac{e^2}{2\pi^2} EB\,. \tag{2.7}$$

[3] One may also allow an infinitesimal axial transformation with vanishing space-time dependence to find Eq. (2.3).

c.f. Eq. (2.2); we see that the relationship indicative of the axial anomaly has been reproduced. Note, to achieve this connection one must perform an integration over space-time. Also, as in the topological axial anomaly case, here too we find that the change of chirality is discrete and so too must be a non-zero discrete topological term.

While the above demonstration made use of an electric field let us emphasize that the CME exists even in the vanishing electric field case. This may be the case for a hot QCD environment with a non-trivial topology or non zero space-time dependent θ angle. Then along with an external magnetic field and a basic requirement for the CME are fulfilled as is defined in Eq. (2.4).

Experimental efforts have been and are currently underway to observe the CME. Notably, in a semimetal, the CME was thought to be observed [5]. Also, enormous effort has been carried out in heavy-ion collision experiments such as at the large hadron collider (LHC) at CERN and the relativistic heavy ion collider (RHIC) at the Brookhaven National Laboratory, however, the CME still has not been confirmed in colliders. However let us first examine the CME in the context of a condensed matter environment.

2.1.2 Chiral Magnetic Effect in Condensed Matter

A relativistic fermionic dispersion relation is a requirement to study chirality and indeed the chiral anomaly and magnetic effects, and there are a number of different condensed matter systems in which such a dispersion is visible. Some include Weyl and Dirac semimetals, graphene, and spin-orbit coupled atomic gases. However, here let us focus on semimetals. A semimetal's valence and conduction band lie between those of a conductor and an insulator and posses a small overlap–in contrast with a semiconductor where it is separated. This small overlap permits interesting electronic and transport properties. With the discovery of graphene [30], a 2 (space) + 1 (time) dimensional analog of a semimetal, it was found a relativistic massless quasiparticle excitation, a Weyl-like fermion, was present. Then with an extension to 3+1 for certain solid-state crystals [6, 7, 31, 32], it was found as well, a Weyl/Dirac spectrum was present with small to vanishing gap.

Chirality in a semimetal is governed by Weyl nodes serving as topological charges stemming from a Berry's phase in crystal quasi-momentum space [33, 34]. Chiral quasiparticle behavior was detected along with the discovery of 3-dimensional Dirac semimetal [6, 7, 31, 32], and has paved the way for testing of the chiral anomaly in condensed matter systems. Indeed in addition to the CME, the chiral anomaly was thought to be observed [35] in Weyl semimetals. Let us see how the chiral anomaly appears in such systems. We confine our attention to the physics of a Weyl semimetal with linear dispersion relation whose Hamiltonian is $\tilde{H} = \vec{p} \cdot \vec{\sigma}$; in this section we use a tilde over variables so as to contrast with the rest of the thesis. Berry's phase represents a non-holonomic addition to the phase of the wavefunction. Here we are in momentum space, and we can determine the phase through a unitary transformation of the Hamiltonian, i.e.,

$$\tilde{H}' = U^\dagger \tilde{H} U - i U^\dagger (\nabla_p U \frac{d\vec{p}}{dt}) \,, \tag{2.8}$$

where Berry's phase is $iU^\dagger \nabla_p U$; however only Berry's curvature, a monopole in momentum space, is observable. The unitary phase can be chosen so as to yield a diagonal (in spinor space) Hamiltonian, and an approximate adiabatic evolution of the Hamiltonian around momentum space is assumed. Then in the presence of an electromagnetic field[4]–we take $\vec{E} \cdot \vec{B} \neq 0$–one may solve the equations of motion of Eq. (2.8) to find an invariance in phase space leading to the anomaly [36], namely

$$\frac{\partial \tilde{n}_5}{\partial t} = \frac{e^2}{4\pi^2} \vec{E} \cdot \vec{B} \,. \tag{2.9}$$

What is interesting here is although the equations of motion are classical, a quantum non-conservation of chirality is obtainable with Berry's phase. Let us now see how one might inspect the CME in a semimetal with the anomaly driven by a finite $\vec{E} \cdot \vec{B}$.

The most recognizable signature of the CME in a semimetal is a quadratic magnetic field dependence in the conductivity, or a negative magnetoresistence [37]. Let us illustrate how this occurs at a cursory level. First, one must outfit the anomaly relation stemming from a Berry's phase, Eq. (2.9), with a subtractive chirality-changing scattering time, t_ν, which is different from the real time, x_0. This amounts to adding a $\tilde{n}_5/t_\nu$ to Eq. (2.9). One can then predict the amount of chiral density growth as (for small chirality-changing scattering times [5]–this in effect negates the effects of $\partial_0 \tilde{n}_5$)

$$\tilde{n}_5 \propto \vec{E} \cdot \vec{B} t_\nu \,. \tag{2.10}$$

And furthermore, one can characterize a many-body system possessing a net chiral density with a chiral chemical potential [4] as

$$\tilde{\mu}_5 \sim \tilde{n}_5 \,, \tag{2.11}$$

where an assumption of small chiral chemical potential to chemical potential and temperature has been made. Now applying the above relation to the defining chiral magnetic effect current, Eq. (2.4), we can find in addition to Ohm's current, a non-zero addition to the electromagnetic current. Then in electric and magnetic fields with strengths E and B respectively, specifically one would find

$$\tilde{j}^i = \tilde{\sigma}^{ij} E \hat{x}^j \,. \tag{2.12}$$

And for the case of parallel electric and magnetic fields, one would then find the conductivity

$$\tilde{\sigma}^{ii} \propto B^2 \,, \tag{2.13}$$

for magnetic field also in the x^j direction; see Ref. [5] for details. Indeed such a quadratic magnetic field dependence was thought to be observed in zirconium pentatelluride, $ZrTe_5$ [5]. However, let us mention here that like the case of the CME in QCD in heavy ion collisions, there is discussion as to whether the quadratic magnetoresistance is solely coming from the CME or something else. In any case, however, observation of the CME in QCD and colliders is a more delicate task–one still not completed.

[4]One actually only needs a magnetic field. Note, however that without an electric field we would not have an anomaly. Also as a side note, in the absence of an electromagnetic field the equations of motion found from Eq. (2.8) would have no Berry's phase contributions [36].

2.1.3 Chiral Magnetic Effect in Heavy Ion Collisions

In off-central heavy-ion collision experiments, an enormous out of plane magnetic field resides, in fact, it possesses the strongest terrestrial value comparable to that of the pion mass or $B \sim m_\pi^2$. The fluid, or QGP, in the resulting high density and temperature environment, possesses many other interesting properties too, such as non-vanishing vorticity [38, 39]. With such a strong magnetic field the CME is thought to appear in conjunction with a net local (as described above) chirality through local parity violation.

While fluctuations in chirality or topology are not directly observable in heavy-ion collisions, one can make use of the azimuthal direction in the transversal plane in which the magnetic field develops to extract meaningful experimental data. Notably, a charge asymmetries of event-by-event correlations can be measured [40]. Groups STAR at the RHIC [41] and ALICE at the LHC [42] have carried out such measurements. While the measurements are consistent with the finding of what a local parity violation and CME are thought to produce, whether the measurements are exclusively coming from the CME or from background effects cannot be differentiated at this time [40]. However, with exacting theoretical analysis of all processes at play, one might be able to differentiate the proper signal of the CME leading to its discovery. To this end, there are still several theoretical shortcomings of the anomaly and CME which require elucidation.

Whether in a condensed matter environment or in a heavy-ion collision a key ingredient in the theoretical analysis of the CME is the insertion of chirality by hand. This could take the form of a spacetime dependent topological $\theta(x)$–and by extension the chiral chemical potential, μ_5; see Eq. (2.5)–or even a straightforward imbalance of chiral density. A noteworthy example lies with the usage of Berry's phase of Weyl fermions to illicit the chiral anomaly and CME [36]. While useful for analytic purposes assuming a finite chiral chemical potential as an initial state we go on to describe is artificial. And if the CME were visible in QFT then one needn't rely on anything but the Dirac equation. Another at-first-glance separate but we will later show a related issue with the CME's analysis is the effects of a fermion mass. A fermion mass is seemingly troublesome as it will mix both left and right parts of the wavefunction but we have in any case Lorentz covariant expectation values with chirality at our disposal. The resolution to both the issue of insertion of chirality by hand and the effects of a fermion mass is provided by the relativistic analog of tunneling in quantum mechanics: the Schwinger mechanism.

2.2 Background Electric Field

2.2.1 Schwinger Mechanism

The Schwinger mechanism predicts the generation of particle anti-particle pairs from the QFT vacuum in the presence of a strong electric field [15, 43, 44]. The Schwinger mechanism can be classified as a QFT vacuum instability; others include Hawking radiation [45], the Unruh effect [46], pair creation from inflation (for example in a Robertson Walker metric), and spontaneous symmetry breaking [47]. The Schwinger mechanism arose as a solution to the Klein paradox [48], which is an application of the Dirac equation to a non-relativistic barrier scattering quantum mechanical

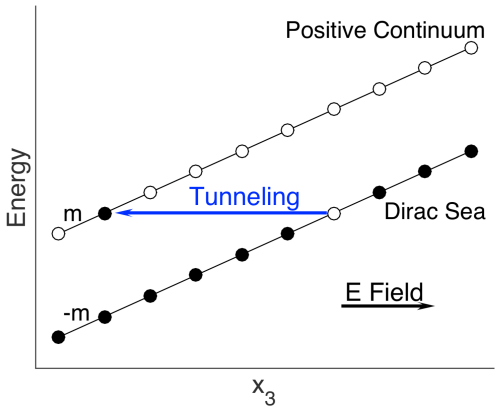

Figure 2.1: Dirac sea picture of the Schwinger mechanism. Dirac spectrum is shown against the coordinate associated with the direction of the homogeneous electric field. Excitations represent particles tunneling from the Dirac sea, whereas their accompanying holes represent anti-particles. The electric field tilts the spectrum enabling a tunneling from the QFT vacuum. The picture of tunneling (as is commonly used) in momentum space is given in Fig. 2.2, with a magnetic field present.

problem. And this finding highlighted the particle number non-conserving nature of relativistic quantum field theories. However, the Schwinger mechanism has still not been observed. Even so, the mechanism lies close to experimental verifiability. In fact, despite the strong homogeneous QED electric fields required, combinations of time-dependent fields, (notably those interpolating between strong and slow and weak and fast electric fields: dynamically assisting electric fields [49]), may reduce the experimental threshold. See Sec. 3.3 for more details. The discovery of the Schwinger mechanism could shed light on other vacuum instability physics purely non-perturbative in nature. For instance, acceleration in a very strong electric field could mimic gravitational effects in Unruh and Hawking radiation [50].

The Schwinger mechanism in fact provides a physically translucent picture of a vacuum instability process. To that end let us make use of a Dirac sea interpretation; see Fig. 2.1. A background electric field with strength E, (here homogeneous in the x_3 direction), tilts the Dirac spectrum Ex_3 enabling quantum tunneling from the Dirac sea to the continuum, leaving an anti-particle (hole) in its place. Here we see a characteristic tunneling length must be penetrated, which we will see is related to a critical electric field. An important feature here is also the traversal of a mass gap. Interesting we may liken the tunneling behavior of the Schwinger mechanism to a Landau Zener crossing in quantum mechanics.

One may also make use of a classically motivated picture in which the vacuum is characterized by a particle anti-particle pair as a condensate. Then a background electric field imparts work to the pair splitting them apart. More generally, but also relevant to the condensate picture, we can picture the Schwinger mechanism process quite simply from a pair, created from the vacuum instability at some point in space-time, then accelerated due to the electric field; see Fig. 1.2 shown earlier. What is more, is we can see a background magnetic field cannot impart work to a particle anti-particle pair and thus we should not expect to see pair production from a sole magnetic field.

Not only for QED but also more generally for Yang-Mills theories can one see Schwinger pair production [51–53]. The Schwinger mechanism is thought to underlie the chromoelectric flux tube breaking leading to hadronization in nucleus-nucleus collisions such as the RHIC and LHC experiments. An Abelian approximation for non-Abelian Schwinger pair production is frequently evoked and this is justified for flux tubes thought formed in colliders with finite topological charge. Thus, here we work in QED, however, with suitable homogeneous chromoelectromagnetic fields, i.e. $G_a^{\mu\nu} = F^{\mu\nu} n_a$ where $n^2 = 1$ for G_a a Yang-Mills field, Fn_a, an Abelian projection, we may infer pertinent QCD pair production physics. Furthermore, of noted interest are field configurations with finite topological charge, $\epsilon_{\mu\nu\sigma\lambda} F^{\mu\nu} F^{\sigma\lambda}$, thought present in HIC[11, 12]. Then upon Lorentz transformation, we find parallel (chromo)electric and magnetic fields. Such a field configuration presents an optimal study of pair production with topological effects, yet without being encumbered by technical details, and serves as the (Abelian) background examined in depth in this thesis. Even with homogeneous fields, the study of the Schwinger mechanism is challenging due to its inherent nonperturbative nature.

The nonperturbative nature of a vacuum instability such as the Schwinger mechanism is most clearly demonstrated through the effective action in Schwinger proper time.[5] A vacuum instability is then characterized by inequivalent vacuum states, $\langle \text{in}| \neq \langle \text{out}|$ at t_{in} and t_{out}, usually taken to $-\infty$ and ∞ respectively. That a vacuum instability is present is most easily seen through a calculation of the S matrix element describing an in to an out vacuum transition, $|\langle \text{out}|\text{in}\rangle|^2$. Then the alternative, namely that something besides the vacuum appears in the out state, (most commonly a pair of particles), is described by,

$$\mathcal{P} \coloneqq 1 - |\langle \text{out}|\text{in}\rangle|^2 \,, \tag{2.14}$$

or the probability that out state contains an excitation. This prediction is referred to as the vacuum non-persistence. But, $\langle \text{out}|\text{in}\rangle$ is simply the partition function

$$c_v \coloneqq \langle \text{out}|\text{in}\rangle = \int \mathcal{D}\bar{\psi}\mathcal{D}\psi \exp\{i \int d^4x [\bar{\psi}(i\not{D} - m)\psi]\} \,, \tag{2.15}$$

here for fermions in some background, non-dynamical, gauge field[6]. The partition function can also be characterized by an effective action,

$$c_v \coloneqq e^{i\Gamma} \,. \tag{2.16}$$

[5] Schwinger proper time is a functional means of expressing full QFT Green's functions and effective actions in terms of a quantum mechanical-like 4+1 dimensional setup; for path integral manifestations see Refs. [54, 55].

[6] Background fields typically solve the homogeneous Maxwell equations for the above QED case and a Yang-Mills homogeneous equation for the non-Abelian equivalent. However, we will also explore more complicated background field types that could be had with the inhomogeneous Maxwell equations.

Let us also mention that if one was to introduce dynamical gauge fields to the above, the prescription would be to replace $A^\mu \to A^\mu + a^\mu$, where a is a dynamical field, and to integrate over the dynamical field, amounting to the addition of $\mathcal{D}a$ in the partition function with gauge fixing terms as well. However, in this work, we restrict our attention to sole background fields. Thus our setup is one-loop exact.

Then we can see that the vacuum non-persistence is

$$\mathcal{P} \approx 2\mathrm{Im}[\Gamma]\,, \tag{2.17}$$

for a small imaginary part of the effective action. This is the simplest measure of a vacuum instability and Schwinger pair production predicts to lowest order the probability of a particle anti-particle pair appearing. Turning our attention to homogeneous fields, with a characteristic electric field strength E and fermion mass, m, one can calculate the effective action to find [15]

$$\mathcal{P} \lessapprox \exp\left(\frac{-\pi m^2 c^3}{eE\hbar}\right). \tag{2.18}$$

This is the probability of a single pair of particles to be produced from a constant electric field due to the Schwinger mechanism. SI units have been explicitly shown here to emphasize the scale of the electric field required to traverse the vacuum mass gap; while significant methods to surpass the critical electric field are underway as explained before. The exponential suppression above, Eq. (2.18), to quadratic order in mass is the defining expression of the Schwinger mechanism and should appear in all final expectation values where the Schwinger mechanism plays a role. Also, notice the placement of the gauge coupling constant, e, in Eq. (2.18), it is in the denominator and therefore the exponential suppression cannot be seen to any order[7] in a perturbative theory. Nonperturbative methods are needed. One such state-of-the-art method lies with a quantum mechanical-like worldline formulation discussed in Sec. 3.2. The Schwinger mechanism promises a fundamental non-perturbative outlook on QFTs and has a basis in many important phenomena, and therefore there have been numerous experimental studies.

The Schwinger mechanism has been sought in many experimental setups including but not limited to condensed matter analog environments and high powered lasers.

2.2.2 Schwinger Mechanism in Condensed Matter

The appeal of utilizing an analog condensed matter environment to study the Schwinger mechanism is readily apparent in that the critical electric field strength required for tunneling is dramatically reduced [57]. The analogy of Schwinger pair production in condensed matter is facilitated through a Landau Zener transition [58, 59], where in place of the positive continuum and the Dirac sea are the conduction band and valence band, respectively:

$$\begin{gathered}\text{Schwinger mechanism} \leftrightarrow \text{Landau Zener tunneling}\\ \text{positive continuum} \leftrightarrow \text{conduction band}\\ \text{Dirac sea} \leftrightarrow \text{valence band}\,.\end{gathered}$$

Some examples environments include Dirac / Weyl semimetals, semiconductors, and graphene, (the 2+1 dimensional corollary to a 3+1 semimetal). The semimetals

[7] If all orders in a perturbation theory are kept, resurgence theory [56] promises to resolve this issue. Then one may connect the nonperturbative and perturbative sectors of a theory through a Borel transformation.

and graphene possess little or no energy gap in their dispersion relations. However, one could construct a semimetal with effective quasi-particle mass in the form of a doped semimetal, with impurities acting as a gap, or even construct a tunable gap [60]. Then in analogy with the QFT case, let us consider a gap Δ. Then one might find in the case of a gapped dispersion the following form for the exponential suppression in Schwinger's formula [61]

$$\mathcal{P}_{LZ} \approx \exp\left(-\frac{\pi\Delta^2}{v_F\hbar eE}\right). \tag{2.19}$$

The advantage of using gapped materials is that a clear indication of Landau Zener transitions is available through the characteristic exponential suppression factor, however using gapped materials come with at a cost. As the signal for the transitions would be highly suppressed with a gap, observing a meaningful signal might pose a challenge. And for the gapless case, it could become unclear whether signals of breakdown are genuinely from Landau Zener tunneling or from some competing mechanism.

The Schwinger mechanism in inhomogeneous fields in semiconductors was analyzed in Ref. [57]. Also gapless dispersions were investigated in graphene in Refs. [62, 63], as well as in semimetals with more realistic dynamics in Ref. [64]. Not only in condensed matter but also in QED the Schwinger mechanism is thought observable.

2.2.3 Schwinger Mechanism in High Powered Lasers

The clearest theoretical study of Schwinger pair production lies in QED and as such, the most important task is its direct observation in strong electromagnetic field, and the strongest pure background fields[8] are obtainable with high powered lasers. One can both directly measure the effects of pair production through the sole use of lasers or indirectly through the collision of a laser beam with particles. Many such facilities devoted to the study of strong QED–the study of QED in strong electromagnetic fields–have been established including the Extreme Light Infrastructure (ELI) and the X-ray Free-Electron Laser Facility (XFEL) in DESY; see Refs. [50, 65, 66] for specific experimental outlooks. However, still the largest peak electric field, $E \sim 10^{-2}E_{crit}$, is still orders of magnitude below the critical electric field strength [67, 68], $E_{crit} \sim 1.3 \times 10^{18}$ V/m. In the coming, we illustrate how this is surpassable with inhomogeneous fields, and therefore verification (or falsification) is expected in the near future. Even with a favorable laser configuration, the realistic modeling of a high powered laser is highly non-linear and requires sophisticated numerical implementation through particle-in-cell simulations [69]. Additionally, backreaction effects are also important. When a pair is spontaneously produced energy is taken from the background field and this too must be simulated accordingly. Furthermore, higher-order effects, beyond 1-loop, become important too. While direct observation from high-powered lasers is at hand, in fact, indirect observation of the Schwinger mechanism in the collision of a particle beam with a high powered laser has been observed at SLAC E-144 laser experiment [70]. There, a low-intensity optical laser was collided with incoming electrons creating high-intensity photons which then

[8] The electromagnetic fields generated in nucleus-nucleus are greater, however, differentiating a non-perturbative characteristic mass gap from other observables is challenging.

recombined with the optical laser producing pair production. It is of great interest to confirm the Schwinger mechanism directly in high powered lasers, and to this end, it has been found that certain background field shapes theoretically better illicit pair production than others.

2.2.4 Inhomogeneous Fields

Homogeneous fields provide an unobstructed with technical detail picture of the Schwinger mechanism process; this is invaluable for theoretical studies. Indeed we primarily use homogeneous fields for addressing Schwinger mechanism mass effects to the chiral anomaly. We can gather physical insight not obtainable with inhomogeneous field backgrounds. However, there are compelling reasons for analyzing inhomogeneous fields: Background fields capable of approaching electric (chromoelectric) field strengths relevant to the Schwinger pair production process in QED (in high powered lasers) and QCD (in heavy-ion collisions) are highly inhomogeneous, and therefore to properly model background in such environments it is essential to go beyond inhomogeneous fields. Furthermore, with certain background field types, such as for a temporally inhomogeneous electric field, the threshold for pair production is, in fact, lessened. As there still is no direct observation of the Schwinger mechanism, the study of inhomogeneous fields that enhance pair production is highly desirable.

Electromagnetic field configurations produced in high powered alternating lasers such as at ELI and XFEL stem from beams of a given frequency and modulation, and as such always contain some inhomogeneity [50, 65, 66]. To properly model such scenarios one must use numerical techniques, such as particle-in-cell simulations [69], and there is generally always spatio-temporal inhomogeneity in both the magnetic and electric fields [71]. Thus it is a crucial task to study more complicated QED backgrounds. Also, by the very transient nature of heavy-ion collisions, chromo-electromagnetic fields generated there are highly inhomogeneous [72, 73]. For example, it was found in a study of the LHC and RHIC that for off-central collision the magnetic field was highly spatially inhomogeneous [74]. Even though the study of inhomogeneous fields is valuable for realistic scenarios, it is at the present experimentally mandatory as the engineering of optical shapes can reduce the threshold for pair production.

In very early studies by Keldysh it was found a temporally inhomogeneous electric field was more likely to illicit Schwinger pair production than a homogeneous one [75]. However, in contrast to a homogeneous field the mechanism for Schwinger pair production is not entirely non-perturbative; coined a “dynamical pair production” pairs generated are dependent on a specific electric field characteristic frequency. A famous example of a temporally inhomogeneous electric field is provided by a Sauter potential, or rather a pulsed electric field in time; here the characteristic frequency is a measure of the width of the pulse in time. In contrast to a temporal inhomogeneity, a spatially inhomogeneous electric field is known to inhibit Schwinger pair production in comparison to a homogeneous field [76, 77]. With the above field types considered it then becomes natural to ask how pair production behaves under a magnetic field, whether spatially or temporally inhomogeneous, or combinations of fields. Indeed such a discipline is widely being researched. Let us visit one important combination of fields first.

Motivated by Keldysh's work [75] employing a dynamical mechanism, and also by unique engineered pulse shapes as used in strong field atomic physics, Schutzhold et al. discovered a combinatory electric field configuration that significantly reduced the threshold for pair production coined the "dynamical assisted Schwinger mechanism [49]." There both a strong and slow electric field (essentially a homogeneous one) was superimposed with a fast but weak one (a Sauter potential [43]); specifically, they used

$$A(x_4) = -iEx_4 - i\varepsilon \tan(wx_4)\,, \tag{2.20}$$

where x_4 is a Euclidean time, $x_0 = -ix_4$, ε is a measure of the amplitude of the small peaked field with characteristic frequency w, and E is the strength of the slow (approximately homogeneous) field. In essence, the weak fast field acts as an optical trap in effect reducing the tunneling length required for pair production. Equipped with more mathematical machinery, we may better describe this process later in Sec. 3.2. Several related works have also been done: The usage of strong spatially modulated and a weak temporally modulated electric fields was examined in Ref. [78]. Also, a quantum kinetic theory extension employing the dynamically assisted mechanism [79], as well as an analysis of the momenta spectra [80], were researched. Then it becomes an interesting question to ask how might one further enhance (or avoid an inhibitability) the Schwinger mechanism process. We find a magnetic field for specific configurations may provide an answer.

2.3 Background Magnetic Field

Above we have looked at the basic effects of a background electric field in a quantum field theoretic system, then it is a natural question to ask how might the above theories be augmented under the influence of a magnetic field. QFTs under a background magnetic field have rich application and also span a wide breadth of application; one of the more prominent examples is the CME, discussed above. In addition to playing an important role in QGPs in heavy-ion collision experiments, magnetic fields are also important in astrophysical contexts such as for neutron stars. For example, magnetars are neutron stars which decay from a very strong magnetic field, 10^{15} G–to put this in context, consider the previous example of an off-central heavy-ion collision; there a magnetic field of 10^{18} G [10] can be generated. It is quite amazing the magnetic field in colliders is so strong. Also, in early universe applications, a magnetic field is thought important. Non-dynamical processes like inflation may in fact seed a primordial magnetic field at the universe's beginnings [81]. Furthermore, enormous effort is being spent on the makeup of a phase diagram in QCD [82], where the nature of QCD under a finite temperature and baryon chemical potential is sought. Not only using such statistical properties but also using a magnetic field as a tunable parameter one can explore symmetry breaking/restoring characteristics of QCD; this is referred to magnetic catalysis [21–23]. While a sole background magnetic field has received considerable attention, in part due to theoretical difficulties the study of a magnetic field with an electric field has received too little attention. And one of the most interesting applications in this research thrust indeed lies with the Schwinger mechanism.

2.3.1 Schwinger Mechanism with Magnetic Field

Into a background electric field let us introduce a parallel magnetic field; the magnetic field gives rise to curious rich new chiral physics, notably chirality generated through the Schwinger mechanism. Let us begin our examination of spawned chirality with a cursory look at Schwinger pair production under the Lowest Landau Level Approximation (LLLA). Parallel homogeneous fields are the simplest possible, (yet unencumbered with technical difficulties), optical field setup which is parity-violating. It is known such fields out-of-equilibrium yield a net chiral density through the Schwinger formula–elaborated below [13]. Even in the highly unequilibrated ion-ion collision scenario chromoelectomagnetic flux tubes are thought to form in the glasma, with features resembling those of parallel Abelian homogeneous fields [11, 12]. And thus parallel fields provide us with an ideal theoretical setup to study both chirality and Schwinger pair production (due to the electric field).

First, let us remark on Schwinger's formula in parallel fields. The vacuum instability manifests itself in the cleanest physical interpretation as an imaginary piece of the effective action of the QFT partition function, Eq. (2.17). And here let us limit our discussion to the probability of only a single pair of particles being produced. Then accounting for a space-time volume measure, Vt in the effective action, one can find the probability of a single particle anti-particle pair[9] to be produced is roughly

$$2\mathrm{Im}[\Gamma] \approx Vt\,\omega\,, \tag{2.21}$$

with ω being the probability density per unit time. Note here that ω is the lowest order in pair production value of the non-persistence probability given in Eq. (2.17).

We select homogeneous parallel electric and magnetic fields with respective strength E and B in the 3-axis direction,

$$\mathbf{B} = B\,\hat{x}_3, \quad \mathbf{E} = E\,\hat{x}_3\,. \tag{2.22}$$

Then, the imaginary piece of the effective action is famously known, (for a comprehensive review, see Ref. [84]), and Schwinger's formula for the pair production rate reads

$$\omega = \frac{e^2 EB}{4\pi^2}\coth\!\left(\frac{B}{E}\pi\right)\exp\!\left(-\frac{\pi m^2}{eE}\right). \tag{2.23}$$

The parallel magnetic field slightly increases the probability of pair production. Also, even with the magnetic field the characteristic exponential suppression, Eq. (2.18), is present. Note that here all the Landau levels are kept; the levels are characterized by the $\coth(\frac{B\pi}{E})$ function above which may be expanded out in an series of exponential terms with the $n = 0$ (LLLA) case given by for large magnetic field $\coth(\frac{B\pi}{E}) = 1$. Even with the LLLA we can see the the magnetic field enhances pair production but only to a linear order whereas the electric field suppresses it exponentially. Most significant about Schwinger's formula, Eq. (2.23), is its connection to chirality.

[9] The effective action contains information on any number of pairs to be produced. Though, we limit our discussion in this section to only the probability of a single pair to be produced. Furthermore, let us note higher orders in the effective action are not directly correlated with a higher number of pairs produced [83]. Afterward, all orders will be considered.

We may use Schwinger's formula in parallel fields to motivate a heuristic calculation of chirality generation through Schwinger pair production. Intuitively, one could consider the scenario of an approximately massless particle anti-particle pair under the influence of a strong magnetic field. There the particles' spins would project to the magnetic field in such a way as to set up a net chirality. Then under the influence of an electric field, the particle pair would accelerate in opposite directions. One ought to measure a net chirality in such a circumstance. See Fig. 1.3 introduced before. Indeed, it was found such a picture was originally found to generate a net chirality in Ref. [13]. Note that this picture also holds in the massive fermion case as well. For a strong enough magnetic field, only the lowest Landau level states will be occupied and this would produce an effective dimensional reduction simulating a system with fixed chirality.

Let us also note that not only the chirality directly but also the CME naturally appears in the context of parallel fields with the Schwinger mechanism. Consider again Fig. 1.3; since the particles are being accelerated due to the electric field, which is parallel to the magnetic field, then a current will be generated along the magnetic field; this is the CME current. While a classically motivated picture provides is indeed helpful, it is imperative to more quantitatively address the phenomena of chirality generation via the Schwinger mechanism, and we can do this through the axial Ward identity.

2.3.2 Axial Ward Identity

A key component of an anomaly, specifically the chiral anomaly, is the existence of the QFT vacuum, which supplies an infinite number of participants from the Dirac sea, making possible the non-conservation of a classical symmetry when an instability may be present [85]. To illustrate this we make use of the anomaly's quintessential Dirac sea interpretation. Previously, we examined the Dirac spectrum in a quasiclassical picture in coordinate, x_3, space where the levels were perturbed by a background electric field by eEx_3. This was shown in Fig. 2.1. The key point is that the electric field, through the Schwinger mechanism, enabled a tunneling of the mass gap. Let us then see how the same process unfolds with the addition of a parallel magnetic field. Here however, it is instructive to make use of the momentum representation of the Dirac sea picture–as is more commonly utilized.

The Dirac sea energy dispersion relation for a massive, with mass, m, fermion in parallel electric and magnetic fields can be seen in Fig. 2.2. The magnetic field is strong and a lowest Landau level approximation (LLLA) is assumed. This is an important point, as for massive particles, only the lowest Landau level may contribute to the chirality, and this is due to the virtue of a definite projection of helicity. The LLLA here amounts to an effective 1+1 dimensional reduction. Then we turn on a parallel electric field, strong enough such that pair production may take place and the mass gap be traversable; a particle (excitation) may tunnel from the Dirac sea, leaving an anti-particle (hole) in its place. Now, due to the strong magnetic field and the LLLA, only chiral right-handed particles and left-handed anti-particles can be produced. We end up with chirality non-conservation in what manifests itself as the axial Ward identity. Since we have an infinite Dirac sea, conservation of chirality can be broken. This is an essential point. Particle non-conservation gives rise to the anomaly from a vacuum instability. Indeed, such a

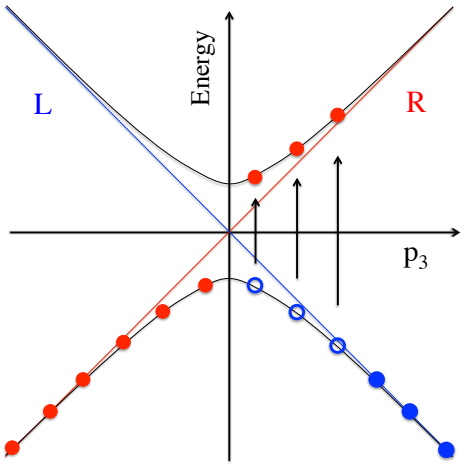

Figure 2.2: Schematic picture of Schwinger pair production and the axial Ward identity in a reduced 1+1 dimensional system due to a LLLA. A Dirac sea dispersion relation is shown in momentum space; particles (anti-particles) are represented as excitations (holes). A strong magnetic field makes possible the LLLA in effect dimensional reducing the system to 1+1. And the Schwinger mechanism makes possible tunneling of the mass gap. Right-handed particles and left-handed anti-particles, and thus a net chirality, are generated from the tunneling mechanism. (Note, pairs produced at higher longitudinal momenta are shown only for illustrative purposes, yet are actually highly suppressed.)

picture is frequently invoked to describe the anomaly for massless particles in a 1+1 dimensional system.[10] However, the problem–we go on to show later in the thesis–is conventional QFT tools are inadequate for treating a vacuum instability.

Turning our attention once again to the vacuum non-persistence we may quantify the rate of chirality generation via the Schwinger mechanism. In the instance of a single pair being produced under the LLLA the chirality would be incremented by two, (one right particle and one left anti-particle),

$$\omega = \frac{e^2 EB}{4\pi^2} \exp\left(-\frac{\pi m^2}{eE}\right) \sim \frac{1}{2}\partial_0 n_5 \,, \tag{2.24}$$

as was found in Ref. [13]. Here, the chiral density, n_5, is an expectation value[11] of the time component of the axial current

$$j_5^\mu := \bar{\psi}\gamma^\mu\gamma_5\psi \,. \tag{2.25}$$

The nonconservation of chirality is famously predicted through the axial Ward identity:

$$\partial_\mu j_5^\mu = -\frac{e^2}{16\pi^2}\epsilon^{\mu\nu\alpha\beta}F_{\mu\nu}F_{\alpha\beta} + 2m\bar{\psi}i\gamma_5\psi \,, \tag{2.26}$$

[10] Note, the picture depicted in Fig. 2.2 relies on tunneling, not a spectral flow, to describe the anomaly and this is a necessary feature for massive systems.

[11] The precise meaning of this expectation value we will elucidate later.

and is exact at the operator level as depicted above. With parallel homogenous electric and magnetic fields, Eq. (2.22), we have $\epsilon^{\mu\nu\alpha\beta}F_{\mu\nu}F_{\alpha\beta} = -8EB$. Also, as will be shown below, $\langle j_5^i \rangle = 0$. Accordingly, one would expect the chirality production heuristically found in Eq. (2.24) to follow as

$$\partial_0 \langle j_5^0 \rangle = \frac{e^2 EB}{2\pi^2} + 2m\langle \bar{\psi} i\gamma_5 \psi \rangle \,. \tag{2.27}$$

However, in fact the pseudoscalar condensate in parallel homogeneous fields was calculated by Schwinger when studying the neutral meson and proton using proper time methods, Ref. [15], and was found to be

$$\bar{P} := \langle \bar{\psi} i\gamma_5 \psi \rangle = -\frac{e^2 EB}{4\pi^2 m} \,. \tag{2.28}$$

Using the above we find the enigma

$$n_5 \neq \langle j_5^0 \rangle \,. \tag{2.29}$$

The chirality found using standard proper time methods, Eq. (2.28), does not agree with the heuristic picture provided in Eq. (2.24). In fact,

$$\partial_0 \bar{n}_5 = 0 \,, \tag{2.30}$$

for any m even the case of $m \to 0$. The massless limit is frequently evoked in literature to drop $m\langle \bar{\psi} i\gamma_5 \psi \rangle$. However, it is prudent to find the mass dependence in the pseudoscalar first before such limits can be taken. Indeed, an Abelian massless theory may differ quite markedly from one in which the $m \to 0$ limit is taken, notably the former possesses a completely shielded electric charge [86]. The resolution to the enigma we find is provided through identification of vacuum states. Indeed depending on which vacuum states are utilized different vacuum expectation values (VEV) can be found.

However, before addressing VEVs under differing vacuum expectation values let us go over some basics of the concept of dynamical symmetry breaking due to a magnetic field in QCD, of which the effects including an electric field and the Schwinger mechanism we go onto elucidate.

2.3.3 Magnetic Catalysis

Symmetries, and their breaking, make up a generous part of our understanding in QFTs. A notable example–as outlined above–lies with the chiral symmetry. The chiral symmetry offers a Lorentz invariant topology [29], Eq. (2.3), leading to the axial anomaly. Then we found for certain parity-violating non-trivial topologies one can find the CME, Eq. (2.4). In turn, breaking of the chiral symmetry is highly important as the mechanism leads to the forming of the bulk of the visible mass in the universe [2, 3]. Not only directly from a dynamical symmetry breaking, forming a condensate in QCD, but also through the addition of a magnetic field can the dynamical mass, or chiral condensate, be affected. This process is commonly known as magnetic catalysis [21–23].

The magnetic catalysis can be essentially understood as a catalyzing effect on a fermion anti-fermion condensate in the presence of a magnetic field [23]. The effect is tantamount to an enhancement of a dynamically generated mass. When a condensate forms, a symmetry (in this case the chiral symmetry) is broken which leads to a dynamically generated mass. Before explaining magnetic catalysis from a dimensionally reduced field theoretic standpoint let us motivate the process through a condensed matter analogy in superconductivity [87].

Indeed, the analogy of superconductivity to QCD was exploited in the explanation of dynamical symmetry breaking [2, 3]. In superconductivity, a condensate is also formed, known as a Cooper pair between two fermions–in contrast to a fermion and anti-fermion for the chiral condensate–due to an electron-phonon interaction. Analogous to QCD a mass forms, or rather an energy gap in BCS theory. However, let us not press the analogy further as there are notable differences. While in QCD the chiral condensate is strengthened due to a magnetic field, the Cooper pair is weakened. This is due to the magnetic moment anti-alignment of the Cooper pair; while one electron's spin is aligned with the magnetic field the other is stuck in a frustrated state–leading to weakening of the condensate as well as the Meissner effect. In contrast, the chiral condensate is charge neutral, both constituents of the condensate are aligned with the magnetic field, and no Meissner effect is present. Let us more formally describe the enhancement of the condensate and dynamical mass in magnetic catalysis.

Here we examine magnetic catalysis in 3 (space) + 1 (time) dimensions–here there is no proper time dimension in contrast to the rest of the thesis; however, with the strong magnetic field the physics is similar to a dimensionally reduced 1+1 system. The dynamical mass, M, can be defined directly from the formed chiral condensate in a magnetic field, B, with bare mass, m (which is later taken to zero):

$$M(m, B) = -G \langle \bar{\psi}\psi \rangle \ . \tag{2.31}$$

G is a coupling constant defined in the Nambu-Jona-Lasinio (NJL) model [88], whose value describes a weak interaction with 2nd order terms bilinear in the Dirac fields. In the NJL model in 3+1 dimensions this would amount to the addition of the terms, $G/2[(\bar{\psi}\psi)^2 + (\bar{\psi} i\gamma_5 \psi)^2]$, into the Dirac Lagrangian, depicted in the partition function Eq. (2.15). Note, the coupling G is distinct from the electromagnetic coupling e. Then the dynamical mass, Eq. (2.31) is determined from integrating out the higher-order terms and constructing a gap equation; see Refs. [21–23] for more details. The chiral condensate is easily solvable, which we do in Sec. 8 with the addition of an electric field, with Schwinger proper time techniques. There is a non-trivial non-vanishing solution to the above for a vanishing pole mass, $m \to 0$ [21–23]:

$$M \propto \exp\left(-\frac{2\pi^2}{GeB}\right); \tag{2.32}$$

the dynamical mass here is similar to an effective mass found in BCS theory. What is more, we see here too the influence of the magnetic field is non-perturbative in nature; c.f. the characteristic Schwinger mechanism exponential suppression is $\exp(-\frac{m^2\pi}{eE})$.

Dimensional reduction from 3+1 to 1+1 is a characteristic feature of magnetic catalysis and can be used to explain pertinent physics. In a background magnetic

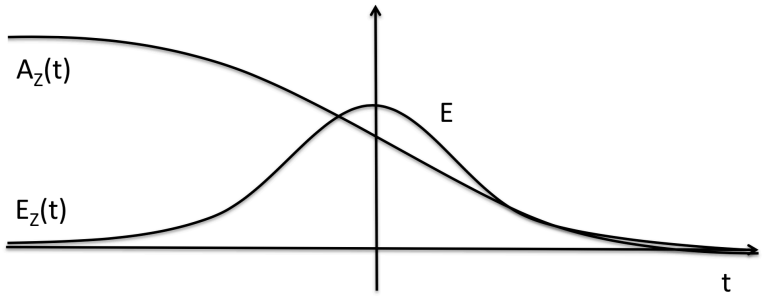

Figure 2.3: Example of inequivalent vacuum state background field: Sauter potential. $E_z(t) = E\cosh^{-2}(t)$ and $A_z(t) = -E\tanh(t) + E$. The field $E(t)$ does indeed vanish at $t \to \pm\infty$. However the gauge, $A_z(t)$ does not. Note we use homogeneous fields and not the above Sauter potential in the evaluation of expectation values under Schwinger pair production. However, the extension to inhomogeneous fields is motivated in Sec. 3.3 later.

field the eigenvalues of the Dirac equation in 3+1 dimensions follow as [23]:

$$E_n = \pm\sqrt{m^2 + 2eBn + p_\parallel^2}\,. \tag{2.33}$$

$n = 0, 1, 2...$ and counts the Landau levels. $p_\parallel$ is momentum parallel to the magnetic field. Then for a sufficiently strong magnetic field only the lowest Landau level, $n = 0$, will be occupied; however, the resulting lowest Landau level expression is identical to the 1+1 spectrum. We can understand this process simply from a classically motivated picture. A strong magnetic field will polarize an electron's spin and will also restrict motion to a cyclotron orbit, only allowing motion in a parallel to the magnetic field direction, effectively reducing the dimensionality. Then, using the classical analogy, one can visualize an energetically favorable configuration of spin alignment of a particle anti-particle pair in the presence of a strong magnetic field, in effect enhancing the condensate.

While our understanding of magnetic catalysis and dynamical symmetry breaking under a strong magnetic field is complete, a fascinating extension lies with the addition of an electric field. As we saw before with an electric field, the vacuum is unstable against the production of pairs. And this process mars our concept of equivalent vacuum states, which one may typically take for granted. Then for the processes leading up to a dynamical mass, Eq. (2.31), under the influence of an electric field how should one even define a meaningful dynamical mass? We address this question in Ch. 8. Let us first address a simpler question: How should one define expectation values under a vacuum instability, such as from Schwinger pair production?

2.4 Observables under a Vacuum Instability

The key observation here is that even if the background field vanishes in the asymptotic $t \to \pm\infty$ limits for configurations which yield Schwinger pair production the gauge does not. A simple example of this is provided by a Sauter electric field potential [43]; see Fig. 2.3. Therefore as our many-body vacuum states are determined

in their asymptotic limits in time as well, the vacuum states are indeed affected by the background field. We must have $|\text{in}\rangle \neq |\text{out}\rangle$, as was described as a definition of Schwinger pair production, Eq. (2.14). Then, a naïve usage of the differing in and out vacuum states for the determination of mean expected value would then entail a different (but physical) observable. Let us emphasize that many standard QFT calculations techniques make use of in-out vacuum states. And in the presence of an electric field then, the physical interpretation of those results is changed. This is true using even worldline or Schwinger proper time methods as well. We find the naïve approach of vacuum states has been employed in Eq. (2.28) when trying to confirm the intuitive process for chirality generation, Eq. (2.24), with concrete calculations. There is nothing physically wrong with the expectation values calculated in Eq. (2.28) using in-out vacuum states; a simple but profound interpretation is merited we will show. How might one perform a calculation in agreement with our physical intuition predicting a mean expected value[12]?

We find mean expectation values can be had with the usage of similar vacuum states. While vacuum states at any time are permissible, it is simplest to employ asymptotic states for their transparent particle pictures; hence in-in vacuum states can be used. Such observables found using in-in vacuum states are consistent with the postulates of quantum mechanical expectation values. And in-in expectation values would coincide with intuition: If one were to turn on an electric field in volume, V, for time, T, and make measurements of an operator $\mathcal{O}$, then the average of all measurement would indeed be $\langle \text{in}|\mathcal{O}|\text{in}\rangle$. Let us go ahead and at this point introduce the following notation to contrast both in-out and in-in expectation values for some given time-dependent operator $\mathcal{O}(t)$ in the Heisenberg representation:

$$\langle \mathcal{O} \rangle := \langle \text{out}|\mathcal{O}(t)|\text{in}\rangle / c_v \,, \qquad \langle\langle \mathcal{O} \rangle\rangle := \langle \text{in}|\mathcal{O}(t)|\text{in}\rangle \tag{2.34}$$

Our in (out) states is defined at some time $t_{in}(t_{out})$, which we later take to negative infinity (positive infinity), whereby we can expand the Dirac operators in terms of creation and annihilation operators acting on either vacuum state. Given the importance of vacuum states for expectation values in unstable QFTs then it is mandatory to address the physical implications of such values.

The Schwinger mechanism, much like other vacuum instabilities, is an inherently out-of-equilibrium phenomenon. Then we find, too, that expectation values consistent with quantum mechanical definitions also describe a situation inherently out-of-equilibrium. And this concept we address with greater mathematical rigor in Ch. 4. Such in-in expectation values are consistent with a Schwinger Keldysh out-of-equilibrium formalism. However, if in-in expectation values represent their mean values in an experiment then what is one to make of in-out expectation values.

The question of an in-out expectation value we can better address with more theoretical results at our disposal. However, we can provide a cursory explanation using arguments laid out for the Schwinger mechanism in Sec. 2.2.1. There we found that the product of the partition function with its Hermitian conjugate, $|\langle \text{out}|\text{in}\rangle|^2$ in Eq. (2.14), described the probability that the vacuum would stay a vacuum and nothing (particle or otherwise) be produced in the out-state. Then from the above

[12]Here, we have temporarily made use of the vocabulary introduced in Ref. [89] for in-in observables. Note, also in Ref. [89] in-out observables are denoted as causal observables in regard to the causality of the in-out Green's function. However, we go to explain in-out (in-in) observables should be likened to a scenario of (out-of) equilibrium.

analogy, one could motivate an in-out expectation value as describing a scenario where nothing appears in the out-state. In other words, if an in-in observable, which contains all the contributions of any number of pairs being produced in the out-state, describes a state out-of-equilibrium, then an in-out observable, which describes a state where no pairs are produced, should describe a situation of equilibrium. One may also reason this by noting that the Minkowski partition function, Eq. (2.15), resembles a Euclidean partition function at zero temperature; see Sec. 4.4 for details. Having put forth the machinery to contrast the two observables we would be in a better position to illustrate the nature of in-out expectation values.

In light of the above arguments, it becomes a prudent question to ask how do the axial anomaly and related quantities behave under in-in or in-out vacuum states. As we have outlined, it is true that the axial anomaly is exact at the operator level, Eq. (2.26). However, a clear recognition of the anomaly's behavior under vacuum unstable conditions has been woefully absent. Before embarking on these calculations let us illustrate some basic elements of the in-in formalism making ties to its out-of-equilibrium description.

Chapter 3

Methods

3.1 In-In Formalism and the Schwinger Keldysh Closed Time Path

Having exposed the importance of inequivalent vacuum states in the determination of expectation values, let us further discuss the relationship between the vacuum states and their in or out-of-equilibrium origins. To achieve this let us illustrate the simplest example of a defining in-in expectation value, whose formulation naturally can be connected to an out-of-equilibrium Schwinger Keldysh closed time path. This object we can show is an ordinary expectation value in quantum mechanics. The essential feature of a closed time path formalism is the involvement of two histories or two time paths in the determination of the expectation value of operators [90]. Let us take for example for a general operator, $\mathcal{O}$, the following expectation value:

$$\langle\psi(t_i)|\,\mathcal{O}\,|\psi(t_i)\rangle = \int dx\,\mathcal{O}|\,\langle x|\psi(t_i)\rangle\,|^2\,, \tag{3.1}$$

valid at some (initial) time, here labeled t_i, and in the Schrödinger representation. Then we express the wavefunction as a path integral shifted to some later time, t_f,

$$\langle y|\psi(t_f)\rangle = \int dx \int_{x'(t_i)=x}^{x'(t_f)=y} \mathcal{D}x'\mathcal{D}p\,\langle x'|\psi(t_i)\rangle\, e^{i\int_{t_i}^{t_f}[p\cdot x' - H]}\,, \tag{3.2}$$

for the Hamilitonian, H, of the Schrödinger equation. Using the path integral form of the wavefunction in the expectation value, Eq. (3.1), we can find that two paths are integrated over, from t_i to t_f then back to t_i:

$$\begin{aligned}\langle\psi(t_f)|\,\mathcal{O}\,|\psi(t_f)\rangle = \int dx_+dx_-\,\mathcal{O}\int \mathcal{D}x_+\mathcal{D}x_-\mathcal{D}p_+\mathcal{D}p_-\,\langle x_+|\psi(t_i)\rangle\,\langle\psi(t_i)|x_-\rangle \\ \times\exp\Big\{i\int_{t_i}^{t_f}[p_+\cdot x_+ - H_+] + i\int_{t_f}^{t_i}[p_-\cdot x_- - H_-]\Big\}\,.\end{aligned} \tag{3.3}$$

Here the closure of the time paths is referred to as the "closed time path" formulation and is often attributed to Schwinger [91] and Keldysh [92]. The above formulation is also referred to as a real-time formalism, so as to contrast it with the imaginary time

formalism where time is Wick rotated to imaginary values descriptive of equilibrated setups.[1]

The extension to a QFT is simple. First let us generalize the above to include quantum statistical information. Consider a density matrix of a given quantum theory that contains all the quantum and statistical information of the theory [93, 94], c.f., Eq. (3.1),

$$\langle \mathcal{O}(t) \rangle = \frac{\mathrm{Tr}[\rho(t)\mathcal{O}]}{\mathrm{Tr}[\rho(t)]} \,. \tag{3.4}$$

For a quantum mechanical setup, $\rho(t) = \sum_n p_n \, |\psi_n(t)\rangle \, \langle \psi_n(t)|$, with p_n being the probability of finding the system in n quantum state. Also, we assume $\mathrm{Tr}[\rho] = 1$ and the probabilities, p_n, must add up to unity. Then, one may expect the states to evolve in time according to the unitary evolution operator,

$$U(t_f, t_i) = T \exp\left[-\frac{i}{\hbar} \int_{t_i}^{t_f} dt' H \right] , \tag{3.5}$$

T indicates a time ordering in the matrix exponential. The density matrix, Eq. (3.4), then evolves in time accordingly,

$$\rho(t_f) = U(t_f, t_i) \, \rho(t_i) \, U(t_i, t_f) \,. \tag{3.6}$$

Applying the above to expectation values we can see

$$\begin{aligned} \langle \mathcal{O}(t) \rangle &= \mathrm{Tr}[\rho(t_f)\mathcal{O}] \\ &= \mathrm{Tr}[\rho(t_i) \, U(t_i, t) \, \mathcal{O} \, U(t, t_i)] \\ &= \mathrm{Tr}[\rho(t_i) \, U(t_i, t) \, \mathcal{O} \, U(t, t_f) U(t_f, t_i)] \,, \end{aligned} \tag{3.7}$$

where we have made use of the cyclicity of the trace and product identities of the unitary evolution operator. The time evolution of the density matrix also satisfies a quantum Louiville equation. Note here as well, even without a path integral formulation, the two time paths in the evolution operators, Eq. (3.6), depicting a closed time path are manifest. Furthermore, upon looking at the expectation value, Eq. (3.7), we can see that the operator at an intermediate time, $t_i < t < t_f$, can be viewed as being inserted along either path on the closed loop.

Let us extend the above to a quantum many-body system. To do so of course one may formulate the above in the Heisenberg notation. Also, let us take the initial and final time to their respective asymptotic limits i.e., $[t_i \, , t_f] \to [-\infty \, , \infty]$. Taking the limits is important so that a well-defined Fock state may be established. As before we assume "in" and "out" ground states are found at $t_i \to -\infty$ and $t_f \to \infty$ respectively. With these steps one may write the above expectation value as

$$\langle \mathcal{O}(t) \rangle = \langle in| \, \mathcal{O}(t) \, |in\rangle \ . \tag{3.8}$$

[1] One may in fact combine imaginary time with a Schwinger Keldysh contour so as to contrast real-time effects against a system at finite temperature. The extended contour penetrates into the imaginary time plane. We will see an example of this in the worldline formalism with the critical electric field strength playing the role of the proper time-like temperature; see Eq. (4.45).

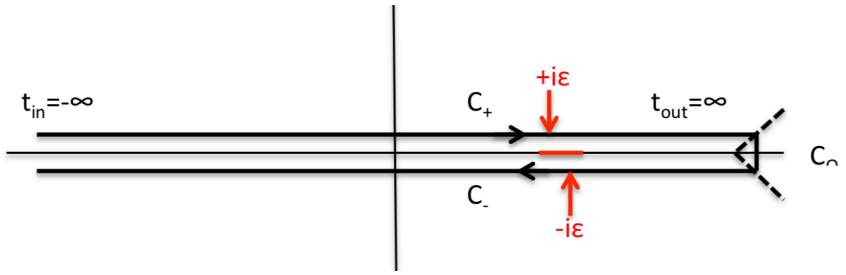

Figure 3.1: Schwinger Keldysh contour $\mathcal{C}$ over x^0 including sections going from in to out, $\mathcal{C}_+$, out to in, $\mathcal{C}_-$, and the connecting piece spanning imaginary time, $\mathcal{C}_\cap$. Note that $\mathcal{C}_+$ corresponds to the time ordered (conventional) path appearing in the QFT partition function–a bilinear in fermion fields placed on the path too would correspond to an in-out value in the absence of a vacuum instability. $\mathcal{C}_-$ corresponds to the anti-time ordered path. Last, $\mathcal{C}_\cap$, (representing the boundary condition at $x^0 = \infty$), is non-trivial in the presence of a vacuum instability.

Here we have made explicit the use of the ground state at $t_{in} = -\infty$ as $\langle\Omega| = \langle in|$. We have found an in-in expectation value. Thus, one may directly relate the above Schwinger Keldysh formalism with that of an in-in prescription.

For the purposes of calculating various observables it is convenient to introduce sources to a general partition function with which to find correlation functions. Also, for later convenience at this point we go ahead and narrow our focus to fermions in a QED background. The generating functional for a Schwinger-Keldysh contour or for an in-in prescription is

$$\mathcal{Z}[\eta,\bar{\eta}] = \int \mathcal{D}\bar{\psi}\mathcal{D}\psi \exp\left[i\int_{\mathcal{C}} dx^0 \int d^3x[\bar{\psi}(i\not{D} - m)\psi + \bar{\eta}\psi + \bar{\psi}\eta\right]. \tag{3.9}$$

Using the above we may also construct a correlation function with time ordering on the entire contour:

$$\begin{aligned} S_{\mathcal{SK}}(x,y) &= i\langle in|\, T_{\mathcal{C}}\psi(x)\bar{\psi}(y)\,|in\rangle \\ &= \theta_{\mathcal{C}}(x^0-y^0)i\langle in|\,\psi(x)\bar{\psi}(y)\,|in\rangle - \theta_{\mathcal{C}}(y^0-x^0)i\langle in|\,\bar{\psi}(y)\psi(x)\,|in\rangle \\ &= i\left[(-i\frac{\delta}{\delta\bar{\eta}(x)})(i\frac{\delta}{\delta\eta(y)})\mathcal{Z}[\eta,\bar{\eta}]\right]_{\eta=\bar{\eta}=0} \Big/ \mathcal{Z}[\eta,\bar{\eta}]|_{\eta=\bar{\eta}=0}\,, \end{aligned} \tag{3.10}$$

The Green's function here can be understood as possessing a matrix structure with elements depicting which part of the contour is being examined. Also the vacuum states are normalized such that $\mathcal{Z}[\eta,\bar{\eta}]|_{\eta=\bar{\eta}=0} = 1$. Let us label parts of the contour[2] as

$$\int_{\mathcal{C}} dx^0 = \int_{-\infty+i\epsilon}^{\infty+i\epsilon} dx^0_+ + \int_{\infty+i\epsilon}^{\infty-i\epsilon} dx^0_\cap - \int_{-\infty-i\epsilon}^{\infty-i\epsilon} dx^0_-\,, \tag{3.11}$$

depicted in Fig. 3.1. The theta function along the real time contour reads

[2]Let us point out here again that one could extend the Schwinger-Keldysh contour so as to include an imaginary portion corresponding to an equilibrium temperature given in the initial density matrix. Thus there is no KMS condition given for the Green's function, Eq. (3.10). (Addition of which, i.e. a finite temperature worldline path integral, would entail a sum over the coordinate path integrals for each periodicity.)

$$\theta_{\mathcal{C}}(x^0 - y^0) = \begin{cases} \theta(x^0_+ - y^0_+) & \text{for} \quad x^0 \in x^0_+, y^0 \in y^0_+ \\ \theta(y^0_- - x^0_-) & \text{for} \quad x^0 \in x^0_-, y^0 \in y^0_- \\ 0 \quad \text{for} \quad x^0 \in x^0_+, y^0 \in y^0_- \\ 1 \quad \text{for} \quad x^0 \in x^0_-, y^0 \in y^0_+ \,. \end{cases} \tag{3.12}$$

The Schwinger-Keldysh propagator satisfies the following differential equation, (for $\not{D}$ acting on x represented by $\not{D}_x$),

$$(i\not{D}_x - m)S_{\mathcal{SK}}(x, y) = -\delta_{\mathcal{C}}(x - y)\,. \tag{3.13}$$

Let us pause here to emphasize that while the above generating functional is in fact reminiscent of the product of two separate generating functionals, c.f., Eq. (2.15), the Schwinger Keldysh formalism is valid for non-trivial vacuum instabilities as well as presented in the previous sections. To illustrate this let us demonstrate the connection to the above from an in-in treatment [95]. We begin with an empty vacuum state and insert in a complete set of out states such that

$$\langle in|in\rangle = \sum_{\alpha} \langle in|out, \alpha\rangle \langle out, \alpha|in\rangle \;; \tag{3.14}$$

here α runs over all possible combinations of out coherent states. Then to express the above in its path integral formulation let us note that the complete set can be expressed in a functional integral form,

$$\begin{aligned} \langle in|in\rangle = \int \mathcal{D}\bar{\psi}_{\cap}\mathcal{D}\psi_{\cap}\mathcal{D}\bar{\psi}_{+}\mathcal{D}\psi_{+}\mathcal{D}\bar{\psi}_{-}\mathcal{D}\psi_{-} \\ \times \exp\Big[i\int d^4x_+[\bar{\psi}_+(i\not{D} - m)\psi_+] - i\int d^4x_-[\bar{\psi}_-(i\not{D} - m)\psi_-]\Big]\,, \end{aligned} \tag{3.15}$$

so long as the following boundary conditions on a common spacelike hypersurface at $t_{out} \to \infty$ be met

$$\psi_+(t_{out}) = \psi_-(t_{out}) = \psi_{\cap}\,. \tag{3.16}$$

Notice in the above that so long as inserted operators at t are placed such that $t < t_{out}$ for either contour, then we see there is no explicit dependence on the out state. Therefore we may absorb the functional integral of $\psi_{\cap}$ into an overall normalization constant for the path integral so long as the boundary condition, Eq. (3.16), be met. This is Eq. (3.9), (with the addition of sources). And we have

$$\langle in|in\rangle = \mathcal{Z}[\eta, \bar{\eta}]|_{\eta=\bar{\eta}=0} \tag{3.17}$$

as anticipated.

Now that we have observed that a Schwinger Keldysh contour is good for calculating a vacuum instability let us round out our previous discussion and address the various individual Green's functions the Schwinger Keldysh propagator contains. The propagator, Eq. (3.10), in matrix notation reads

$$(i\not{D}_x - m) \otimes \begin{pmatrix} S^c_{in}(x, y) & -S^<_{in}(x, y) \\ S^>_{in}(x, y) & S^{\bar{c}}_{in}(x, y) \end{pmatrix} = \begin{pmatrix} -\delta(x - y) & 0 \\ 0 & \delta(x - y) \end{pmatrix}. \tag{3.18}$$

Let us define each propagator separately as the following

$$S^{c}_{in}(x,y) = i\,\langle in|\,\theta(x_0-y_0)\psi(x)\bar{\psi}(y) - \theta(y_0-x_0)\bar{\psi}(y)\psi(x)\,|in\rangle\ , \tag{3.19}$$

$$S^{\bar{c}}_{in}(x,y) = i\,\langle in|\,\theta(y_0-x_0)\psi(x)\bar{\psi}(y) - \theta(x_0-y_0)\bar{\psi}(y)\psi(x)\,|in\rangle\ , \tag{3.20}$$

$$S^{>}_{in}(x,y) = i\,\langle in|\,\psi(x)\bar{\psi}(y)\,|in\rangle\ , \tag{3.21}$$

$$S^{<}_{in}(x,y) = i\,\langle in|\,\bar{\psi}(y)\psi(x)\,|in\rangle\ . \tag{3.22}$$

The propagator S^{c}_{in} is the usual time-ordered propagator used in most QFT applications and will serve us for bulk of our discussion hereafter.

While the above set of propagators provide us with all the dynamical and quantum information of the system it is also convenient to introduce the statistical and spectral propagators [96] to round out our discussion here. To do so note the Schwinger Kelydsh propagator may be expressed as

$$S_{\mathcal{SK}}(x,y) = F(x,y) + \frac{i}{2}\rho(x,y)(\theta_{\mathcal{C}}(z_0) - \theta_{\mathcal{C}}(-z_0))\,, \tag{3.23}$$

$$F(x,y) = \frac{i}{2}\,\langle in|\,[\psi(x),\bar{\psi}(y)]\,|in\rangle\ , \tag{3.24}$$

$$\rho(x,y) = \langle in|\,\{\psi(x),\bar{\psi}(y)\}\,|in\rangle\ , \tag{3.25}$$

where F and ρ are the spectral and statistical propagators respectively. Then using the expression $S^{c}_{in} + S^{\bar{c}}_{in} = S^{<}_{in} - S^{>}_{in}$ we can construct

$$F(x,y) = \frac{1}{2}(S^{c}_{in} + S^{\bar{c}}_{in}), \tag{3.26}$$

$$\rho(x,y) = i(S^{<}_{in} + S^{>}_{in})\,. \tag{3.27}$$

Note that the statistical and spectral equations satisfy the following differential equations

$$(i\not{D}_x - m)\,F(x,y) = 0\,, \tag{3.28}$$

$$(i\not{D}_x - m)\,\rho(x,y) = 0\,. \tag{3.29}$$

With the addition of dynamical gauge boson in addition to the background field, the above two could be supplemented with collisional effects in a 2PI formalism. To this end one would need in addition to the generating Lagrangian given in Eq. (3.10) an additional 2 point source term in fermions and gauge bosons along with a single gauge boson generator. However, as a first approximation let us ignore dynamical gauge bosons. For the strong background fields required to surpass the Schwinger critical electric field strength, this approximation is just.

Having presented a suitable formalism for calculating in-in observables we are tasked with non-perturbative and intractable problems in chirality and the Schwinger mechanism. Let us also point out that the Schwinger mechanism was first studied under non-equilibrium settings in Ref. [97] applying Keldysh's techniques [91, 98]. Let us also mention that the Schwinger mechanism under a Schwinger Keldysh contour has also been examined in Refs. [99, 100]. However, with further modification, we can apply well established mathematical techniques, worldline techniques, to address the Schwinger mechanism and chirality generation out-of-equilibrium.

3.2 Worldline Formalism

Above, we have looked at a nonequilibrium setting for a QFT in the form of a distorted and closed time path and how this may be interpreted as an equivalent, e.g., "in-in," vacuum state formulation. However, we are tasked with performing chirality and Schwinger pair production-related calculations impregnable to usual methods. This is where the worldline formalism comes in. Early applications of the worldline formalism include topics in chirality and the Schwinger mechanism thus its usage here is intuitive. However, the combination of worldline methods with an in-in prescription will be reserved for later topics in the thesis. Here we introduce essential findings of the worldline formalism including a terse derivation of the worldline path integral and Schwinger's formula[3], Eq. (2.23), as well as worldline instantons and their relationship to pair production.

Feynman, in two groundbreaking papers, Ref. [101, 102], laid out what would become the underlying structure of QED. While largely second quantization was used, (and predominantly adopted later), in Feynman's papers, relegated to the appendix, a first quantized path integral formulation appeared. This first quantized formulation is what would become the worldline formalism. While the worldline approach had until recently received little attention, in part due to its ease in handling intractable calculations, e.g. diagrammatic multi-loop QCD, has found renewed interest. Let us present here the clearest example of the worldline method with an abbreviated proof, (later we will derive the Green's function on the worldline in its entirety), of the QED effective action in a background field.

Let us begin with the QED effective action defined after integrating out the fermions from the QED partition function, Eq. (2.15):

$$i\Gamma[A] = \mathrm{Tr}\ln(i\not{D} - m)\,. \tag{3.30}$$

Note, more generally the above effective action includes the energy associated with the background gauge field, $i\int d^4x \frac{1}{4}F_{\mu\nu}F^{\mu\nu}$. Also moreover, the effective action is defined such that infinite volume terms in the absence of fields are subtracted, i.e. $\mathrm{Tr}[\ln(i\not{D} - m) - \ln(i\not{\partial} - m)]$. The trace here indicates a summation over Dirac as well as functional degrees of freedom. Then consider the insertion of γ_5 into the functional trace. Using the anticommutative property of γ_5 with γ^μ and the cyclic property of the trace, we may also consider

$$\begin{aligned} i\Gamma[A] &= \mathrm{Tr}\ln(-i\not{D} - m) \\ &= \frac{1}{2}\mathrm{Tr}\ln[(i\not{D} - m)(-i\not{D} - m)]\,. \end{aligned} \tag{3.31}$$

Then using the Laplace transform,

$$\ln[\mathcal{O} - i\epsilon] = -\int_0^\infty \frac{ds}{s}\,\exp[-i(\mathcal{O} - i\epsilon)s]\,, \tag{3.32}$$

[3]Schwinger has many attributed formulae; here we refer to Schwinger's formula as the approximated rate of pair production in parallel fields.

where we require the use of an implicit small imaginary piece in the mass term for convergence, we find the effective action becomes

$$i\Gamma[A] = -\frac{1}{2}\,\mathrm{Tr}\int_0^\infty \frac{ds}{s}\exp[-i(\not{D}^2 + m^2)s]\,. \tag{3.33}$$

Then, let us interpret the functional trace in coordinate space such that

$$i\Gamma[A] = -\frac{1}{2}\,\mathrm{tr}\int d^4x\int_0^\infty \frac{ds}{s}\,\langle x|\exp[-i(\hat{\not{D}}^2 + m^2)s]\,|x\rangle\ . \tag{3.34}$$

Here we denote functional operators with a hat, i.e., $\hat{\mathcal{O}}$; also here the trace, tr, acts only on the Dirac indices. The above illustrates the novelty of the Schwinger proper time method, namely we have reduced a quantum field theory problem to a quantum mechanical-like 4+1 dimensional problem with time replaced with proper time.

It is physically illuminating to view the above kernel within the effective action in a path integral form. We present this transformation in detail in the next section. Briefly, however, let us make use of the relationship between the operator and path integral representations,

$$\langle x|e^{-i\hat{H}s}|y\rangle = \int_{x(0)=y}^{x(s)=x}\mathcal{D}x\,\mathcal{P}e^{i\int_0^s d\tau\mathcal{L}}\,, \tag{3.35}$$

where $\hat{H}$ here is the Hamiltonian of our 4+1 quantum mechanical-like system with accompanying Lagrangian, $\mathcal{L}$, found using a Legendre transformation. Using the above we can find the effective action becomes in its path integral form

$$i\Gamma[A] = -\frac{1}{2}\int_0^\infty ds\,e^{-im^2s}\oint\mathcal{D}x\exp\Big\{-i\int_0^s d\tau\Big[\frac{1}{4}\dot{x}_\mu\dot{x}^\mu + eA_\mu\dot{x}^\mu\Big]\Big\}\Phi(x) \tag{3.36}$$

$$\Phi(x) = \mathrm{tr}\,\mathcal{P}\exp\Big\{-i\int_0^s d\tau\frac{e}{2}\sigma_{\mu\nu}F^{\mu\nu}\Big\}\,. \tag{3.37}$$

Most significant in the above we see is the replacement of ordinary time with proper time, τ, as the time in our quantum mechanical path integral, and hence why the above is coined the worldline formalism. Owing to the functional trace we see the above effective action depicts the sum over closed worldline loops and hence $\oint\mathcal{D}x = \int dx\int\mathcal{D}x'$ for the boundary condition $x'(0) = x'(s) = x$. $\Phi(x(\tau))$ is the spin factor and contains all the information dealing with the gamma matricies. Furthermore, we can see the path integral for fermions above factors into a Boson portion and spin factor portion, but is connected through the s integral. Further conventions are listed below in Sec. 1.4. Upon expanding about the gauge field, here only considered as a background field, we find the effective action describes perturbatively a 1-loop calculation as in Fig. 3.2. While such a perturbative expansion is physically illuminating, for the purposes of studying the Schwinger mechanism a non-perturbative treatment is needed. To that end let us digress into a nonperturbative treatment of the effective action which highlights the tunneling nature of the Schwinger mechanism; that is using worldline instantons.

Worldline instantons are found from a steepest descent approximation to the effective action in Euclidean spacetime. After making a Wick rotation to a Euclidean metric, and making a change of variables in the proper time, $\tau\to\tau s$, we expand about $x\to x+\eta$ for fluctuations, η, about the classical value. We find worldline

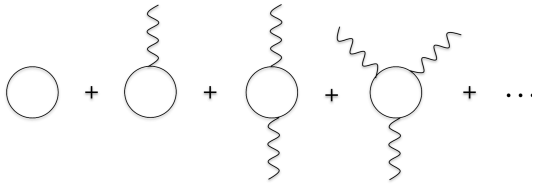

Figure 3.2: Effective action, $\Gamma[A]$, expanded about the gauge, A. For sole background fields, the effective action is 1-loop exact with any number of background photons. Note, the diagram with no lines represents an infinite volume term, and is assumed to be removed through regularization; however, imaginary pieces in Γ, such as due to the Schwinger mechanism, are insensitive to regularization and thus regularization will be a non-issue in this work.

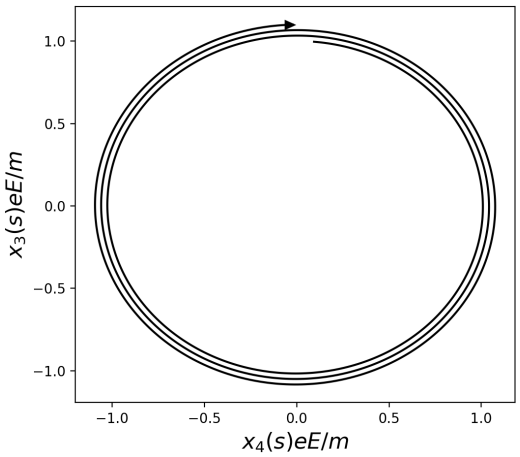

Figure 3.3: Worldline instanton sample trajectory in homogeneous fields. n, the worldline instanton winding number is related to the number of pairs of produced particles. Periodic, (and circular for homogeneous electric fields), paths are a product of periodic boundary conditions. x_4 is a Euclidean time, and hence worldline instantons describe a tunneling phenomenon.

instantons must satisfy the following Lorentz force equation[4] in Euclidean spacetime for periodic boundary conditions [103, 104]:

$$\ddot{x}_\mu = -\frac{ie|\dot{x}|}{m} F_{\mu\nu}\dot{x}^\nu \,. \tag{3.38}$$

Such solutions are worldline instantons. Multiple solutions exist for $|\dot{x}| = \sqrt{\dot{x}_\mu \dot{x}^\mu}$. For the case of homogeneous fields worldline instantons trace out circles periodic in the direction of the electric field and Euclidean time, x_4; see Fig. 3.3. Worldline instantons offer an intuitive interpretation of Schwinger pair production: at some point in spacetime a particle is created for forward times and an antiparticle is created for backward times forming a loop in spacetime. We may interpret this as a pair of particles being spontaneously created from the vacuum. And the number of

[4]Note here that the spin factor, Eq. (3.37), has been excluded from the equations of motion under the assumption that it weakly contributes. It does not contribute for the case of homogeneous fields, and the treatment is exact.

loops of the instanton approximately corresponds to the number of particles being produced. Inserting the worldline instantons into the effective action one can readily find the imaginary part of the effective action, i.e., the real part of the Euclidean effective action, at the classical level as

$$-\operatorname{Re}[\Gamma_{\text{Euclidean}}] = \operatorname{Im}[\Gamma_{\text{Minkowski}}] \propto \exp\Big(-\frac{m^2\pi}{eE}\Big)\,, \tag{3.39}$$

which is Schwinger's formula for pair production, Eq. (2.14). In fact, if we evaluate the imaginary part of the effective action by steepest descents using worldline instantons we can arrive at the exact imaginary part of the effective action. See Ref. [105] for explicit calculations; note for homogeneous fields fluctuations in the fields are at most quadratic order and therefore steepest descents is exact.

Armed with the worldline instanton technique we can better explain qualitatively the dynamically assisted Schwinger mechanism with configuration given in Eq. (2.20). For homogeneous fields, the periodic paths traced by the worldline instanton in $x_4(0) = x_4(s)$ follow along with an effective potential set by the gauge. However with the addition of a weak pulsed field, poles, due to the tangent functions in Eq. (2.20), constrict the motion of the instanton creating a tightened instanton path in effect reducing the tunneling length required for Schwinger pair production.

The worldline formalism is not only useful for QED but also non-Abelian gauge fields as well. The extension is intuitive. The worldline representation of a non-Abelian gauged scalar one-loop effective action is given as a simple replacement of the Wilson loop, with $A_\mu(x) = A^a_\mu(x)T^a$ and T^a being the generators of the gauge group:

$$\exp\Big\{-ie\int_0^s d\tau A_\mu \dot{x}^\mu\Big\} \to \operatorname{tr}\mathcal{P}\exp\Big\{-ig\int_0^s d\tau g A_\mu \dot{x}^\mu\Big\}\,. \tag{3.40}$$

We have simply acquired a trace over the gauge group and a path ordering. Note that the extension to non-Abelian fields is somewhat more involved for fermions, however, essentially the only difference lies in the replacement of the field strength in the spin factor, Eq. (3.37), with its equivalent, that is $F_{\mu\nu} \to G_{\mu\nu} = \partial_\mu A_\nu - \partial_\nu A_\mu + ig[A_\mu, A_\nu]$. Also, the path ordering encompasses the spin factor as well. To a large extent the discussions in this thesis will be limited to homogeneous fields. For homogeneous fields in color space an Abelian rotation can always be performed allowing the fields, F, and gauge, A, to be diagonal and hence omit the path ordering. Thus QED is a good approximation of the behavior of non-Abelian QFT's in homogeneous Abelianized fields. Let us note in passing that non-Abelian homogeneous fields may also be found from a non-spacetime dependent gauge. For example for $SU(2)$ let $A_1 \propto \sigma_1$ and $A_2 \propto \sigma_2$, then one can see $F \propto \sigma_3$. However, this configuration does not produce pair production as there is no time dependence in the background field and therefore we confine our attention to the Abelian-like case of $A \propto x^a T^a_{diagonal}$.

We have explored the utility of worldline methods for treating the Schwinger mechanism, particularly looking at the worldline instanton method. The instantons are capable of treating inhomogeneous background fields otherwise intractable through other means. Let us explore this formalism along with a parallel inhomogeneous magnetic field in an interesting application to the generation of chirality.

3.3 Schwinger Mechanism Enhancement in Inhomogeneous Parallel Fields

In the previous chapters we have outlined the necessary physics and techniques to understand chirality generation via the Schwinger mechanism. Before analyzing concrete applications of an out-of-equilibrium in-in formalism and a traditional QFT in-out formalism, let us apply the heuristic picture of chirality production introduced in Sec. 2.3.2 to inhomogeneous fields. We will indeed find that the heuristic picture is a correct one describing an out-of-equilibrium spontaneous production of chirality. The usage of inhomogeneous fields, as alluded to earlier, lessens the Schwinger mechanism threshold for pair production for certain field shapes, and from the heuristic picture one may also infer an enhancement of the production of chirality. We found chirality production can be had from the imaginary part of the effective action predicting Schwinger pair production, Eq. (2.14). Using the vacuum non-persistence at lowest order (again Eq. (2.14)) one may count the net chirality change induced from a single particle anti-particle pair produced. Therefore for inhomogeneous fields we focus our efforts, rather, on finding the lowest order contributions to the imaginary part of the effective action. Then, based on non-persistence we motivate likely observable setups in heavy-ion colliders and Dirac semimetals; this is done in Sec. 3.3.4 below. Let us first here look at the effective action in inhomogeneous fields, specifically we discuss spatially inhomogeneous magnetic fields and temporally inhomogeneous electric fields.

Let us mention that the contents of this chapter are not central to our main arguments and results of chirality production through a vacuum state identification, and thus for a first reading of this thesis may be passed over. The discussion of vacuum unstable states and observables continues in Sec. 4.

3.3.1 Electric and Magnetic Field Kernels

We are primarily concerned with background fields in QED (and non-Abelian extensions) that are parity violating, i.e. ones with $\epsilon_{\mu\nu\sigma\lambda}F^{\mu\nu}F^{\sigma\lambda} \neq 0$. And these field types, specifically the parallel electric and magnetic field variety, admit a major simplification: the worldline kernel, Eq. (3.35) is factorizable into separate electric and magnetic field parts. More specifically we restrict field types such that the electric and magnetic fields are parallel in the x_3 direction,

$$\mathbf{E}(x) = E(A_4(x_3), A_3(x_4))\hat{x}_3\,, \quad \mathbf{B}(x) = B(A_1(x_2), A_2(x_1))\hat{x}_3\,. \tag{3.41}$$

First, it proves convenient to introduce a Euclidean metric here as we employ the worldline instanton method, Eq. (3.38), which would require complex solutions in a Minkowski metric, unnecessarily complicating matters. See Sec. (1.4) for notations. The Euclidean worldline effective action is given in Eq. (3.36). Let us also note that upon performing a Wick rotation the imaginary part of the effective action in Minkowski spacetime is given in Euclidean spacetime as

$$\omega = 2\mathrm{Im}(\Gamma_{\mathrm{Minkowski}}|_{n=1}) = -2\mathrm{Re}(\Gamma_{\mathrm{Euclidean}}|_{n=1})\,, \tag{3.42}$$

and here we make explicit the approximation of a single pair of particles produced from the vacuum with $n = 1$; see also Eq. (2.17). In the Euclidean convention no

$i\epsilon$ factor is present and rather the quadratic mass term ensures convergence. Also, to avoid confusion with the Minkowski expression listed later, we use T for the proper time parameter in Euclidean spacetime. The effective action in contrast to the propagators always has periodic boundary conditions over paths in coordinate space, $x_\mu(0) = x_\mu(T)$.

Under the condition of parallel field types given in Eq. (3.41) one can find that similar to the case of homogeneous fields, Eq. (4.24), the spin factor, Eq. (3.37), diagonalizes and the path ordering is subsequently removed. Moreover, we can find that the kernel can be factored into electric and magnetic parts:

$$\Gamma[A] = -2\int_0^\infty \frac{dT}{T} e^{-m^2 T}\mathcal{K}_B\mathcal{K}_E, \tag{3.43}$$

$$\begin{aligned}\mathcal{K}_B(T;A_1,A_2) \coloneqq \oint \mathcal{D}x_1\mathcal{D}x_2 \cosh\left(e\int_0^T d\tau B(x)\right)\\ \times \exp\left\{-\int_0^T d\tau\left[\frac{1}{4}\left(\left(\frac{dx_1}{d\tau}\right)^2+\left(\frac{dx_2}{d\tau}\right)^2\right)+ieA_1\frac{dx_1}{d\tau}+ieA_2\frac{dx_2}{d\tau}\right]\right\},\end{aligned} \tag{3.44}$$

$$\begin{aligned}\mathcal{K}_E(T;A_3,A_4) \coloneqq \oint \mathcal{D}x_3\mathcal{D}x_4 \cos\left(e\int_0^T d\tau E(x)\right)\\ \times \exp\left\{-\int_0^T d\tau\left[\frac{1}{4}\left(\left(\frac{dx_3}{d\tau}\right)^2+\left(\frac{dx_4}{d\tau}\right)^2\right)+ieA_3\frac{dx_3}{d\tau}+ieA_4\frac{dx_4}{d\tau}\right]\right\}.\end{aligned} \tag{3.45}$$

Let us point out that although both kernels factor they are connected through the proper time, T, integral. It is also convenient to make use of the functional representation, where here too the worldline Hamiltonian may be separated into electric and magnetic parts. The functional representation reads

$$\mathcal{K}_B = \mathrm{Tr}\exp\left\{\left[-(\partial_1+ieA_1)^2-(\partial_2+ieA_2)^2\right]T\right\}\cosh\Big(eB(x)T\Big), \tag{3.46}$$

$$\mathcal{K}_E = \mathrm{Tr}\exp\left\{\left[-(\partial_3+ieA_3)^2-(\partial_4+ieA_4)^2\right]T\right\}\cos\Big(eE(x)T\Big)\,. \tag{3.47}$$

Furthermore, the separation in the kernel is also convenient in the sense that Schwinger pair production is solely associated with the electric field, and hence the imaginary pieces found in the proper time integral can be found by restricting our attention to the electric field contour, Eq. (3.45). This important step permits steepest descents (the worldline instanton approximation Refs. [103, 104]) in the worldline integral for parts associated with the electric field. As expected since there are no imaginary pieces in the effective action associated with homogeneous magnetic fields, there too are no instantons in the path integral formalism [106].

As a first step of the calculational techniques, we first examine homogeneous fields, then having benchmarked the technique we move onto inhomogeneous fields.

For the case of homogeneous fields the magnetic kernel, Eq. (3.44), can be easily solved using either its path integral form or functional form. Specifically the gauge we use is $A_1 = -(B/2)x_2$ and $A_2 = (B/2)x_1$. The steps are similar to those performed in Sec. 4.2. If one were to apply functional methods, Eq. (3.46) may be readily solved by simply summing over the eigenvalues of the Dirac equation in a magnetic field in a reduced dimension system–essentially just the Landau levels.

Ultimately we find the exact result, using path integral techniques, of

$$\mathcal{K}_B = \frac{eB}{4\pi}\coth(eBT)\,. \tag{3.48}$$

For a homogeneous electric field, one may find an analogous, albeit complex, solution using similar techniques. However, we perform the worldline instanton approximation which requires more steps but allows calculation of more complicated field types.

We begin with the worldline instanton method by first performing the Laplace method in proper time, T. This first step is not mandatory [107], and one may first take steepest descents in coordinate space associated with the electric field, however doing so simplifies matters and makes more explicit the physical picture of the instantons. Before performing the Laplace method let us take $\tau \to Tu$ in Eq. (3.43), rescaling the kernels. We also use the notation $\dot{x}_\mu = dx_\mu/du$. We find the electric field kernel, Eq. (3.45), becomes

$$\mathcal{K}_E = \oint \mathcal{D}x_3\mathcal{D}x_4 \exp\left\{-\int_0^1 du\left(\frac{1}{4T}\dot{x}^2 + ieA_3\dot{x}_3 + ieA_4\dot{x}_4\right)\right\}\cos\left(eT\int_0^1 duE\right). \tag{3.49}$$

We may go ahead and take the Laplace method in proper time above. T then is minimized as a function of the mass, m, and the coordinates, $\dot{x}_3$ and $\dot{x}_4$: $T^* = \sqrt{\int du \frac{1}{4m^2}(\dot{x}_3^2 + \dot{x}_4^2)}$. Note here that the electric field contributions arising from the spin factor will not contribute to minimum as they are purely imaginary. Also, the magnetic field contributions to the stationary point are assumed to be small. Therefore, stationary points, T^* in proper time are the same for the fermionic as well as bosonic cases. The total effective action, Eq. (3.43), becomes–here we still have not introduced the homogeneous electric field[5]:

$$\mathrm{Re}\Gamma \simeq \frac{-2}{m}\oint \mathcal{D}x_3\mathcal{D}x_4\sqrt{\frac{\pi}{T^*}}\cos\left(eT^*\int_0^1 duE\right)e^{-S_w}\mathcal{K}_B(T^*)\,, \tag{3.50}$$

$$S_w = m\sqrt{\int_0^1 du(\dot{x}_3^2 + \dot{x}_4^2)} + \int_0^1 du(ieA_3\dot{x}_3 + ieA_4\dot{x}_4)\,. \tag{3.51}$$

S_w is a dimensionally reduced worldline action, c.f., Eq. (4.28). Performing steepest descents in x_3 and x_4 coordinate space will yield a reduced dimension Lorentz force equation in Euclidean spacetime,

$$m\frac{\ddot{x}_i}{\sqrt{\int \dot{x}_3^2 + \dot{x}_4^2}} = ie(\partial_i A_j - \partial_j A_i)\dot{x}_j \tag{3.52}$$

for $i, j = 3, 4$. c.f., Eq. (3.38) for the 4+1 dimensional case. Periodic solutions to Eq. (3.52) are worldline instantons [103, 104]. For the case of homogeneous fields the worldline instantons read

$$x_3(u) = \frac{m}{eE}\cos(2\pi n u), \quad x_4(u) = \frac{m}{eE}\sin(2\pi n u)\,, \tag{3.53}$$

[5]While homogeneous fields have been provided for homogeneous fields, Eq. (3.48), we may evaluate the kernel before taking the Laplace approximation in proper time for any give magnetic field so long as the stationary points are not appreciably changed.

whose paths trace out circles in x_3 and x_4; see Fig. 3.3 in the background. n is the worldline instanton number and coincides with the pole number in proper time of the in-out propagator. Worldline instantons in homogeneous electric fields are the simplest solution depicting the Schwinger mechanism tunneling behavior. At some given point in spacetime–owing to the isotropy of homogeneous fields any point will do–a particle anti-particle pair are produced. The particle going forward in time and the anti-particle backwards in time, which is depicted in the wordline instanton trajectory upon switching to Minkowski spacetime, and also letting $u \to iu$. This is reflected in periodic paths in a Euclidean metric. Similarly we also found for the in-in propagator a dependence on imaginary time for the pieces associated with pair production even though we were in Minkowski spacetime; thus imaginary time solutions or tunneling are essential features of the Schwinger mechanism.

Using the worldline instanton solutions, Eq. (3.53), in homogeneous fields one may evaluate the effective action, Eq. (3.50), exactly. As was illustrated before in Sec. 4.2, since the path integral is quadratic steepest descents is exact. Here calculations are also similar to those carried out in Sec. 4.2, and if we include contributions from a fluctuation prefactor, c.f., Eq. (4.28), then we can find to lowest order in Schwinger pair production, $n = 1$, Schwinger's formula for the probability for a single particle anti-particle pair to be produced or Eq. (2.23). Since it was confirmed that the separation of kernels into electric and magnetic field parts was valid for homogenous fields, let us move onto the inhomogeneous case. Here, we first explore spatially inhomogeneous magnetic fields both for the pulsed case in space and some novel setups.

3.3.2 Spatially Inhomogeneous Magnetic Field

An important background magnetic field that approximates well realistic setups is one with a spatial inhomogeneity. It has been argued in off central heavy-ion collisions at the LHC and RHIC the magnetic field may be highly spatially inhomogeneous [74]. Also, we find for specific inhomogeneous background magnetic fields the threshold for Schwinger pair production may be lessened [105], which is interesting since for perpendicular magnetic field types the threshold decreases.

Fortunately the Dirac equation is exactly solvable for a Sauter-type magnetic field peaked in space. Specifically we analyze

$$\mathbf{B}(x) = B\,\mathrm{sech}^2(\kappa x_1)\hat{x}_3\,. \tag{3.54}$$

Refs. [108, 109] have solved the above in both 3+1 and 4+1 dimensions exactly. We employ similar methods, however, making use of a worldline formalism as outlined above. An important limit is for a small inhomogeneity, $\kappa \to 0$, which becomes a constant magnetic field. It is convenient to express the magnetic kernel, Eq. (3.46), in functional form to the following:

$$\mathcal{K}_B = \sum_{\pm} \frac{1}{2}\,\mathrm{Tr}\exp(-H_B^{\pm}T)\,, \tag{3.55}$$

$$H_B^{\pm} := -\partial_1^2 - \left[\partial_2 + \frac{ieB}{\kappa}\tanh(\kappa x_1)\right]^2 \pm eB\,\mathrm{sech}^2(\kappa x_1)\,, \tag{3.56}$$

where we have introduced two effective Hamiltonians. The appeal of doing so is apparent in that we have reduced the problem to a set of one-dimensional Schrödinger-like equations. No approximation is required to split up the Hamiltonian. However, we are restricted to only parallel inhomogeneous electric and magnetic fields. Another drawback is that the background field, aside from homogeneous fields and other exclusions, can only satisfy the inhomogeneous Maxwell equations. And the solutions of which are simply hypergeometric equations. From which one may apply the method of resolvents [108, 109] to determine the eigenspectrum. The eigenvalues of the effective Hamiltonians, Eq. (3.56), are

$$\lambda_n^{\pm} = p_2^2\left[1-\frac{(eB)^2}{(\kappa^2\tilde{n}-|\kappa^2/2\pm eB|)^2}\right]\mp eB-\left((\kappa\tilde{n})^2-2\tilde{n}\left|\frac{\kappa^2}{2}\pm eB\right|+\frac{\kappa^2}{4}\right),$$
$$n\in\left[0,\left|\frac{1}{2}\pm\frac{eB}{\kappa^2}\right|-\frac{1}{2}-\sqrt{\frac{p_2eB}{\kappa^3}}\right); \tag{3.57}$$

$\tilde{n}=n+1/2$. In contrast to the constant magnetic field case, the eigenspectrum is finite and moreover has a transverse momentum dependence. One can verify that the eigenspectrum once summed over as a trace of eigenvalues in the kernel, Eq. (3.46), in the small inhomogeneity limit, $\kappa\to 0$, one can correctly reproduce the constant field case given in Eq. (3.48).

We next proceed by looking for the dominant contributions to the magnetic kernel and these are provided by the lowest eigenvalues, the ground state eigenvalue and the lowest excited states. It can be verified that as in the constant field case the lowest eigenvalue is zero–the lowest Landau level. What is fascinating and non-trivial here is the contributions to the eigenspectum given by the transverse momentum, p_2, for higher excited states. These contributions we will show in fact lower the Schwinger pair production threshold moreso than does constant fields. Again, however, the exponential suppression given by the electric field provides the dominant contribution to pair production. Let us begin elaborating on this reduction by first writing the magnetic kernel as a sum over eigenvalues, specifically we use Eq. (3.57), summing over both sets of eigenvalues:

$$\mathcal{K}_B=\int_{-\infty}^{\infty}\frac{dp_2}{2\pi}\sum_n e^{-\lambda_n T}. \tag{3.58}$$

We restrict our attention to weakly varying inhomogeneous fields such that $2eB>\kappa^2$. Then we can find for large enough transverse momentum in Eq. (3.58) the bound state will disappear. Thus we introduce a transverse momentum cutoff at $\pm p_2^{max}$. After taking the transverse momentum integral we find dominant contributions to the magnetic kernel occur at p_2^{max} and these are at the eigenvalues, Eq. (3.57), evaluated at p_2^{max}, which reduce to

$$\lambda_n^{+}=4n^2\kappa^2-\frac{4n^3\kappa^4}{eB}+\left(\frac{n^2\kappa^3}{eB}\right)^2, \tag{3.59}$$
$$\lambda_n^{-}=4(n+1)^2\kappa^2-\frac{4(n+1)^3\kappa^4}{eB}+\left(\frac{(n+1)^2\kappa^3}{eB}\right)^2. \tag{3.60}$$

The eigenspectrum is dipicted in Fig. 3.4 for the first five eigenvalues or Landau levels. And for the case of a small inhomogeneity parameter in contrast to the

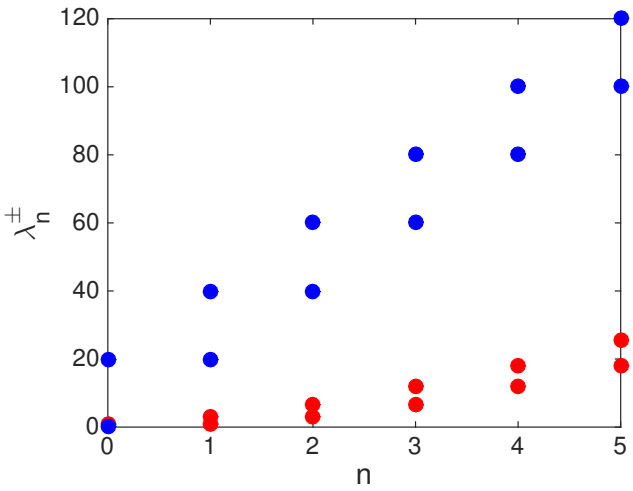

Figure 3.4: Graph of first five eigenvalues (Landau levels) for both the homogeneous case, blue dots, and the inhomogeneous case, red dots. For both cases, a strength of $B = 10m^2$ is used, and for the inhomogeneous case, $\kappa^2 = 0.2m^2$. Eigenvalues too are given in units of dimension mass squared. Lower (upper) values denote spin alignment (anti-alignment) with the magnetic field, with the inhomogeneous case lower (upper) values are given in Eq. (3.60) ((3.59)). Notice the collapse of the excited Landau level for even a small inhomogeneity.

magnetic field strength, $B \gg \kappa^2$, we find the spectrum is shifted as

$$m^2 \to m^2 + 4n^2\kappa^2 \,. \tag{3.61}$$

Therefore, we find that the excited Landau level states, that remain, are significantly lowered for even a small inhomogeneity. This effect is thought important in the observability of the Schwinger mechanism in that both the probability for Schwinger pair production is increased, and because inhomogeneous magnetic fields are more applicable to realistic settings. Let us point out that, similar to the homogeneous case, no spatially inhomogeneous magnetic field can produce Schwinger pair production in isolation–an electric field is required. Also, the only field type discussed here is a magnetic field parallel to the electric field.

Considering the above shift in mass, Eq. (3.61), it is a curious question to ask if one could engineer the magnetic field profile so as to find a negative shift. Indeed we can find such profiles. At a cursory level, let us consider the analytic continuation in inhomogeneity such that $\kappa \to i\kappa$, then the above could read $m^2 \to m^2 - 4n^2\kappa^2$. Such a magnetic field profile would resemble a Sauter-potential but inverted, specifically

$$\mathbf{B}(x_1) = B\sec^2(\kappa x_1)\hat{x}_3 \,, \tag{3.62}$$

$$A_2(x_1) = \frac{B}{\kappa}\tan(\kappa x_1) \,. \tag{3.63}$$

Let us analyze the small transverse momentum case, $p_2 \to 0$, then the magnetic Hamiltonian becomes approximately

$$H_B^{\pm} = -\partial_1^2 + \left(\frac{B}{\kappa}\right)^2\Big[\sec^2(\kappa x_1) - 1\Big] \pm B\sec^2(\kappa x_1) \,. \tag{3.64}$$

Then we look at the specific case in which $B = \kappa^2$, for a strong inhomogeneity. Then we find for the spin aligned case

$$H_B^- = -\partial_1^2 - \kappa^2 \,, \tag{3.65}$$

which clearly has a negative eigenvalues at

$$\lambda = -\kappa^2 \,. \tag{3.66}$$

Motivated by such an inverted field, let us analyze another concrete example displaying a similar structure and which also possesses a negative eigenvalue. It is one reminiscent of a Coulomb potential in one dimension. Specifically we use a Coulomb-like magnetic field well:

$$\mathbf{B}(x_1) = \frac{B}{\kappa^2 x_1^2}\hat{x}_3 \,, \tag{3.67}$$

$$A_2(x_1) = -\frac{B}{\kappa^2 x_1} \,. \tag{3.68}$$

This resembles a Coulomb potential found in hydrogen; however, κ in our context serves to ensure proper dimensions in the potential. With a decreasing κ one would see a contracted well in one dimension. And as expected for the case of a Coulomb potential in hydrogen, there are indeed bound states, negative eigenvalues, for the magnetic well case. We have for the magnetic Hamiltonian, which can be likened to a one-dimensional Schrödinger equation,

$$H_B^{\pm} = -\partial_1^2 + p_2^2 - \frac{2p_2 b}{x_1} + \frac{b^2}{x_1^2} \pm \frac{b}{x_1^2} \,. \tag{3.69}$$

Here $b := eB/\kappa^2$ is used in analogy to a Coulomb potential in hydrogen and in fact takes on quantized values for bound states. Specifically in analogy with orbital angular quantum number for our magnetic well case we find bound states for $b(b\pm 1)$ with $b \geq 2 \in \mathcal{Z}^+$. Bound eigenvalues of Eq. (3.69) for the "+" Hamiltonian can be readily found as

$$\lambda_n = -\left[\left(\frac{b}{n}\right)^2 - 1\right] p_2^2 \,. \tag{3.70}$$

We find here, as well as was found for the Sauter-like magnetic field case, a large transverse momentum negates the bound state. As before we therefore introduce a cutoff. Going through similar procedures as done for the Sauter-like magnetic field above, we find for the maximum transverse momentum $p_2^{max} \sim eB/\kappa$. And we find for the bound states at maximum transverse momenta the following eigenvalues

$$\lambda_n = -\left[\left(\frac{b}{n}\right)^2 - 1\right]\left(\frac{eB}{\kappa}\right)^2 \,. \tag{3.71}$$

Once again we see the appearance of negative eigenvalues or bound states for the magnetic portion of our kernel.

Having discovered several examples of spatially inhomogeneous magnetic fields which may reduce the threshold for pair production assuming a parallel electric field, let us turn our attention to the electric field itself. We confine our attention here,

however, to the known case of the "dynamically assisted Schwinger mechanism [49]" profiles.

3.3.3 Temporally Inhomogeneous Electric Field

Before, when dealing with the magnetic kernel we largely used the functional form as a trace over the magnetic Hamiltonian's eigenvalues. However, in fact the merit of introducing a path integral notation for the kernel, Eq. (3.45), is that one may apply the worldline instanton technique to analyze field configurations which would otherwise be unsolvable. This is readily apparent with the "dynamically assisted Schwinger mechanism [49]." The specific form of the gauge field was introduced in Sec. 2.2.4 as Eq. (2.20), and is repeated here for convenience: $A_3(x_4) = -iEx_4 - i\varepsilon\tan(wx_4)$, where we have $E, w \gg \varepsilon$. The field configuration is one of a strong but slowly varying pulse combined with a weak but fast one.

Then as anticipated earlier with the homogeneous field case, while both kernels are factorizable they are still connected through the proper time integral. Moreover, in the execution of the worldline instanton method, the magnetic field only contributes as an effective mass shift,

$$m^2 \to \widetilde{m}^2 = m^2 + \lambda_n \,, \tag{3.72}$$

where λ_n is given from the magnetic kernel listed in the previous section. The worldline instanton technique is reliant on a weak electric field or large mass approximation [104] therefore we assume that with a magnetic eigenvalue (especially one that is negative) that $m^2 + \lambda_n \gg 0$. All eigenvalues of the magnetic kernel are then summed over as in Eq. (3.58).

Let us examine the dynamical mechanism profile with the worldline instanton equation, Eq. (3.52). Let us first note that $\dot{x}_3^2 + \dot{x}_4^2 = C$ for some constant C that is quantized in periodicity of instanton solutions. Then inserting the profile, Eq. (2.20), into Eq. (3.52) we find the following differential equation:

$$\dot{x}_4^2 = C^2\left[1 - \left(\frac{e\varepsilon}{\widetilde{m}w}\right)^2\left(\frac{Ewx_4}{\varepsilon} + \tan(wx_4)\right)^2\right]. \tag{3.73}$$

We can find approximated periodic solutions to the above differential equation; these are solutions that are bound by the poles in the weak fast Sauter field, $\tan(wx_4)$. See Fig. 3.5. We can reflect the instanton path in the worldline action, Eq.(3.51), through an augmentation of the proper time parameter as

$$S_w \simeq \frac{4\widetilde{m}}{C}\int_0^{u*} du\dot{x}_4^2 \,, \tag{3.74}$$

where $u*$ is the turning point, the wall, of the instanton and it is given as

$$u* = \frac{1}{2\pi n}\arcsin\left(\frac{\pi}{2\gamma}\right) \,, \tag{3.75}$$

$$\gamma = \frac{\widetilde{m}w}{eE} \,. \tag{3.76}$$

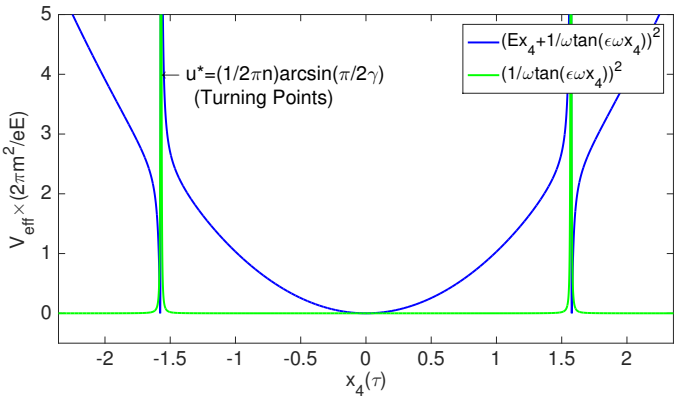

Figure 3.5: Dynamically assisting electric field mechanism. An effective potential is set up by the gauge fields. The green line represents the weak fast field contribution to the effective potential, and the blue line represents both the weak fast and strong slow fields' contributions to the effective potential. The fast weak field sets up walls at $\pm\tan(\omega x_4)$ by which the instanton solutions are bounded in between for periodic solutions. The path in between the weak fast field follows along that of a homogeneous electric field.

Here γ is an adiabaticity parameter, inspired by Keldysh [75]. The worldline action becomes

$$S(\kappa,w)\simeq\begin{cases}\frac{\widetilde{m}^2\pi}{eE} & \text{for}\quad 0<\gamma\leq\frac{\pi}{2}\\ \frac{2\widetilde{m}^2}{eE}\left[\arcsin\left(\frac{\pi}{2\gamma}\right)+\left(\frac{\pi}{2\gamma}\right)\sqrt{1-\left(\frac{\pi}{2\gamma}\right)}\right] & \text{for}\quad \gamma\geq\frac{\pi}{2}\,.\end{cases}\tag{3.77}$$

One can see that for a large adiabaticity parameter the threshold for Schwinger pair production is drastically reduced; see Ref. [49] for more details.

Then approximating the spin factor of the magnetic kernel and the fluctuation prefactor with that of a homogeneous field we find the following final form for the non-persistence of the vacuum:

$$\omega(\kappa,w)=\frac{e^2EB}{(2\pi)^2}\sum_{\lambda_n}\exp(-S(\kappa,w))\,.\tag{3.78}$$

c.f. Eq. (2.23); there we use w to represent the non-persistence in homogeneous fields. In this way, we have shown that we can implement chirality generation under more complex fields to further improve the Schwinger mechanism as well as chirality generation.

3.3.4 Enhancement Comparison

Enhancements to Schwinger pair production for the case of a spatially inhomogeneous Sauter-like magnetic pulse are small. This enhancement is, as was shown in Eq. (3.61), the result of augmentation to the higher excited Landau levels. However, motivated by the profile of an inverted field, we found cases that possessed a bound state, Eqs. (3.66) and (3.71). The enhancement provided by such cases is significantly greater and we illustrate here the enhancement due to both the dynamically

assisted Schwinger mechanism characterized by w and the spatial inhomogeneity, κ. For the case of a bound state, we illustrate the mass shift found in Eq. (3.66). Let us examine two background field strength cases thought relevant for high energy collisions and high powered lasers and semimetals. The former is predicted to easily furnish Schwinger pair production and has strengths $E = B = m^2$, whereas for the latter only weak fields are obtainable and we use $E = B = 10^{-2}m^2$. We plot both cases as a function of κ and w in Fig. 3.6 for strong fields and Fig. 3.7 for weak fields. ω is the probability of pair production per unit time and volume. It can be

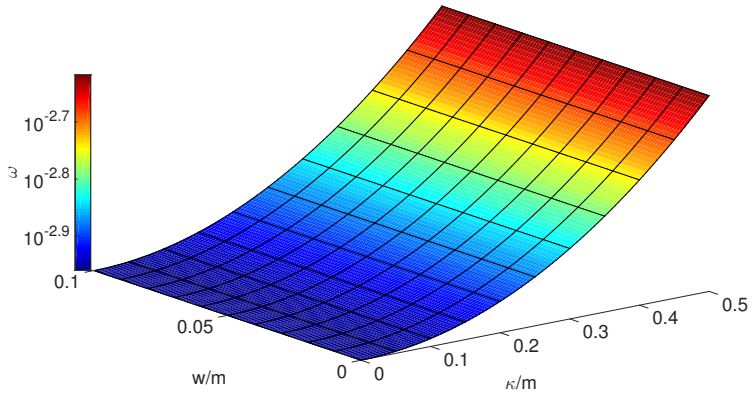

Figure 3.6: Comparative plot of Schwinger mechanism enhancement from both a spatially inhomogeneous magnetic field, characterized with inhomogeneity κ, and a temporally inhomogeneous electric field, w. Here the case of strong fields, $B = E = m^2$, is given, which are thought relevant in nucleus-nucleus collisions. The enhancement attributed to κ does not saturate for strong fields, and thus it is a robust feature in heavy ion collisions.

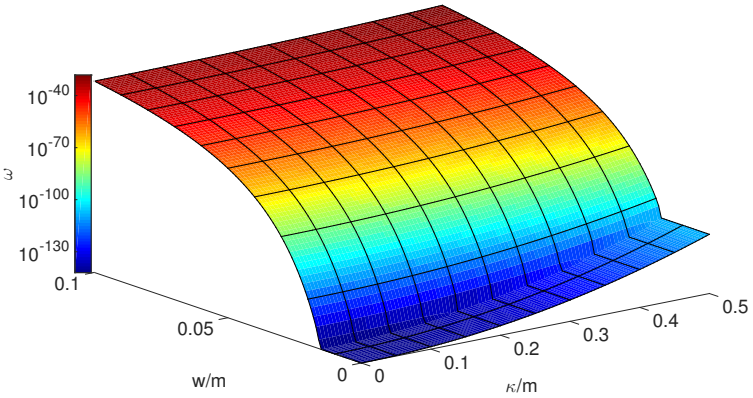

Figure 3.7: Here the case of weak fields, $B = E = 10^{-2}m^2$, is given, which are thought relevant in high powered lasers as well as semimetal applications. For large w, it can be seen the enhancement from the dynamical electric field is dominant, and it is therefore of greater applicability in high powered lasers.

seen that the enhancement coming from κ does not saturate at high field strengths as does w. Thus we consider the spatial enhancement from magnetic fields to be a

robust feature for strong fields. For weak fields however it can be seen the dynamical mechanism is dominant for large w. We have established several inhomogeneous profiles that may improve the probability to observe Schwinger pair production. Let us now, using the heuristic picture highlighted earlier, explore some environments that may be applicable; these are in heavy-ion collisions and Dirac semimetals.

In the heuristic picture we discovered that the generated chirality was twice the non-persistence probability, Eq. (2.24). Then for a large chirality changing scattering time [5], t, we can find for the chiral charge density

$$n_5 \simeq 2t\omega(\kappa, w)\,. \tag{3.79}$$

It helps to relate the above in terms of the chiral chemical potential, μ_5, which is affected by thermodynamic variables [4], so as to see the chiral magnetic effect. It has been found [5] for chemical potential, μ, and temperature, T, the following relationship exists for the chiral chemical potential

$$n_5 \simeq \frac{\mu_5}{3}\left(T^2 + \frac{\mu^2}{\pi^2}\right). \tag{3.80}$$

This hold under the conditions $|eB| < \mu_5^2$, $\mu_5 \ll \mu, T$, and for large particle momentum to the particle mass. Inverting the above for μ_5 one can find the chiral chemical potential. While the above is a valid description in either heavy-ion collisions or semimetals we find how the chirality is generated differs.

For the heavy-ion collision case, the non-persistence probability is generated entirely through the chromo-electromagnetic fields. Whereas the magnetic field in the equation for the chiral magnetic effect, Eq. (2.4), is the out-of-plane electromagnetic field generated in off-central collisions. Schematically the process can be seen in Fig. 3.8. Thus we can find for the case of a heavy-ion collider the following formula

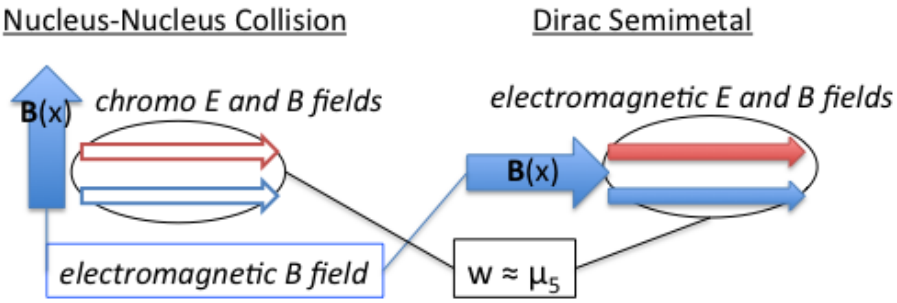

Figure 3.8: How chirality, n_5 and hence the chiral chemical potential μ_5 in Eq. (3.80), is generated in heavy ion colliders and in Dirac semimetals differs. For the former case the chirality is generated solely through chromoelectromagnetic fields and the magnetic field of the CME is perpendicular to the plane of interaction; there are two fields. For the case of the Dirac semimetal only one field is present, the electromagnetic field. Both the chirality generation and the magnetic field of the CME are driven by the same electromagnetic fields. Also for the semimetal case, the field sourcing the anomaly and the CME are parallel.

for chirality generated by the Schwinger mechanism leading to the CME as

$$\mathbf{j}_{cme} \simeq \frac{3te^2}{2\pi^2}\omega(\kappa, w)\mathbf{B}(\mathbf{x})\left(T^2 + \frac{\mu^2}{\pi^2}\right)^{-1}. \tag{3.81}$$

B is the out-of plane magnetic field given in (bold) cartesian coordinates.

For the case of a Dirac semimetal the major difference is given by the fact that both the chirality and the CME are generated by the same background electromagnetic field. See the schematic in Fig. 3.8. It can be seen for the construction of parallel fields that both the electric and magnetic fields contribute to the anomaly, and also the same magnetic field sources the CME. For the semimetal let us consider a highly magnetoresistive layered orthorhombic crystal structure semimetal such as $ZrTe_5$ [110–112]. There instead of the mass of an electron we have an effective quasiparticle mass due to spin splitting driven by magnetic impurities [112], Δ. And we also have for the Fermi velocity, v_f. To contrast this with the speed of light among other variables we use S.I. variables here. While most of our above analysis remains valid in the semimetal environment we must change the worldline action in homogeneous fields to $S_0 = \frac{\pi}{v_f \hbar e E}\left[\Delta^2 - (2\hbar v_f \kappa)^2\right]$, and therefore the action with the dynamically assisted Schwinger mechanism reads

$$S(\kappa, w) \simeq \begin{cases} S_0 & \text{for} \quad 0 < \zeta \leq \frac{\pi}{2} \\ \frac{2S_0}{\pi}\left[\arcsin\left(\frac{\pi}{2\zeta}\right) + \left(\frac{\pi}{2\zeta}\right)\sqrt{1 - \left(\frac{\pi}{2\zeta}\right)}\right] & \text{for} \quad \zeta \geq \frac{\pi}{2}\,, \end{cases} \tag{3.82}$$

with new adiabaticity parameter $\zeta = \frac{w\sqrt{\Delta^2 - (2\hbar v_f \kappa)^2}}{e v_f E}$. Finally with the above substitutions the vacuum non-persistence and the CME current can be found as

$$\omega(\kappa, w) = \frac{e^2 E B}{(2\pi\hbar)^2 c} \coth\left(\frac{\pi B}{cE}\right) \exp\left(-S(\kappa, w)\right)\,, \tag{3.83}$$

$$\mathbf{j}_{cme} \simeq \frac{3 t v_f^3 e^2}{2\pi^2} \omega(\kappa, w) \mathbf{B}(x) \left(T^2 + \frac{\mu^2}{\pi^2}\right)^{-1}. \tag{3.84}$$

Here as expected we can clearly see the emergence of the characteristic quadratic magnetic field [37, 113]. Like the case of the heavy-ion collision indeed the CME current is enhanced for the same field configurations that also enhance the Schwinger mechanism. Usage of the special inhomogeneous fields may offer a method to observe the CME with mass effects.

We have seen that the enhancement of the Schwinger mechanism elicits an enhancement to the produced chirality for parity violating fields using the heuristic picture. However, we still must explain the heuristic production of chirality from a more concrete theoretical standpoint. To do so, we find, one must make use of an identification of vacuum states.

Chapter 4

Vacuum States and Observables

It was introduced in Sec. 2.4 the importance of vacuum states for expectation values. Even the simplest of case such as homogeneous fields or a pulsed field the concept of equivalent vacuum states at $t \to \pm\infty$ is invalid. We saw in Sec. 3.1 that an in-in prescription is identifiable with an out-of-equilibrium Schwinger Keldysh contour. And in Sec. 3.2 we showed the ease of worldline methods in handling the non-perturbative phenomena such as the Schwinger mechanism. Here, let us join the two, that is a non-equilibrium worldline prescription. However, to do so it is worthwhile to first address the equilibrium in-out propagator in the worldline form. Before doing so let us specifically characterize the definition of our Dirac operators in an external field and contrast the operator's in-in and in-out propagators.

Our in (out) states is defined at some time $t_{in}(t_{out})$, which we later take to negative infinity (positive infinity), whereby we can expand the Dirac operators in terms of creation and annihilation operators. Specifically

$$\begin{aligned}\psi(x) &= \sum_n a_n^{in}\phi_{+n}^{in}(x) + b_n^{in\,\dagger}\phi_{-n}^{in}(x) \\ &= \sum_n a_n^{out}\phi_{+n}^{out}(x) + b_n^{out\,\dagger}\phi_{-n}^{out}(x)\,. \end{aligned} \tag{4.1}$$

Both representation are valid over all time. Eigenvectors of the Dirac equation are denoted with positive energy solutions as ϕ_{+n}, with eigenvalue n, or negative energy solutions as ϕ_{-n}, also with eigenvalue n. Note here the eigenvalues may run over momentum and thus the summation here implicitly includes the relevant integral. a_n and b_n respectively represent annihilation operators for a fermion (here in the in basis) such that

$$a_n^{in}\,|in\rangle = b_n^{in}\,|in\rangle = \langle in|\,a_n^{in\,\dagger} = \langle in|\,b_n^{in\,\dagger} = 0\,, \tag{4.2}$$

with anti-commutation relations, $\{a_n^{in}, a_m^{in\,\dagger}\} = \{b_n^{in}, b_m^{in\,\dagger}\} = \delta_{nm}$ which also hold for the out representation.

All of our expectation values are assumed to be in the Heisenberg representation and thus an implicit time ordering will be present[1]. Therefore, the qualitative and quantitative differences between the in-in(out) expectation values can be best captured through an in-depth look at their respective propagators, in fact their

[1] Alternatively in the path integral representations either for the in-out, Eq.(2.15), or Schwinger Keldysh, Eq. (3.10), cases a time ordering too will be implicitly present in expectation values.

causal propagators (here we make explicit the time ordering):

$$S^{c}(x,y) = i\langle T\psi(x)\bar{\psi}(y)\rangle\,, \tag{4.3}$$
$$S^{c}_{in}(x,y) = i\langle\!\langle T\psi(x)\bar{\psi}(y)\rangle\!\rangle\,. \tag{4.4}$$

Both satisfy the following differential equation

$$-(i\not{D}_x - m)S(x,y) = \delta(x-y)\,. \tag{4.5}$$

Yet the properties and boundary conditions of both propagators differ markedly. The expectation values derived from the in-in propagator are Hermitian and real and can be written as a sum over respective eigenvectors of the Dirac equation whose solutions predict similar particle types. In contrast, expectation values derived from the in-out propagator are not Hermitian and may contain imaginary pieces. However, in contrast to the in-in propagator the in-out propagator permits an expansion about the gauge one may characterize using functional methods; this enables the worldline method directly, simplifying matters. Let us first examine the in-out propagator. However, before doing so let us spell out our main results concerning chirality generation via the Schwinger mechanism using both the in-out and in-in formalisms. Doing so will give context to parts of the following technical discussions in the coming pages.

4.1 Summary of Chirality Production Results

Using both the in-out, Eq. (4.3), and in-in, Eq. (4.4), propagators we can directly calculate their corresponding expectation values. First let us begin with the in-out values. After some steps outlined below we find for the pseudoscalar condensate, axial Ward identity, and vector currents (associated with the CME) as

$$\begin{aligned}\langle\bar{\psi}i\gamma_5\psi\rangle &= -\lim_{y\to x}\mathrm{tr}[\gamma_5 S^{c}(x,y)]\\ &= -\frac{e^2EB}{4\pi^2 m}\,,\end{aligned} \tag{4.6}$$
$$\partial_\mu\langle\bar{\psi}\gamma^\mu\gamma_5\psi\rangle = 0\,, \tag{4.7}$$
$$\langle\bar{\psi}\gamma^\mu\psi\rangle = 0\,. \tag{4.8}$$

We find the pseudoscalar condensate contributions have exactly cancelled the anomaly contributions in the axial Ward identity, and hence why the divergence of the chiral current is zero. Likewise we have also discovered that the current has vanished.

However, when we calculate the same observables but in the in-in representation we find very different values for the pseudoscalar condensate, axial Ward identity, and vector currents:

$$\begin{aligned}\langle\!\langle\bar{\psi}i\gamma_5\psi\rangle\!\rangle &= -\lim_{y\to x}\mathrm{tr}[\gamma_5 S^{c}_{\mathrm{in}}(x,y)]\\ &= -\frac{e^2EB}{4\pi^2 m}\left[1-e^{-\pi m^2/(eE)}\right],\end{aligned} \tag{4.9}$$

$$\partial_\mu \langle\!\langle \bar{\psi}\gamma^\mu\gamma_5\psi \rangle\!\rangle = \frac{e^2 EB}{2\pi^2} e^{-\pi m^2/(eE)} \tag{4.10}$$

$$\langle\!\langle \bar{\psi}\gamma^\mu\psi \rangle\!\rangle = \frac{e^2 EB\, t}{2\pi^2} \coth\Big(\frac{\pi B}{E}\Big) e^{-\pi m^2/(eE)} \delta^\mu_3 \,. \tag{4.11}$$

The contributions to the Schwinger mechanism for the in-in case are manifest. Moreover, we find agreement to the heuristically motivated picture introduced in Sec. 2.3.1.

We may understand the contrast between both the in-out and in-in observables from an in and out-of-equilibrium description. An in-out description is formally equivalent, after taking a Wick rotation to Euclidean time, to a zero temperature equilibrated system. On the other hand, as explained in Sec. 3.1, in-in observables capture out-of-equilibrium phenomena. Therefore we can understand the anomaly and CME as being inherently out-of-equilibrium. Or rather, they do not exist in equilibrium. Likewise we can also see an exponential suppression of quadratic mass in the in-in quantities indicative of the Schwinger mechanism. Therefore, we can see how the axial Ward identity and the CME behave under a finite mass. We elaborate in depth these points in the coming pages. Notably, after the in-out and in-in formalism are established, at the end of this chapter in Sec. 4.4, we illustrate the differences between both formalisms. Then in Secs. 5 and 6 the above summarized anomaly and CME respectively are elaborated.

4.2 In-Out Propagator

Let us begin our discussion of vacuum state dependent propagators with the in-out case. As outlined before this represents a matrix element with unique and different ground states at asymptotic times: $t \to -\infty$ for the in state and $t \to \infty$ for the out state. The in-out propagator enjoys a simple transformation to Schwinger proper time or the worldline. Let us first represent the propagator, Eq. (4.3), formally as:

$$\begin{aligned} S^{\rm c}(x,y) &= \langle {\rm x}| \frac{-1}{i\hat{\not{D}} - m} |{\rm y}\rangle \\ &= (i\not{D}_x + m) \langle {\rm x}| \frac{1}{\hat{\not{D}}^2 + m^2} |{\rm y}\rangle \end{aligned} \tag{4.12}$$

Brakets with positions denote space-time states. Information about the time ordering and direction of the in and out ground states are conveniently captured with an implicit small imaginary portion in the mass term, $m^2 \to m^2 - i\epsilon$. The small imaginary piece guarantees convergence in the infrared limit. Also notice in Eq. (4.12), one may expand about the external gauge field to find the in-out propagator represents the sum over all external photon contributions as in Fig. 4.1; c.f., see the expansion of effective action in Fig. 3.2.

Also let us contrast the above with the effective action, Eq. (3.31), presented in Sec. 3.2. Similar to there, one may use a Laplace transform,

$$\hat{\mathcal{O}}^{-1} = i \int_0^\infty ds\, \exp(-i\hat{\mathcal{O}} s) \,, \tag{4.13}$$

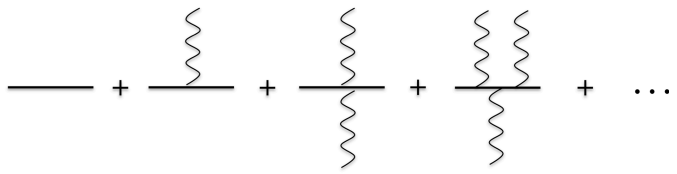

Figure 4.1: Expansion of in-out propagator, S^c, about the gauge field, A. Propagator is the sum over all external photon lines and is exact to one loop.

to make the transformation to Schwinger proper time. Then we can clearly see the emergence of a quantum mechanical-like 4+1 dimensional system–space and time give us 4 dimensions with proper time providing an additional dimension. Then the in-out propagator (4.12) becomes

$$S^{\rm c}(x,y) = (i\not{D}_x + m)\int_0^\infty ds\, g(x,y,s)\,, \tag{4.14}$$

$$g(x,y,s) \coloneqq i\langle {\rm x}|e^{-i\hat{H}s}|{\rm y}\rangle\,, \tag{4.15}$$

$$\hat{H} \coloneqq \hat{\not{D}}^2 + m^2\,. \tag{4.16}$$

Here we have characterize a worldline kernel, Eq. (4.15), which satisfies a quantum mechanical-like Schrödinger equation,

$$\Big(\frac{d}{ds} - H\Big)g(x,y,s) = 0\,, \tag{4.17}$$

with Hamiltonian, H. $\hat{\not{D}}^2 = \hat{D}^\mu\hat{D}_\mu + \frac{1}{2}F\sigma$. This is the functional form first envisioned by Schwinger [15]. And, for certain applications calculations can be considerably simplified as we will demonstrate. In passing let us mention that using the small imaginary piece one can readily identify Eq. (4.12) as a solution to the defining differential equation in Eq. (4.5).

Our next task is to cast the kernel, Eq. (4.15) into a path integral form. We stated this result in the previous section; see Eq. (3.34) and arguments which follow, and as advertised let us construct the path integral in detail. This process is accomplished through identifying the worldline Lagrangian, $\mathcal{L}$ from the Hamiltonian, Eq. (4.16), and using a Legendre transform [114]. Then we make use of Eq. (3.34). There, we use $x(\tau = 0) = y$ and $x(\tau = s) = x$ as boundary conditions. The worldline operators follow appropriate Heisenberg equation of motion in proper time,

$$\frac{d\hat{\mathcal{O}}}{d\tau} = -i[\hat{\mathcal{O}}, \hat{H}]\,, \tag{4.18}$$

as well as a 4+1 dimensional extension of the canonical commutation relation, $[\hat{p}_\mu, \hat{x}_\nu] = ig_{\mu\nu}$. We find for the velocity

$$\dot{\hat{x}}_\mu \coloneqq \frac{d\hat{x}_\mu}{d\tau} = -i[\hat{x}_\mu, \hat{H}] = 2(\hat{p}_\mu - A_\mu(\hat{x}))\,. \tag{4.19}$$

Then using the above the corresponding Lagrangian can be found as

$$\hat{\mathcal{L}} = \hat{p}_\mu \frac{\partial \hat{H}}{\partial \hat{p}^\mu} - \hat{H} \tag{4.20}$$

$$= -\frac{1}{4}\dot{\hat{x}}^2 - A(\hat{x})\dot{\hat{x}} - \frac{1}{2}F(\hat{x})\sigma - m^2\,. \tag{4.21}$$

Here and throughout "dots" represent derivatives with respect to τ. Going from an operator formalism to a classical variable for the path integral, we find the kernel, Eq. (4.15), of the in-out propagator may be read as

$$g(x,y,s) = i\int \mathcal{D}x\,\mathcal{P}\exp\Big\{i\int_0^s d\tau\Big[-\frac{1}{4}\dot{x}^2 - A\dot{x} - \frac{1}{2}F\sigma - m^2\Big]\Big\}\,. \tag{4.22}$$

The Lorentz indices have been suppressed here and also hereafter where appropriate; where confusion might be present, we make explicit the indices. Thus complete the formulation of the worldline path integral. Eq. (4.22) and the in the in-out propagator are valid for any QED background field. However, at this point let us restrict our attention to parallel homogeneous fields.

The derivation of the fermion propagator in homogeneous fields using functional means is well known [15, 114], but let us spell out the explicit steps, as for later calculations we will need to make use of some details outlined here.

The homogeneous field we use are indicated in Eq. (2.22); they are parallel on the x_3 direction. Also the energy density of the configuration, i.e. $F_{\mu\nu}F^{\mu\nu}$, need not be zero; of course we have $\epsilon_{\mu\nu\alpha\beta}F^{\mu\nu}F^{\alpha\beta} \neq 0$. A significant simplification in homogeneous fields involves the breakup of the integrand in the path integral into a spin factor, (we saw before in Eq. (3.37)), and a bosonic path integral factor.

It is convenient to first address the spin factor in the path integral, Eq. (3.37), contained in both the effective action and propagator. Under homogeneous fields the argument simplifies and the path ordering disappears. Furthermore using a Weyl representation for our gamma matrices the argument of the spin factor, $F\sigma$, takes on a diagonal form and the spin factor, Eq. (3.37), becomes

$$\Phi = \begin{pmatrix} e^{-e(E-iB)s} & & & 0 \\ & e^{e(E-iB)s} & & \\ & & e^{e(E+iB)s} & \\ 0 & & & e^{-e(E+iB)s} \end{pmatrix} \tag{4.23}$$

It is also convenient to represent the above in terms of Dirac matrices:

$$\Phi = [\cos(eBs) + i\sin(eBs)\sigma^{12}] \times [\cosh(sEs) + \sinh(eEs)\gamma_5\sigma^{12}]\,, \tag{4.24}$$

with $\sigma^{12} = \mathrm{diag}[1,-1,1,-1]$. The spin factor solely determines the gamma matrix nature of expectation values, e.g. through only a cursory look at the spin factor one can determine whether a pole in proper time is present–we will later demonstrate poles we will be of order $\sinh^{-1}(eEs)$.

Equipped with the spin factor, which does not affect the path integration, we turn our attention to the remaining bosonic portion of the path integral. The bosonic portion reads

$$b(x,y,s) \coloneqq \int \mathcal{D}x\,\exp\Big\{i\int_0^s d\tau[-\frac{1}{4}\dot{x}^2 - eA\dot{x}]\Big\}\,, \tag{4.25}$$

Any background the fermionic worldline path integral, Eq. (4.22), may be split into multiplicative bosonic and spin factors, yet a connection between the two is provided through s and a sum over coordinate paths x. For the case of homogeneous field, however, the two are only connected through s. Let us proceed with the evaluation of the bosonic part through the worldline instanton method introduced in Eq. (3.38). Here, however, our classical paths are quite generic with s dependence and the imaginary part we will see stems from singularities in the proper time integral. We solve the path integral by expanding around classical paths

$$x_\mu(\tau) = x^{cl}_\mu + \eta_\mu(\tau); \tag{4.26}$$

here η represents fluctuations around the classical path which disappear at end points, $\eta(0) = \eta(s) = 0$. Owing to the virtue of a quadratic in x_μ Lagrangian higher order functional expansions disappear and the treatment here is exact. Performing steepest decents on Eq. (4.25), where the worldline action is $S_b = \int_0^s d\tau[-\frac{1}{4}\dot{x}^2 - eA\dot{x}]$ of $b = \exp(iS_b)$; we find

$$b(x,y,s) = e^{iS_b(x^{cl})}\mathcal{F}\,, \tag{4.27}$$

$$\mathcal{F} \coloneqq \int \mathcal{D}\eta\, \exp\Big\{i\int_0^s d\tau[-\frac{1}{4}\dot{\eta}^2 + \frac{1}{2}\eta^\mu eF_{\mu\nu}\dot{\eta}^\nu]\Big\}\,. \tag{4.28}$$

With our Fock-Schwinger gauge choice, $A_\mu(x) = -\frac{1}{2}F_{\mu\nu}x^\nu$, we see the fluctuation path integral is that of the original one but periodic about zero, simplifying matters.

Let us treat the classical part first. Considering the boundary conditions in the prefactor fluctuation, the classical part must contain all endpoint, x and y, information. Solutions of the classical equations of motion can be found simply by treating the Lorentz force equation as a time-independent like Schödinger equation. We find the Lorentz force equation with general solution as

$$\ddot{x}^{cl\,\mu}(\tau) = 2eF^\mu_{\ \nu}\dot{x}^{cl\,\nu}(\tau) \tag{4.29}$$

$$\dot{x}^{cl\,\mu}(\tau) = \Big[e^{2eF\tau}\Big]^\mu_{\ \nu}\dot{x}^{cl\,\nu}(0). \tag{4.30}$$

Also making note of the boundary conditions, $\int_0^s d\tau\dot{x}^{cl\,\mu}(\tau) = z^\mu$, and inserting Eq. (4.30) we can find that $(e^{2Fs}-1)^\mu_{\ \lambda}\dot{x}^{cl\,\lambda}(0) = 2F^\mu_{\ \lambda}z^\lambda$. After some manipulations we can arrive at the following form for the classical action

$$\varphi \coloneqq S_b(x^{cl}) = \frac{1}{2}x_\mu eF^\mu_{\ \nu}y^\nu - \frac{1}{4}z_\mu[\coth(eFs)]^\mu_{\ \nu}eF^\nu_{\ \lambda}z^\lambda\,. \tag{4.31}$$

The above classical action is gauge dependent in the Fock gauge. The important thing to bare in mind is that the action goes to zero as $x \to y$. It is also convenient to expand the Lorentz contracted terms here as well. We find for the classical action also, after summing over indices in the cotangent function

$$\varphi(x,y,s) = \frac{1}{2}x_\mu eF^\mu_{\ \nu}y^\nu + \frac{1}{4}\Big[(z_3^2 - z_0^2)eE\coth(eEs) + (z_1^2+z_2^2)eB\cot(eBs)\Big]. \tag{4.32}$$

The remaining part of the path integral, the fluctuation prefactor, Eq. (4.28), can be found directly through an expansion about Fourier modes:

$$\eta_\mu(\tau) = a_{\mu_0} + \sum_{n=1}^{\infty}\left[a_{\mu\, n}\cos\left(\frac{2\pi n\tau}{s}\right) + b_{\mu\, n}\sin\left(\frac{2\pi n\tau}{s}\right)\right]. \tag{4.33}$$

The factors in the integrand and measure, with measure constant $\mathcal{N}$, in the path integral become

$$\int_0^s d\tau\, \dot\eta^2 = \frac{s}{2}\sum_{n=1}^{\infty}\left(\frac{2\pi n}{s}\right)^2 (a_{\mu n}a_n^\mu + b_{\mu n}b_n^\mu)\,, \tag{4.34}$$

$$\int_0^s d\tau\, \eta^\mu eF_{\mu\nu}\dot\eta^\nu = \frac{s}{2}\sum_{n=1}^{\infty}\left(\frac{2\pi n}{s}\right)(a_n^\mu eF_{\mu\nu}b_n^\nu - b_n^\mu eF_{\mu\nu}a_n^\nu)\,, \tag{4.35}$$

$$\int \mathcal{D}\eta = \mathcal{N}\prod_{n=1}^{\infty} da_n db_n\,. \tag{4.36}$$

We may evaluate the determinant with the help of the normalization of the path integral in the absence of external fields, $\mathcal{D}\eta\, e^{i\int_0^s d\tau[-\frac{1}{4}\dot\eta^2]} = -i/(4\pi s)^2$, also Fourier expanded. After some steps we find the fluctuation prefactor becomes

$$\mathcal{F} = -i\frac{e^2EB}{(4\pi)^2}\sin^{-1}(eBs)\sinh^{-1}(sEs)\,. \tag{4.37}$$

The kernel, Eq. (4.15), finally reads

$$g(x,y,s) = \frac{e^2EB}{(4\pi)^2}\exp(-im^2s + i\varphi(x,y,s))\sin^{-1}(eBs)\sinh^{-1}(eEs)\Phi\,. \tag{4.38}$$

The kernel and expectation values derived from it are exact to one loop. The kernel also contains all the information of Schwinger pair production through its essential singularity in φ and isolated singularity in $\sinh^{-1}(eEs)$. All the Landau levels are contained in the various $\cot(eBs)$ functions. Also, let us note, after taking the covariant derivative the in-out propagator, in homogeneous parallel fields, is found to be translational invariant with the exception of the gauge dependent Wilson line factor. Equipped with the in-out propagator, let us move onto the in-in propagator.

4.3 In-In Propagator

The worldline methods depicted for in-out states above have been widely used to study the Schwinger mechanism, and it would be highly advantageous to extend the worldline formalism to in-in states. Fortunately for the case of parallel homogeneous fields this has been accomplished by Fradkin et. al. in Ref. [89], whose construction differs from Eq. (4.12) only through an augmentation of the proper time integral. Before illustrating calculational steps let us first motivate a physical manifestation of the in-in propagator provided through a canonical operator formalism stemming from a Schwinger Keldysh contour. Such a treatment can also provide physical information of the vacuum non-persistence, Eq. (2.14).

4.3.1 Matrix Element Expansion

Let us begin our discussion of the in-in propagator through an examination of its form in a canonical operator approach, introduced in Eqs. (4.1). Doing so makes clear the physical ramifications of the in-in propagator versus the in-out one. We take as our starting point the Schwinger Keldysh generating functional defined without sources. The generating functional, Eq. (3.9), is formally derivable beginning with an in-in construction [95]. And in this sense, we may formally evaluate the SK path integral to find the generating functional as

$$\mathcal{Z}_{\eta=0} = \sum_{\alpha} |\,\langle \alpha, out|in\rangle\,|^2 = 1\,. \tag{4.39}$$

α runs over all possible eigenstates of the given background. It can be found that the only non-vanishing contribution are matrix elements where any number of particle antiparticle pairs are produced from the vacuum [89]:

$$\mathcal{Z}_{\eta=0} = \sum_{N=0}^{\infty} \frac{1}{N!^2} \sum_{\substack{m_1 \ldots m_N \\ n_1 \ldots n_N}} |\langle a^{out}_{m_N} \ldots a^{out}_{m_1} b^{out}_{n_N} \ldots b^{out}_{n_1}\rangle|^2\,. \tag{4.40}$$

Here, again we use the following notation: $\langle \mathcal{O}\rangle := \langle \text{out}|\mathcal{O}(t)|\text{in}\rangle/c_v$. Rearranging the above by moving the $N=0$ contribution to the left we can see how the in-in generating functional contains information of the vacuum non-persistence, Eq. (2.14),

$$1-|c_v|^2 = \sum_{n_1,m_1} \langle b^{\dagger\,out}_{n_1} a^{\dagger\,out}_{m_1}\rangle^* \langle a^{out}_{m_1} b^{out}_{n_1}\rangle |c_v|^2 + \frac{1}{2!^2} |\sum_{\substack{m_1,m_2 \\ n_1,n_2}} \langle a^{out}_{m_2} a^{out}_{m_1} b^{out}_{n_2} b^{out}_{n_1}\rangle|^2 |c_v|^2 + \ldots\,, \tag{4.41}$$

where we have made use of the notation for anti-time ordered correlation function via

$$\langle \mathcal{O}\rangle^* := \langle in|\,\mathcal{O}\,|out\rangle\,/c_v^*\,, \tag{4.42}$$

The vacuum non-persistence is measuring the probability for any number of pairs of particles to be produced from the vacuum. Matrix elements here obey the usual Wick contractions; see Ref. [89] for details. Let us take the Wick contraction of $\langle b^{\dagger\,out}_{n_1} \ldots b^{\dagger\,out}_{n_N} a^{\dagger\,out}_{m_1} \ldots a^{\dagger\,out}_{m_N}\rangle$. Notice that due to the symmetry of the Hermitian conjugate no matter which permutation contraction of $b^{\dagger\,out}_n$ and $a^{\dagger\,out}_m$ we get we may always rearrange the associated operator on the un-contracted side to find

$$\frac{1}{|c_v|^2} = \langle \exp\Big[\sum_{n,m} a^{out}_n b^{out}_m \langle b^{\dagger\,out}_m a^{\dagger\,out}_n\rangle^*\Big]\rangle\,, \tag{4.43}$$

Into any of these generating functionals we may insert operators to construct in-in expectation values. We will do so with the in-in time ordered propagator. First, however, let us look at the first term in the expanded exponential above; one can see this quantity shares a close connection to the vacuum non-persistence, Eq. (2.14). In fact, they are identical to $\mathcal{O}(n=1)$ in the non-perturbative expansion of pair production, $\exp(-\frac{\pi n m^2}{eE})$. The quantity is the probability for a *single* particle antiparticle pair to be spawned from the vacuum. Using the definitions for the canonical

operators, Eq. (4.1), and the in-out propagator, Eq. (4.12) we can find

$$\sum_{n,m}\langle a_n^{out} b_m^{out}\rangle\langle b_m^{\dagger\, out} a_n^{\dagger\, out}\rangle^* = \frac{e^2 EBVt}{4\pi^2}\sum_{n=1}^{\infty}\coth\Big(\frac{n\pi B}{E}\Big)\exp\Big(-\frac{n\pi m^2}{eE}\Big)\,. \tag{4.44}$$

Notice here the probability for a single pair of particles includes contributions from all n poles. What we can gather from this is that the pole number n does not correspond to the particle number. Casting the above in a worldline formalism and completing the sum over n we can identify what the sum over all n is associated with.

$$\sum_{n,m}\langle a_n^{out} b_m^{out}\rangle\langle b_m^{\dagger\, out} a_n^{\dagger\, out}\rangle^* \propto \mathrm{tr}\,\langle x|\,\frac{1}{1-e^{\hat{H}\frac{\pi}{eE}}}\,|x\rangle\ . \tag{4.45}$$

Here we see the sum over n in the proper time, s, corresponds to a Boson-like distribution in proper time with Hamiltonian $\hat{H}$, Eq. (4.16), with $\pi/(eE)$ depicting a temperature in proper time. That a Boson-like distribution is present as opposed to a Fermi-Dirac distribution is because the Schwinger mechanism process is insensitive to spin dynamics. Indeed, one can find a similar expression as above for Bosons.

Equipped with the above let us reexamine the in-in propagator. This is in operator notation, utilizing both in and out representations, (but we may use any representation we like),

$$S^{\rm c}_{\rm in}(x,y) = i\sum_n \langle\!\langle T[a_n^{out}\phi_{+n}^{out}(x) + b_n^{out\,\dagger}\phi_{-n}^{out}(x)]\bar{\psi}_{in}(y)\rangle\!\rangle\,. \tag{4.46}$$

We insert in a complete set of states finding again that only Bogoliubov coefficients predictive of pair production contribute to the final expression. We can see this more clearly, using Eq. (4.43), expressing the above as

$$S^{\rm c}_{\rm in}(x,y) = i|c_v|^2\langle\exp\Big[\sum_{n,m} a_n^{out} b_m^{out}\langle b_m^{\dagger\, out} a_n^{\dagger\, out}\rangle^*\Big] T\psi(x)\bar{\psi}(y)\rangle\,. \tag{4.47}$$

We can see that the first term in an expansion of the exponential resembles $S^{\rm c}$, however there is the $|c_v|^2$ term which we can show disappears after taking the contraction of each term in the series. To illustrate this fact let us examine one specific contraction:

$$\langle\!\langle a_n^{out} a_m^{in\,\dagger}\rangle\!\rangle = |c_v|^2\langle\exp\Big[\sum_{m_1,n_1} a_{m_1}^{out} b_{n_1}^{out}\langle b_{n_1}^{\dagger\, out} a_{m_1}^{\dagger\, out}\rangle^*\Big] a_n^{out} a_m^{in\,\dagger}\rangle\,. \tag{4.48}$$

Proceeding with the Wick contraction, let us show how the infinite sum simplifies through a recursive analysis. Let us consider an element with N pairs of particles and then apply Wick's theorem. We sum over every possible permutation, where we denote here $\omega_n^{out} = b_m^{out}\langle b_m^{\dagger\, out} a_n^{\dagger\, out}\rangle^*$

$$\begin{aligned}
&\sum_{\substack{m_1\ldots m_N\\ n_1\ldots n_N}} \langle a_{m_1}^{out}\omega_{m_1}^{out} a_{m_2}^{out}\omega_{m_2}^{out}\ldots a_{m_N}^{out}\omega_{m_N}^{out} a_n^{out} a_m^{in\,\dagger}\rangle \\
&= \sum_{\substack{m_1\ldots m_N\\ n_1\ldots n_N}} \Big\{\langle \boxed{a_{m_1}^{out}\omega_{m_1}^{out} a_{m_2}^{out}\omega_{m_2}^{out}\ldots a_{m_N}^{out}\omega_{m_N}^{out}}\, \overbrace{a_n^{out} a_m^{in\,\dagger}}\rangle \\
&+ N\,\langle \boxed{a_{m_2}^{out}\omega_{m_2}^{out}\ldots a_{m_N}^{out}\omega_{m_N}^{out}}\, \overbrace{a_{m_1}^{out}\omega_{m_1}^{out} a_n^{out} a_m^{in\,\dagger}}\rangle
\end{aligned}$$

$$+ N(N-1)\left\langle \boxed{a^{out}_{m_3}\omega^{out}_{m_3}...a^{out}_{m_N}\omega^{out}_{m_N}}\, a^{out}_{m_1}\omega^{out}_{m_1}a^{out}_{m_2}\omega^{out}_{m_2}a^{out}_{n}a^{in\,\dagger}_{m}\right\rangle + ...\Big\}\,. \tag{4.49}$$

Here boxed elements represent every possible contraction of contained operators. Let us imagine the set which includes a contraction of just $a^{out}_n a^{in\,\dagger}_m$, in first expression of Eq. (4.49) along with everything else, then imagine the next set of contractions which include one pair of $a^{out}_{m_1}\omega^{out}_{m_1}$ for each N pairs, the second expression in Eq. (4.49). Continuing the set which includes two pairs, the final expression in Eq. (4.49), we see a pattern emerge. Disconnected pieces would be contained in the previous sets, and all possible fully connected permutations are accounted for in the truncated $N!$ term. Making use of Eq. (4.43) we find Eq. (4.49) becomes a geometric series

$$\begin{aligned}\langle\!\langle a^{out}_n a^{in\,\dagger}_m\rangle\!\rangle &= \langle a^{out}_n a^{in\,\dagger}_m\rangle + \sum_{m_1,n_1}\langle b^{out}_{n_1}a^{out}_n\rangle\langle b^{\dagger\,out}_{n_1}a^{\dagger\,out}_{m_1}\rangle^*\langle a^{out}_{m_1}a^{in\,\dagger}_m\rangle \\ &+ \sum_{\substack{m_1,m_2\\ n_1,n_2}}\langle b^{out}_{n_2}a^{out}_n\rangle\langle b^{\dagger\,out}_{n_2}a^{\dagger\,out}_{m_2}\rangle^*\langle b^{out}_{n_1}a^{out}_{m_2}\rangle\langle b^{\dagger\,out}_{n_1}a^{\dagger\,out}_{m_1}\rangle^*\langle a^{out}_{m_1}a^{in\,\dagger}_m\rangle + \dots\,. \end{aligned}\tag{4.50}$$

Finally, we can see that the $|c_v|^2$ term has been absorbed through the contraction process. Furthermore, we can see from inference that the in-in propagator is then a series of matrix elements of pairs of particles in the out state. The first of which is the in-out propagator and physically describes a scenario with no particles in the out state.

4.3.2 Dirac Eigendecomposition

While the above treatment was physically illuminating actual calculations are challenging owing to the infinite products over matrix elements of pairs from the out state. However, a major simplification is achievable if we represent the out state in the in-out propagator in terms of its transformed in state representation. We again make use of the canonical operator approach used above. Using Eq. (4.1) but in the in state representation, we find for the in-out propagator

$$S^{\rm c}(x,y) = i\sum_{N=0}^{\infty}\frac{1}{N!^2}\sum_{\substack{m_1...m_N\\ n_1...n_N}}\langle b^{in\,\dagger}_{n_1}...b^{in\,\dagger}_{n_N}a^{in\,\dagger}_{m_1}...a^{in\,\dagger}_{m_N}\rangle\langle\!\langle a^{in}_{m_N}...a^{in}_{m_1}b^{in}_{n_N}...b^{in}_{n_1}T\psi(x)\bar\psi(y)\rangle\!\rangle\,. \tag{4.51}$$

Let us consider here $\psi(x)$ and $\bar\psi(y)$ both in the in representation. Then using the anticommutative properties of the creation and annihilation operators one can confirm that only the $N=0,1$ states remain after expressing the above in its normal ordering. We find for the in-out propagator

$$S^{\rm c}(x,y) = S^{\rm c}_{\rm in}(x,y) + i\sum_{n,m}\langle b^{in\,\dagger}_n a^{in\,\dagger}_m\rangle\langle\!\langle a^{in}_m b^{in}_n T\psi^{in}(x)\bar\psi^{in}(y)\rangle\!\rangle\,. \tag{4.52}$$

Let us express the Dirac operator in terms of eigenvectors of the Dirac equation, then the above can be written as

$$\begin{aligned}S^{\rm c}(x,y) &= S^{\rm c}_{\rm in}(x,y) + i\sum_{n,m}\langle b^{in\,\dagger}_n a^{in\,\dagger}_m\rangle\Big[\theta(z_0)\phi^{in}_{-n}(x)\bar\phi^{in}_{+m}(y) + \theta(-z_0)\bar\phi^{in}_{+m}(y)\phi^{in}_{-n}(x)\Big] \\ &= S^{\rm c}_{\rm in}(x,y) + S^{a}(x,y)\end{aligned}\tag{4.53}$$

$$S^a(x,y) \coloneqq \sum_{n,m} \phi^{in}_{-n}(x)\langle b^{in\,\dagger}_n a^{in\,\dagger}_m\rangle \bar{\phi}^{in}_{+m}(y)\,. \tag{4.54}$$

The calculation of S^a is not central to discussions presented later; the final form of the expression can be found below in Eq. (4.76).

Let us evaluate the above addition to the propagator, S^a, through an eigendecompostion of the Dirac equation. This was first performed in Ref. [89], and we review essential points of their calculation here. We verified above that to construct an in-in propagator one should calculate the Green's function depicting any number of pairs being produced from the vacuum, which serves as an addition to the in-out propagator. ϕ is a solution to the Dirac equation, but it is convenient to rather solve the quadratic Dirac equation given by

$$(\not{D}^2 + m^2)\tilde{\phi}_n(x) = 0\,, \tag{4.55}$$

$$(i\not{D} + m)\tilde{\phi}_n(x) = \phi_n(x)\,. \tag{4.56}$$

Let us evaluate the quadratic Dirac equation explicitly in parallel homogeneous field given by Eq. (2.22). First, let us point out two major simplifications. Considering the makeup of our gauge fields, we can find for the momentum in the x_3 and x_1 directions, we should have a factor of $\exp(ip_A x_A)/L$ in ϕ for $x_A \coloneqq (0,-x^1,0,-x^3)$. Also as we found before the argument of the spin factor, Eq. (3.37), is diagonal therefore we can find the eigenvectors–whose explicit form is not required–associated with Dirac matrices simply as well, in fact only two are required:

$$-2i\gamma^1\gamma^2 u_k = k u_k\,, \quad 2\gamma^0\gamma^3 u_k = u_k\,, \quad \text{for} \quad k = \pm 1\,. \tag{4.57}$$

$k = 1(-1)$ denotes spin alignment (anti-alignment). We can find for the quadratic Dirac equation, Eq. (4.55), the following form

$$\Big\{\partial_0^2 - \partial_2^2 + (p_1 + eBx_2)^2 + (p_3 - eEx_0)^2 + m^2 + keB - ieE\Big\}\tilde{\phi}_n(x) = 0\,, \tag{4.58}$$

which permits a clear separation into electric and magnetic eigenvectors. Gathering the magnetic pieces we find ϕ contains an eigenvector solution for the Landau levels, l.

$$\Big\{\partial_2^2 - (p_1 + eBx_2)^2 + eB(2l+1)\Big\}\xi^B_l = 0\,, \quad \text{for} \quad l = 0,1,2... \tag{4.59}$$

$$\xi^B_l = (\tfrac{eB}{\pi})^{1/4}\frac{1}{\sqrt{2^l l!}} H_l[\tfrac{1}{\sqrt{eB}}(p_1 + eBx_2)]\exp[-\tfrac{1}{2eB}(p_1 + eBx_2)^2]\,. \tag{4.60}$$

The eigenvectors of Hermite polynomials are orthogonal in Landau level, i.e., $\int dx_2 \xi^B_l \xi^B_{l'} = \delta_{ll'}$. Finally we may characterize the remaining eigenvectors associated with the electric field as

$$\Big\{\partial_0^2 + (p_3 - eEx_0)^2 + m^2 + eB(2l+1-k) - ieE\Big\}\xi^E_{\pm k} = 0\,. \tag{4.61}$$

Unlike the magnetic field, solutions here contain complex arguments depictive of particle and anti-particle solutions. Particle (anti-particle) solutions are given as positive (negative) eigenvalue solutions to $[-i\gamma^0\vec{D}\vec{\gamma} + A^0 + m\gamma^0]\phi_n = \lambda(t)\phi_n$. There are two separate representations, for either in or out asymptotic times, for the

Hamiltonian. Since the Green's function, Eq. (4.54), is entirely constructed from in states we only report such eigenfunctions. We have

$$\xi^E_{+k} = \frac{p_3 + \sqrt{p_3^2 - 2ieEa}}{\sqrt{2eE}} e^{\frac{i\pi a}{4}} D_{a-1}[\tfrac{1}{\sqrt{eE}}(1-i)(p_3 - eEx_0)]\,, \tag{4.62}$$

$$\xi^E_{-k} = -\frac{p_3 + \sqrt{p_3^2 - 2ieEa}}{\sqrt{-2ieEa}} e^{\frac{i\pi a}{4}} D_{-a}[\tfrac{1}{\sqrt{eE}}(1+i)(p_3 - eEx_0)]\,, \tag{4.63}$$

$$a := \frac{i(m^2 + eB(2l+1-k))}{2eE} \tag{4.64}$$

D is a parabolic cylinder function. Gathering the electric field and magnetic field eigenvectors we compactly write the orthonormalized solutions for the Dirac equation as

$$\phi^{in}_{\pm n\in k,l,p}(x) = (i\not{D} + m)e^{ip_A x_A}\frac{u_k}{L}\xi^B_l \xi^E_{\pm k}\,. \tag{4.65}$$

The covariant derivative can readily be taken by pointing out that the 2nd order differential equations, Eqs. (4.60) and (4.63), can be expressed in a linear form.

With the eigenfunctions in hand one can then calculate the matrix element in S^a. Then with the help of the in-out propagator, Eq. (4.14), written in operator form the matrix element representing pair creation in the in state can be found as

$$\langle b^{in\,\dagger}_n a^{in\,\dagger}_m\rangle = -i\int d^3x' d^3y' \phi^{in\,\dagger}_{-n}(x') S^{\rm c}(x',y')\gamma^0 \phi^{in}_{+m}(y')\,, \tag{4.66}$$

with $x'_0 \to -\infty$ and $y'_0 \to \infty$. Taking the asymptotic limits of the above eigenvectors and in-out propagator one can eventually find

$$\langle b^{in\,\dagger}_n a'^{in\,\dagger}_n\rangle = \frac{a}{2\pi} e^{\frac{i\pi a}{2}}\Gamma(a)\delta_{ll'}\delta_{kk'}\delta(p_1 - p'_1)\delta(p_3 - p'_3)\,. \tag{4.67}$$

Γ here is denoted as the gamma function.

Gathering the matrix elements and eigenvectors we can find

$$S^a(x,y) = \sum_{l=0}^{\infty}\sum_{k=\pm 1}\int \frac{dp_{1,3}}{(2\pi)^2}\frac{ia}{2\pi}\Gamma(a)e^{\frac{i\pi a}{2}}\phi^{in}_{-,k,l,p}(x)\bar{\phi}^{in}_{+,k,l,p}(y)\,. \tag{4.68}$$

Let us examine the p_3 integral as this is where the non-trivial proper time integration path stems from. After taking the covariant derivatives of the above parabolic cylinder functions, Eqs. (4.63), one can find that the p_3 integral reduces to the following two sets of integrals:

$$I_{p_3} = \int dp_3\, e^{-ip_3 z_3} D_{-a}[\tfrac{1}{\sqrt{eE}}(1+i)(p_3 - eEx_0)] D_{-a}[\tfrac{1}{\sqrt{eE}}(1+i)(p_3 + eEx_0)]\,, \tag{4.69}$$

and the other set can be found with the replacement $-a \to -a-1$ in the parabolic cylinder function. This integral may be solved exactly provided we split it into arguments of the z_3 and z_0 variables. After a change of variables to $q = \frac{1}{\sqrt{eE}}(p_3 - \frac{eE}{2}(x_0 + y_0))$, the above integral can be found as [89]

$$\begin{aligned} I_{p_3} = \sqrt{eE}e^{\frac{i}{2}eEz_3(x_0+y_0)}[&\theta(z_0+z_3)\theta(-z_3)J_1 + \theta(z_0 - z_3)\theta(z_3)J_2 \\ &+ \theta(-z_0 - z_3)\theta(-z_3)J_3 + \theta(-z_0 + z_3)\theta(z_3)J_4]\,, \end{aligned} \tag{4.70}$$

$$J_1 = J_2 = \int dq\, D_{-a}[(1+i)(q-\tfrac{eE}{2}\sqrt{z_0^2-z_3^2})]D_{-a}[(1+i)(q-\tfrac{eE}{2}\sqrt{z_0^2+z_3^2})]$$
$$= \frac{\sqrt{\pi}eE}{\Gamma(a)}\int_0^\infty ds\, e^{-\frac{i\pi}{4}+i\pi a+eE(1-2a)s+i\frac{eE}{4}(z_3^2-z_0^2)\coth(eEs)}\sinh^{-1}(eEs)\,, \tag{4.71}$$
$$J_3 = \int dq\, e^{-i\sqrt{eE(z_0^2-z_3^2)}q}D_{-a}[(1+i)q]D_{-a}[(1+i)q] = J_1 \tag{4.72}$$
$$J_4 = \int dq\, e^{i\sqrt{eE(z_0^2-z_3^2)}q}D_{-a}[(1+i)q]D_{-a}[(1+i)q]$$
$$= \frac{\sqrt{\pi}eE}{\Gamma(a)}e^{i\frac{\pi}{4}+i\frac{\pi}{2}(a-1)}\Big\{\int_0^{-\infty} ds\, e^{i\pi a+eE(1-2a)s+i\frac{eE}{4}(z_3^2-z_0^2)\coth(eEs)}\sinh^{-1}(eEs)$$
$$+\int_{-\infty}^{\infty} ds\, e^{-i\pi a+eE(1-2a)s+i\frac{eE}{4}(z_3^2-z_0^2)\tanh(eEs)}\cosh^{-1}(eEs)\Big\}\,. \tag{4.73}$$

The important thing to notice here is in the final expression, J_4, after a change of variables to $s' = s + i\pi/2eE$, the integrand can be made to resemble that of J_{1-3} and moreover the kernel, Eq. (4.38). However, doing so gives us an additional factor of $i\pi/2eE$ in proper time along with a $\theta(z_3)$ dependence, qualitatively changing the propagator. After the above step, the Landau levels can be summed over and p_1 integrated over to make the connection to the kernel. It is found

$$S^a(x,y) = (i\not{D}_x + m)\Big\{\theta(z_3)\theta(z_0^2-z_3^2)\Big[\int_{-\infty-\frac{i\pi}{2eE}}^{\infty-\frac{i\pi}{2eE}} + \int_{0^--\frac{i\pi}{eE}}^{-\infty-\frac{i\pi}{eE}}\Big]$$
$$+(\theta(z_3)\theta(z_0^2-z_3^2)+\theta(-z_3))\int_{0^+-\frac{i\pi}{eE}}^{\infty-\frac{i\pi}{eE}}\Big\}ds\, g(x,y,s)\,, \tag{4.74}$$

with the kernel given by Eq. (4.38). Last we can simplify the above by noting the following relationship for the discontinuity about $s = -i\pi/eE$ for the upper half:

$$\theta(z_0^2-z_3^2)\int_{\gamma^h} ds\, g(s,y,s) = 0\,; \tag{4.75}$$

the contour γ^h is given in Fig. 7.1 below. We finally find

$$S^a(x,y) = (i\not{D}_x + m)\Big\{\theta(z_3)\Big[\int_{-\infty-\frac{i\pi}{2eE}}^{\infty-\frac{i\pi}{2eE}} + \int_{0^--\frac{i\pi}{eE}}^{-\infty-\frac{i\pi}{eE}}\Big] + \theta(-z_3)\int_{0^+-\frac{i\pi}{eE}}^{\infty-\frac{i\pi}{eE}}\Big\}ds\, g(x,y,s)\,. \tag{4.76}$$

The physical ramification of $\theta(z_3)$ terms we will illustrate with concrete examples in the coming sections; however let us mention that such terms will find to give rise to a real-time dependence. Let us write the above propagator more compactly. Combining the above with the in-out propagator, Eq. (4.53), one can find the final expression for the in-in propagator as [89]

$$S^{\rm c}_{\rm in}(x,y) = (i\not{D}_x + m)\int_{in} ds\, g(x,y,s) \tag{4.77}$$
$$\int_{in} ds := \Big[\theta(z_3)\int_{\Gamma>} ds + \theta(-z_3)\int_{\Gamma<} ds\Big]\,, \tag{4.78}$$

with contours depicted in Fig. 4.2. Let us point out that here that although the contours seem to be valid to only $\mathcal{O}(n=1)$ of $\exp(-\frac{nm^2\pi}{eE})$, the in-in propagator contains, in fact, all n orders.

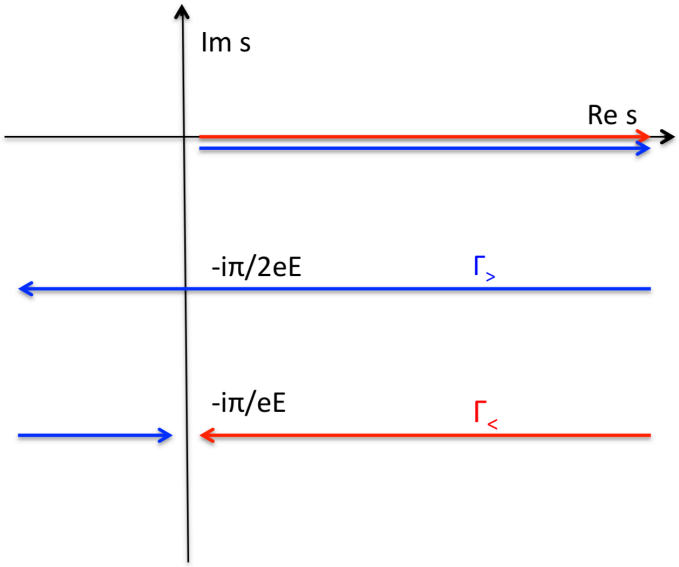

Figure 4.2: In-In propagator, $S^{\rm c}_{\rm in}$, integral contours in proper time s. There is an essential singularity about $s = -i\frac{\pi}{eE}$. $\Gamma^{>}(\Gamma^{<})$ is valid for positive (negative) z_3.

4.3.3 Schwinger Keldysh Real Time Correlators

We have in the previous section examined the in-in real-time propagator, or rather the time ordered causal correlator. However, as we saw in Sec. 3.1 there are multiple in-in correlators, Eqs. (3.19) - (3.22), one may find from an SK contour. Let us treat these here. However let us note that this section may be passed over to Sec. 4.4 for a first reading, as the discussions here are not directly used for later results. We round out our discussion by listing the remaining in-in or SK correlators; let us also note that the following correlators, like the time ordered one Eq. (4.78), were first derived in Ref. [89]. Additionally, hereafter, even equipped with all correlators, we elect to use the time-ordered propagator, Eq. (4.78), to determine real-time expectation values. Mostly, this is because in a path integral or Heisenberg notation the path-ordering would emerge naturally and thus provide a clear definition of our expectation values. Next, to address point split quantities the causal propagators provide an implicit averaging over fermion operators. Last, expectation values found from the in-in time ordered propagator, can be readily contrasted with those found from the in-out propagator. Despite the above arguments, however, one can find that any of the following SK correlation functions may be used to find equivalent results. What is more is we can confirm statistical characteristics and ensure causality of our formalism.

Let us begin by directly evaluating $S^{\bar{c}}_{in}$, which is simple considering it's relationship to S^{c}_{in}:

$$\begin{aligned} S^{\bar{c}}_{in}(x,y) &= -\gamma_0[S^{c}_{in}(y,x)]^{\dagger}\gamma_0 \\ &= (i\not{D}_x + m)\Big[\theta(-z_3)\int_{\Gamma_{>^*}} + \theta(z_3)\int_{\Gamma_{<^*}}\Big] ds\, g(x,y,s)\,. \end{aligned} \tag{4.79}$$

The contours of the in-in anti-time ordered propagator are depicted in Fig. 4.3.

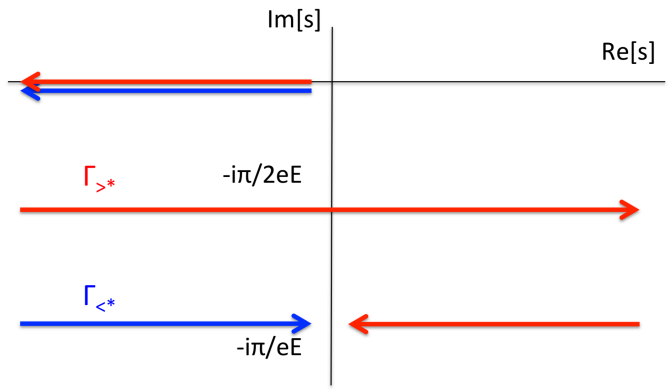

Figure 4.3: In-In anti-time propagator, $S^{\bar{c}}_{in}$, integral contours in proper time s. There is an essential singularity about $s = -i\frac{\pi}{eE}$. $\Gamma^{>^*}(\Gamma^{<^*})$ is valid for $-$ $(+)$ z_3.

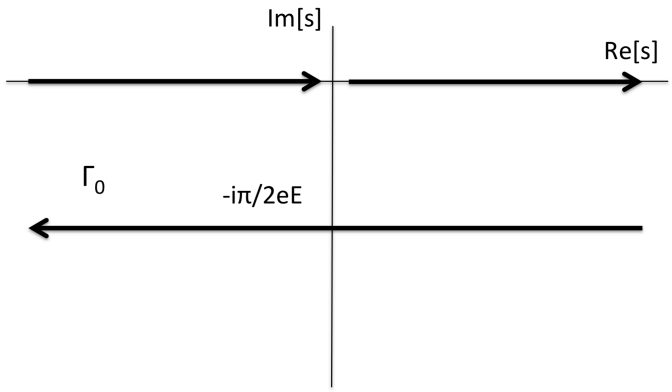

Figure 4.4: Contour about origin in proper time, s. There is an essential singularity about $s = 0$.

Then equipped with above we can quickly determine the statistical Green's function, Eq. (3.26). This is just

$$F(x,y) = (i\not{\partial}_x + m)\Big[\theta(z_3)\int_{\Gamma_>} + \theta(-z_3)\int_{\Gamma_<} - \frac{1}{2}\int_{\Gamma_0}\Big] ds\, g(x,y,s) \tag{4.80}$$

with contours similar to those given in the time ordered propagator; see Fig. 4.2. Also we have an additional contour surrounding the origin in proper time; this is given in Fig. 4.4. We can gather two things from the statistical propagator. One, this represents an averaged expression of both time and anti-time ordered expressions, and expectation values derived from it are consistent with either for equal time, $z_0 = 0$. Thus the statistical propagator may be utilized in an Wigner non-equilibrium framework capable of furnishing a Boltzmann equation [115, 116]–with Schwinger mechanism effects. This step is left for further investigation, however. Two, a statistical propagator is associated with the imaginary part of a Wightman function, and indeed we see the pieces associated with imaginary parts are consistent with the Schwinger mechanism in Eq. (4.80). However, the spectral part is associated with the real parts and let us show there is no contribution from the Schwinger mechanism there.

Let us find the other characteristic equation from a Schwinger Keldysh path: the spectral function, Eq. (3.27). Again we can do this readily. Here we use the relationship $S^{\bar{c}}_{in}(x,y) - S^{c}_{in}(x,y) = i\,\mathrm{sgn}(z_0)\rho(x,y)$, where $\mathrm{sgn}(z_0) = \theta(z_0) - \theta(-z_0)$. Let us note that by the very construction of our Dirac operators for equal time we must have $\lim_{x_0\to y_0}\rho(z) = i\delta(\vec{z})$ and therefore the $\mathrm{sgn}(z_0)$ commutes through the covariant derivative to find for the spectral propagator

$$\rho(x,y) = -i(i\not{D}_x + m)(\theta(z_0) - \theta(-z_0))\int_{\Gamma_0} ds\, g(x,y,s)\,. \tag{4.81}$$

We can confirm causality with the above expression. The vanishing of anti-commutation of a fermion and an anti-fermion operator outside the light cone serve as a measure of causality enforcement [114], and indeed the spectral propagator manifestly vanishes outside the light cone. Also, there are no Schwinger pair production effects present in the spectral correlator.

Having explored all the different types of SK contours[2], we have the necessary tools to calculate in-in real time expectation values. Yet, before calculating actual observables, it is important to discuss the physical ramifications of both in-in and in-out expectation values.

4.4 Euclidean (In-Out) and Real Time (In-In) Expectation Values

In the previous sections the in-out and in-in propagators were examined. In so doing, a suggestive glimpse into their physical nature was made visible. That is the in-in propagator contains all the squared matrix elements, (coming from the imaginary part of the in-out propagator), of any number of produced pairs. And the in-out propagator is the first term, $N = 0$, of the in-in propagator predictive of no pairs of produced particles:

$$S^{\mathrm{c}}_{\mathrm{in}} = S^{\mathrm{c}} + i\sum_{n,m}\langle a^{out}_n\psi\rangle\langle a^{\dagger\,out}_n b^{\dagger\,out}_m\rangle^*\langle b^{out}_m\bar{\psi}\rangle + \dots\,. \tag{4.84}$$

What we can gather from this expression is that while the in-in propagator predicts any number of pairs being produced in the out state the in-out propagator predicts that no particles are spawned in the out state. Let us first discuss in-in observables then we confront the more non-trivial in-out observables.

An in-in or SK formalism is well established for computing real-time out-of equilibrium observables. Indeed, using the in-in propagator, Eq. (4.4), one can see that observables follow from basic postulates of quantum mechanics; see Sec. 3.1 in the

[2] To complete the SK correlators let us write down the remaining ones; these are the Wightman functions, Eqs. (3.21) and (3.22), which can be inferred from the above correlators. They are

$$S^{>}_{in}(x,y) = (i\not{D}_x + m)\Big[\theta(z_3)\int_{\Gamma_>} + \theta(-z_3)\int_{\Gamma_<} - \theta(-z_0)\int_{\Gamma_0}\Big] ds\, g(x,y,s)\,, \tag{4.82}$$

$$S^{<}_{in}(x,y) = -(i\not{D}_x + m)\Big[\theta(z_3)\int_{\Gamma_>} + \theta(-z_3)\int_{\Gamma_<} - \theta(z_0)\int_{\Gamma_0}\Big] ds\, g(x,y,s)\,. \tag{4.83}$$

However, they are not explicitly used, but can be used as a check of the formalism.

methods chapter. A distinct merit of the SK formalism is real observables guaranteed from the hermiticity of the in-in construction,

$$\langle\langle \bar{\psi}\mathcal{O}\psi \rangle\rangle = [\langle\langle \bar{\psi}\mathcal{O}\psi \rangle\rangle]^\dagger \,; \tag{4.85}$$

this is not necessarily the case with in-out observables, however, with $\langle \bar{\psi}\mathcal{O}\psi \rangle \neq [\langle \bar{\psi}\mathcal{O}\psi \rangle]^\dagger$ for certain operators, $\mathcal{O}$. We use a complex conjugated dagger here so as to contrast the anti-time ordered element notation introduced in Eq. (4.42). Using the hermiticity of the SK formalism one can readily see that the in-in expectation values above, Eq. (4.85), integrated over space $\int d^3x$, are nothing but the definition of a quantum mechanical expectation value.

Real-time dependence follows directly from a SK contour or closed time path. In an imaginary time formalism one must give up explicit time dependence for the benefit of thermal QFT computations. However if a closed time path, such as discussion in Sec. 3.1, is connected to an imaginary time thermal state then one can make use of both explicit time dependence and thermal characteristics of the system. In our prescription, however, we have only made use of a closed time path, and our in-in propagator, Eq. (4.4), does not describe finite temperature. Doing so would amount to the insertion of a thermally equilibrated initial density matrix for some inverse temperature, β, i.e. $\sum_\alpha |in_\beta, \alpha\rangle \langle in_\beta, \alpha|$ with $\langle in| \neq \langle in_\beta|$.

Real time dependence in Eq. (4.4) emerges in a non-trivial way we will illustrate in the coming chapters. Also, for the case of a vacuum instability in homogeneous fields the real time dependence emerges not from an operator insertion at some time, but rather is a measure of the total time necessary to observe Schwinger pair production. But, moreover we can equally well show no such real time dependence resides in in-out expectation values.

Then it is a prudent question to address the physical ramifications of in-out observables. For the case of a vacuum instability present this can be challenging; in the context of cosmological pair creation it was found in Ref. [95] the metric generally contained imaginary pieces–marring physical interpretation. We too find an imaginary part in our the in-out propagator. However, with some exceptions–see the chapter on the dynamical chiral condensate in Sec. 8–the most physically translucent in-out observables in regards to pair production are real and zero. This behavior we argue is to be expected. To reiterate, while the in-in propagator predicts any number of pairs in the out state the in-out propagator is a matrix element of no pairs of generated particles from the out vacuum; Eq. (4.84). However, why should this be the case?

We argue observables found using an in-out propagator represent those of a Euclidean metric in equilibrium, or rather with zero temperature. Consider a Wick rotation of the generating in-out functional, Eq. (2.15), such that $x^0 = -ix^4$. Then the action becomes one of a Euclidean metric

$$\int_0^\beta dx^4 \int d^3x [\bar{\psi}(i\not{D} - m)\psi] \,, \tag{4.86}$$

at zero temperature, $\beta \to \infty$; one can construct an equivalent statistical QFT. We should expect that in-out observables correspond to observables in a Euclidean metric at equilibrium. Even with such a standard step found in several QFT textbooks,

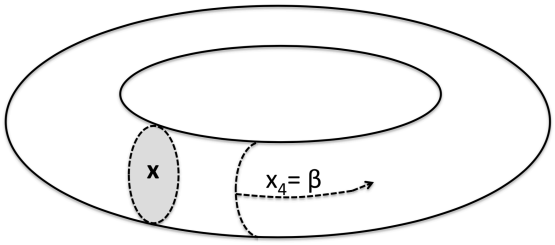

Figure 4.5: Periodicity of Euclidean vacuum states, $\langle x_4|$, for $x_4 = 0$ (in) to $x_4 = \beta$ (out) over some manifold in space, $\mathbf{x}$, at some given point in Euclidean time.

there are subtle contrasts between in-out expectation values and an equilibrium Euclidean expectation values.

The Euclidean partition function and observables derived from it possesses a periodicity in its vacuum states[3] owing to a periodicity in Euclidean time. Specifically we have

$$\langle x^4_{in} = 0| = \langle x^4_{out} = \beta| \ . \tag{4.87}$$

We can denote the periodicity of Euclidean vacuum states figuratively as in Fig. 4.5. The above distinction of vacuum states ensures a real (equilibrated) expectation value.

Turning our attention to the in-out Minkowski case, again keeping in mind Eq. (4.85), observables found using an in-out construction are simply the matrix element which predicts no pairs having been generated from the vacuum. This is in essence a scenario without pair production and with no instability and hence one is to expect in-out observables would coincide with those of a Euclidean equilibrium QFT. As before we discussed the vacuum non-persistence, Eq. (2.14), as describing a case where the vacuum stays the vacuum and anything else would predict pair production. Here as well, we have an observable which predicts a case where the vacuum will stay as a vacuum.

Strictly speaking, however, a Euclidean QFT is defined under all real fields in $U_A(1)$ and all real Hermitian real fields under a non-Abelian $SU(N)$ theory. Then the notion of a Wick rotation is not so trivial. Indeed if one were to start with a Minkowski space time background electric field E, (a real constant field), then perform a Wick rotation, one would end up with imaginary electric fields,

$$\text{Minkowski}\, E \rightarrow \text{Euclidean}\, iE \, . \tag{4.88}$$

Not only just for homogeneous fields but in fact this procedure is present for all fields whether Abelian or non-Abelian. Therefore, a vacuum instability QFT generally possesses a sign problem. Furthermore, the resulting fields are generally complex with a magnetic field and enlarge the gauge group; for example a Minkowski $SU(2)$ theory would need to accommodate imaginary pieces as well becoming $SL(2, C)$ in Euclidean space time[4]. Complex fields in a Euclidean theory are generally required to see pair production; this step serves as a starting point for many analytic tools

[3]Note the periodicity in Euclidean time and the vacuum state should not be mistaken for an anti-periodicity of Dirac determinant derived quantities such as boundary conditions on grassman variables stemming from the anti-commutivity of fermions.

[4]Lefschetz/Picard-Morse theory could potentially be used as a set of theoretical tools with which to study a gauge extension to complex values.

of pair production including the worldline instantons [103, 104]. In a non-Abelian gauge theory defined on the lattice using Monte-Carlo techniques [117], in fact it was found one may avoid the sign problem and complex fields using an opposite charged flavor isospin, which yields a real electric field. However, no pair production was seen. Also, an example of no pair production in a Euclidean theory is provided though the use of background BPST instantons [29]–different from worldline instantons. Instantons with winding number, ν, describe tunneling from a state with winding number $\langle \nu_{in}|$ to a state $\langle \nu_{out}|$ such that $\nu = \nu_{out} - \nu_{in}$ in a non-Abelian theory. QCD–or $SU(N)$ related theory–possesses a vacuum periodic in ν, with instantons being minimum energy self-dual solutions of the Yang-Mills action. But it has been determined that the fermion determinant for BPST ($\nu = 1$) instantons does not have an imaginary piece [118, 119], despite the fact that $\nu_{out} \neq \nu_{in}$. Therefore no Schwinger pair production is seen under a BPST instanton background consistent with the above Euclidean equilibrium expectation value argument.

While one may formally describe in-out expectation values as similar to Euclidean equilibrium ones, let us emphasize that still an imaginary part is present in the in-out propagator, that points to the vacuum instability. This is however not the case for the real part. No such exponentially suppressed quadratic mass term, $\exp(-\frac{n\pi m^2}{eE})$, is present for the real part. Indeed, simply examining the combined proper time structure of the above in homogeneous fields, we can conclude that the poles are bypassed. And therefore, the real part of the in-out propagator would represent a physical measurement coinciding with equilibrium.

A final difficulty of a real time, out-of-equilibrium, interpretation lies with the treatment of the background electric field itself. This problem falls under the umbrella of backreaction effects. Naïvely, the explanation is a background field must be finite and as such when pairs are produced they too must interact with and affect the background field. We have assumed a large enough field such that this issue can be ignored. We will find in the coming sections that there will be a linear time dependence in real time observables, suggesting that as time proceeds the system goes further out of equilibrium. However, as pairs are produced–such as would be expected in collider experiments–and affect the electric field, then the background field approximation fails, and indeed this step would be beyond the scope of our calculations. Furthermore, the Euclidean equilibrium interpretation is valid in the sense that no pairs are produced in the out state. Now, the in state too, (for both real time and Euclidean values), is devoid of pairs and therefore at real-time $t = 0$, we expect both the real time and Euclidean observables to coincide. Real time values are prepared in an equilibrium state.

Chapter 5

Axial Ward Identity

5.1 Pseudoscalar Condensate

5.1.1 Euclidean Equilibrium

Equipped with the in-out, Eq. (4.14), and in-in, Eq. (4.77), propagators we may readily illustrate in and out-of-equilibrium phenomena through investigating the axial Ward identity, Eq. (2.27).

In homogeneous fields the VEV behavior of $\epsilon^{\mu\nu\alpha\beta}F_{\mu\nu}F_{\alpha\beta}$ is trivial; i.e. $\langle\epsilon^{\mu\nu\alpha\beta}F_{\mu\nu}F_{\alpha\beta}\rangle = \langle\!\langle\epsilon^{\mu\nu\alpha\beta}F_{\mu\nu}F_{\alpha\beta}\rangle\!\rangle = \epsilon^{\mu\nu\alpha\beta}F_{\mu\nu}F_{\alpha\beta}$. And therefore our primary consideration belongs to the pseudoscalar condensate portion.

Owing to the virtue of Schwinger proper time the pseudoscalar can easily be calculated. Indeed Schwinger first performed this for the interaction between the neutral meson and proton in Ref. [15]. Let us repeat this in-out calculation.

$$\bar{P} \coloneqq \langle\bar{\psi}i\gamma_5\psi\rangle = -\lim_{y\to x}\mathrm{tr}[\gamma_5 S^c(x,y)]\,. \tag{5.1}$$

Taking the Dirac trace we find the $\not{D}$ term will not contribute due to an odd number of gamma matrices being traced over. More generally, $\not{D}$ acting on the kernel, Eq. (4.38), for point split expectation values will vanish and this is due to translational invariance; $g(x,y) = g(x-y)$. Moreover, we see upon taking the trace that contributions coming from the bosonic part, Eq. (4.25), cancel with those coming from the spin factor, Eq. (4.24). While there are essential singularities in φ from the cotangent function, all vanish upon taking the limit. The essential singularity and poles will be handled judiciously below. We find for the in-out Euclidean equilibrated pseudoscalar condensate the following:

$$\begin{aligned}\bar{P} &= -\lim_{y\to x} 4i\frac{me^2EB}{(4\pi)^2}\int_0^\infty ds\, e^{-im^2s+i\varphi(x,y,s)} \\ &= -\frac{e^2EB}{4\pi^2 m}\,.\end{aligned} \tag{5.2}$$

What is profound about $\bar{P}$ is its cancellation with $\epsilon^{\mu\nu\alpha\beta}F_{\mu\nu}F_{\alpha\beta}$ in the axial Ward identity,

$$\partial_0\bar{n}_5 = 0\,, \tag{5.3}$$

for any m! It is common to omit the pseudoscalar term in the QCD Lagrangian when examining small mass scenarios, however, we find here that the pseudoscalar term plays a critical role. What is more, as the above expectation value is valid for any mass we are left with an apparent contradiction in comparison with the physically motivated LLLA result reasoned above, Eq. (2.24). In fact, in the zero mass limit, one would expect for the physically motivated case

$$\omega \overset{B\gg E,\, m\to 0}{\longrightarrow} \frac{e^2EB}{4\pi^2} = \frac{1}{2}\partial_0 n_5 \,. \tag{5.4}$$

As alluded to above, there is in fact no contraction. The in-out expectation value is one of an equilibrium scenario, or defined in Euclidean spacetime, and does not factor in non-equilibrium phenomena like the Schwinger mechanism. Thus the in-out pseudoscalar condensate, Eq. (5.2) and in-out axial Ward identities, Eq. (5.3), are values to be expected in the absence of Schwinger produced pairs.

Having seen that there is no anomaly, or that the axial Ward identity is zero and chirality be conserved, for homogeneous parallel fields in Euclidean equilibrium, let us illustrate how the anomaly arises out-of-equilibrium utilizing the real-time or in-in formalism.

5.1.2 Real-Time

Before embarking on explicit real-time calculations, let us motivate real-time observables by recapping essential points of the expected chirality generation from the Schwinger mechanism. Out-of-equilibrium the Schwinger mechanism in parallel electric and magnetic fields should continually produce particle anti-particle pairs along the fields. Since it was found the non-persistence of the vacuum, Eq. (2.21), should go to linear order in time, one would expect out-of-equilibrium expectation values such as the generated current should also go to linear order in time. Then, for a strong magnetic field, the produced pairs would have their spins aligned with the magnetic field, generating chirality. The essential calculation to illustrate this is with the divergence of the chiral density current (or the axial Ward identity); we do that here. Later, we explicitly support our pseudoscalar calculations with calculations of the chiral density, Sec. 5.2.2.

As anticipated in the previous section we may directly calculate the real-time or out-of-equilibrium expectation values associated with the Schwinger mechanism using the in-in propagator, Eq. (4.77), and confirm the physically motivated case, Eq. (2.24). Following similar steps as in the equilibrium case we may arrive at

$$\begin{aligned} P &\coloneqq \langle\!\langle \bar{\psi} i\gamma_5 \psi \rangle\!\rangle = -\lim_{y\to x} \mathrm{tr}[\gamma_5 S^c_{in}(x,y)] \\ &= -\lim_{y\to x} i\frac{me^2EB}{4\pi^2}\left[\theta(z_3)\int_{\Gamma_>} + \theta(-z_3)\int_{\Gamma_<}\right] ds\, e^{-im^2 s + i\varphi(x,y,s)} \,. \end{aligned} \tag{5.5}$$

The pseudoscalar condensate is unaffected by regularization and this fact is reflected in the fact that we may use either $\Gamma_>$ or $\Gamma_<$ (or both averaged) in its calculation. Here, we elect to use a point split averaged notation. The Green's function is defined in a symmetric fashion when evaluated at common points i.e., $S(x,x) = \frac{1}{2}[S(x,x+0) + S(x+0,x)]$. This also yields $\lim_{y\to x}\theta(\pm z_3) = 1/2$. Again the pole contributions cancel out here as well upon taking the limit. We may deform the

contour to arrive at an expression indicative of the addition of Schwinger effects. We ultimately find

$$\begin{aligned} P &= -4i\frac{me^2EB}{(4\pi)^2}\left[\int_0^\infty ds - \int_{-i\frac{\pi}{eE}}^{\infty - i\frac{\pi}{eE}} ds\right] e^{-im^2 s} \\ &= -\frac{e^2EB}{4\pi^2 m}\left[1 - e^{-\pi m^2/(eE)}\right], \end{aligned} \tag{5.6}$$

which decidedly predicts the generation of chirality from the Schwinger mechanism. Naturally, there is perfect agreement with the expression Eq. (2.24). Using the axial Ward identity, Eq. (2.26), under in-in vacuum states the divergence of the chiral density in real-time is found as

$$\partial_0 n_5 = \frac{e^2EB}{2\pi^2} e^{-\pi m^2/(eE)}\,. \tag{5.7}$$

Amazingly we find no other contributions to the axial Ward identity than the Schwinger mechanism, indicating that indeed the mechanism is solely responsible for the anomalous generation of chirality. Let us also note here that Eq. (5.6) was inferred in Ref. [120] from the Schwinger mechanism. Here however we make clear the difference in vacuum state expectation values.

Using the real-time formalism we arrive at the generated chiral density directly in an independent calculation to confirm the above. Likewise, we also show the absence for the in-out equilibrium case. But first, let us shortly digress on the utility of Schwinger proper time methods for handling observables like the pseudoscalar condensate.

Fujikawa first formulated [1] the anomaly as arising from the measure in the path integral. There, careful regulation is required in defining the functional trace of γ_5. Of most relevant for our discussion, in the Fujikawa method the following is utilized (here we are in a Euclidean spacetime)

$$\mathrm{tr}(\gamma_5 e^{\frac{1}{2}eF_{\mu\nu}\sigma^{\mu\nu}/M^2}) = \frac{i}{2M^4}\epsilon^{\mu\nu\alpha\beta}F_{\mu\nu}F_{\alpha\beta} \tag{5.8}$$

to regulate the trace of γ_5. A large cutoff mass, M, is used and only the leading terms in M are considered above. Contrast this with the trace taken in pseudoscalar calculation. We found

$$\mathrm{tr}(\gamma_5 \mathcal{P} e^{-i\int_0^s d\tau \frac{1}{2}eF_{\mu\nu}\sigma^{\mu\nu}}) = 4i\sin(eBs)\sinh(eEs), \tag{5.9}$$

Here we are in Minkowski spacetime and the fields are constant; and upon a Wick rotation in τ and large s limit we can find Fujikawa's result, Eq. (5.8). But what is important here is that without the Schwinger proper time realization one would find a trivial result. This is because the proper time method naturally incorporates a heat kernel regularization. And thus the proper time formulation not only easily enables (as we discovered above) but also handles the non-trivial regularization within calculations with γ_5 and concerning chirality.

5.2 Chiral Density

5.2.1 Euclidean Equilibrium

Having discussed the benefit of the worldline formalism and how it enables calculations such as the equilibrium and real-time pseudoscalar we now confirm our results by calculating the chiral density equivalents. Of particular importance, we see how time dependence arises in real-time through the phase space. However, before that let us ensure the Euclidean equilibrated chiral density,

$$\bar{j}_5^\mu := \langle \bar{\psi}\gamma^\mu\gamma_5\psi\rangle = i\lim_{y\to x}\mathrm{tr}[\gamma^\mu\gamma_5 S^c(x,y)]\,, \tag{5.10}$$

vanishes.

We may immediately take the Dirac trace, and so find that only the covariant derivative piece of the propagator contributes.

$$\bar{j}_5^\mu = -i\lim_{y\to x}\mathrm{tr}[\gamma^\mu\gamma_5 \not{D}_x \int_0^\infty ds\, g(x,y,s)]\,. \tag{5.11}$$

We expect the equilibrium chiral current to vanish due to translational invariance of the Green's function, and hence kernel, g. But let us illustrate this. First allowing the derivative to act on the kernel we find

$$\begin{aligned}\not{D}_x g(x,y,s) &= (\partial_\mu - \frac{i}{2}eF_{\mu\nu}x^\nu)\gamma^\mu g(x,y,s)\\ &= -\frac{1}{2}\Big[ieF_{\mu\nu} + (\coth(eFs)eF)_{\mu\nu}\Big]z^\nu\gamma^\mu g(z,s)\,.\end{aligned} \tag{5.12}$$

We can gather that so long as the kernel remain analytic and finite as $x\to y$ or $z\to 0$ then due to the z out front the above expression will vanish in the limit. This is clearly the case outside of the singularities in g, and it also case for the singularities, but requires more effort. First let us close the proper time contour as depicted in Fig 5.1. There is a semicircle contour about $-i\frac{k\pi}{eE}\,\forall\, k\in\mathbb{R}^+$. However we have an essential singularity in the classical piece of the kernel, $\varphi(z,s)$, Eq. (4.32). For a semicircle contour about $-i\frac{k\pi}{eE}$ on the kernel the following residue may be found

$$-i\pi\mathrm{Res}\Big(g,-i\frac{k\pi}{eE}\Big) = \frac{-i\pi}{(k-1)!}\lim_{s\to 0}\frac{d^{k-1}}{ds^{k-1}}\Big[\Big(s+\frac{ik\pi}{eE}\Big)g(s)\Big]\,. \tag{5.13}$$

However, it can be seen that any such term after being acted on by the covariant derivative will contain some power of z and hence

$$\lim_{y\to x}\not{D}_x\,\mathrm{Res}\Big(g,-i\frac{k\pi}{eE}\Big) = 0\,. \tag{5.14}$$

Pieces of integration between the essential singularities can be seen to also vanish in the $z\to 0$ limit. Therefore we find as expected the equilibrium chiral density vanishes,

$$\bar{j}_5^\mu = 0\,. \tag{5.15}$$

in agreement with the pseudoscalar computation. This, however, is not the case out-of-equilibrium.

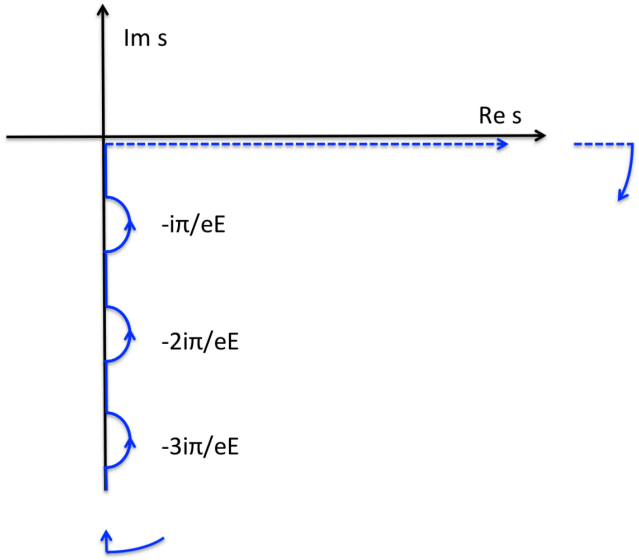

Figure 5.1: Contour of proper time, s, to imaginary values after Wick rotation. Contributions on the semicircle $|s| \to \infty$ vanish owing to convergence provided by the $m^2 - i\epsilon$ term in the worldline action. Imaginary parts of the kernel are associated with singularities at $s = -in\pi/eE$, and the principal part of the kernel is associated with regions in-between singularities.

5.2.2 Real-Time

The real-time chiral density reads

$$j_5^\mu := \langle\!\langle \bar{\psi}\gamma^\mu\gamma^5\psi \rangle\!\rangle = i \lim_{y\to x} \mathrm{tr}[\gamma^\mu\gamma_5 S_{in}^c(x,y)] \,. \tag{5.16}$$

We can make similar manipulations with the Dirac trace as before to find

$$j_5^\mu = -i \lim_{y\to x} \mathrm{tr}[\gamma^\mu\gamma_5 \not{D}_x \int_{in} ds\, g(x,y,s)] \,. \tag{5.17}$$

The essential difference here as opposed to the Euclidean equilibrium case discussed earlier is the addition of $\theta(\pm z_3)$ terms, and upon being acted on by the covariant derivative give rise to a phase space term identifiable with real time. Let us first, though, press on with the calculation, particularly around the singularity.

Proceeding with the calculation of the real-time chiral density, we see that the integration contours can be subtracted with a semicircle contour about the singularity $-i\pi/eE$; see Fig. 7.1. However here, we only have the upper half contour of the singularity about $-i\pi/eE$ as opposed to entire contour about $-in\pi/eE$. Recall the above argument about the singularities in g, Eq. (5.13). There every term contained some power of $z_3^2 - z_0^2$ and therefore vanished in the $z \to 0$ limit. However, here we have the covariant derivative not acting on the kernel and we find non-vanished pieces. They are the pieces that contain a hyperbolic sine factor in the spin factor, Eq. (4.24). Let us illustrate this with the following integral:

$$I_h = \int_h ds\, e^{-im^2 s + i\varphi(x,y,s)} \cot(eBs) \coth(eEs) \,. \tag{5.18}$$

First we shift the proper time s by $s \to s' + \frac{i\pi}{eE}$, keeping only the leading terms in the integrand. The origin of the semicircle contours is shifted to $s = 0$ by this process. Even though there is an essential singularity here, keeping the leading terms here does reproduce the exact result when the $x \to y$ limit is taken. Later we will need to keep all orders.

$$I_h = e^{-\frac{i}{2}xFy - \frac{m^2\pi}{eE} - \frac{1}{4}(z_1^2+z_2^2)eB\coth(-\frac{\pi B}{E})} \frac{i\coth(\frac{\pi B}{E})}{eE} \int_{h+i\frac{\pi}{eE}} \frac{ds}{s} e^{-\frac{i}{4s}(z_0^2-z_3^2)} \,. \tag{5.19}$$

Now redefining $\eta = 1/s$ we can find

$$\int_{h+i\frac{\pi}{eE}} \frac{ds}{s} e^{-\frac{i}{4s}(z_0^2-z_3^2)} = \int_{-\infty}^{\infty} \frac{d\eta}{\eta} e^{-\frac{i}{4}(z_0^2-z_3^2)\eta} = -2\pi i\,\theta(z_3^2 - z_0^2) \tag{5.20}$$

the Heaviside step function. The integral becomes

$$I_h = e^{-\frac{m^2\pi}{eE}} \frac{2\pi}{eE} \coth\!\left(\frac{\pi B}{E}\right)\theta(z_3^2 - z_0^2) \,. \tag{5.21}$$

We may perform a similar set of calculations but without the $\coth(eEs)$ factor

$$\begin{aligned} &\int_h ds\, e^{-im^2 s + i\varphi(x,y,s)} \cot(eBs) \\ &= e^{-\frac{m^2\pi}{eE}} \frac{i\pi}{2} \coth\!\left(\frac{\pi B}{E}\right)(z_3^2 - z_0^2)\,\theta(z_3^2 - z_0^2) \,, \end{aligned} \tag{5.22}$$

which goes to zero after taking its derivative then the $\lim_{x\to y}$. Integrals without the $\cot(eBs)$ can be found by replacing the above final expression with $\coth(eBs) \to -i$. Note, the above result may also be found by closing the semicircle contour to a full closed contour about $-i\pi/eE$, $\int_{\gamma_h} ds = \theta(z_3^2 - z_0^2) \int_{\gamma_f} ds$; see Fig. 7.1. Then one may apply the residue formula, Eq. (5.13), where all higher order contributions from the essential singularity will vanish.

Now we take the Dirac trace, keeping only pieces of the spin factor which contain a $\cosh(eEs)$, (which gives us a $\coth(eEs)$ factor in the integrand). We find

$$\begin{aligned} \mathrm{tr}\gamma_0\gamma_5 \not{D} \exp(-\frac{i}{2}eF\sigma s) = D_\nu \Big[&i\sin(eBs)\cosh(eEs)\,\mathrm{tr}(\gamma_0\gamma_5\gamma^\nu\sigma^{12}) \\ &- \frac{1}{2}\sin(eBs)\sinh(sEs)\,\mathrm{tr}(\gamma_0\gamma_5\gamma^\nu\gamma_5\sigma^{12}) + \cos(eBs)\sinh(eEs)\,\mathrm{tr}(\gamma_0\gamma_5\gamma^\nu\gamma_5\sigma^{12})\Big] \,. \end{aligned} \tag{5.23}$$

Only the top term above with the $\cosh(eEs)$ will remain as it is the only one with a non-vanishing singularity after taking the $x \to y$ limit. Then we have for the chiral current

$$j_5^\mu = \lim_{x\to y} i\frac{e^2 EB}{4\pi^2} \partial^3\theta(z_3)\delta_3^\mu \int_h ds\, \coth(eEs) e^{-im^2 s + i\varphi(x,y,s)} \,. \tag{5.24}$$

We can now see the key difference of the real-time expression here is the introduction of a theta term, $\theta(\pm z_3)$, indicative of time dependence in our system. The delta term here is a measure of the phase space of the system, and we identity it with total

time dependence, t, in our system.

$$\lim_{y\to x}\delta(z_3)=\lim_{y\to x}\int\frac{dp_3}{2\pi}e^{ip^3z^3}=\frac{eEt}{2\pi}. \tag{5.25}$$

In a homogeneous field, such identification is just [121]. Consider the quantum mechanical setup in homogeneous fields. One would have two harmonic oscillator solutions for both the electric and magnetic parts. The electric field harmonic oscillator would have energies independent of p_3 due to a quadratic shift, and the wavepacket position in time would be shifted by p_3/eE. Then one could envision an integration over all p_3, (as is done in effective action calculations), as being analogous over one of total time. Alternatively, we can also understand this from a classical perspective as well. Consider a pair being accelerated by a electric field in the 3-axis direction, then knowledge of the pairs' p_3 (given at some time, t, assumed from a static initial state) would give us a measure of the total time in the system. This is because at some initial time, the kinetic momentum of the pairs is zero, which implies $p_3 = eEt$.

We finally find for the real-time chiral density

$$j_5^\mu=\frac{e^2EB\,t}{2\pi^2}\exp\Big(-\frac{\pi m^2}{eE}\Big)\delta_3^\mu\,, \tag{5.26}$$

where we have used Eq. (5.25) and Eq. (5.21), (replacing $\coth(\pi B/E)$ with $-i$). Then the divergence of the chiral current is completely in agreement with the psuedoscalar and the axial Ward identity.

It is curious why one ought to see a vanishing chiral density. To address this let us note that $\partial_0\bar{n}_5 = 0$ in a Euclidean picture, i.e. $\langle\partial_4\, j_5^4\rangle = 0$. Then let us consider Euclidean ground state for the $m = 0$ case. There topological properties are independent of the θ angle and hence one would not expect a nonzero topological charge and or net chirality. Before embarking on the qualitative differences between the in-out and in-in expectation values let us examine the vector current to ensure similar findings for the CME.

Chapter 6

Chiral Magnetic Effect

6.1 Euclidean Equilibrium

Above we found the Euclidean equilibrated chiral density vanished and equilibrium in-out pseudoscalar condensate also showed a vanishing anomaly. It is then an important task to verify similar behavior also for the CME current. The CME current should be entirely contained in our in-out and in-in formalisms, i.e. no artificial placement of chirality or a chiral chemical potential should be necessary. All the chirality generated we found before was spawned through the Schwinger mechanism in parity violating fields.

Proceeding as before we may calculate the vector current using in-out and in-in vacuum states. These are

$$\bar{j}^{\mu} := \langle \bar{\psi}\gamma^{\mu}\psi \rangle = i \lim_{y\to x} \mathrm{tr}\Big[\gamma^{\mu} S^{\mathrm{c}}(x,y)\Big]\,, \tag{6.1}$$

$$j^{\mu} := \langle\!\langle \bar{\psi}\gamma^{\mu}\psi \rangle\!\rangle = i \lim_{y\to x} \mathrm{tr}\Big[\gamma^{\mu} S^{\mathrm{c}}_{\mathrm{in}}(x,y)\Big]\,. \tag{6.2}$$

Once again, here the mass portion of the Dirac trace vanishes and we are left with the following

$$\bar{j}^{\mu} = -i \lim_{y\to x} \mathrm{tr}[\gamma^{\mu} \not{D}_x \int_0^{\infty} ds\, g(x,y,s)]\,, \tag{6.3}$$

$$j^{\mu} = -i \lim_{y\to x} \mathrm{tr}[\gamma^{\mu} \not{D}_x \int_{in} ds\, g(x,y,s)]\,. \tag{6.4}$$

Let us address the in-out current first. Using arguments in the calculation of the chiral density, namely that the covariant derivative acting on the kernel both outside of the poles and around the poles, Eq. (5.14), vanishes. Thus like the equilibrium chiral density the equilibrium CME current too vanishes:

$$\bar{j}^{3} = 0\,. \tag{6.5}$$

Using similar arguments one may also verify that indeed all the equilibrium current vanishes, $\bar{j}^{\mu} = 0$.

As we analyzed before there were no matrix element contributes of out state generated particles and thus it is easy to see that no current would arise. There is no insertion of a chiral chemical potential, or other device which mimics an out-

of-equilibrium scenario either. All the generated current as we found for the chiral density must be sourced through an out-of-equilibrium real-time prescription.

6.2 Real-Time

The CME current, as anticipated, for the real-time expectation value does not vanish as we will show. The calculations here are similar to the real-time chiral density case, therefore we only give a brief overview here. First, let us confirm that for the produced pairs we have charge conservation and that only the x_3 direction current remains. The only other term possessing z_0 dependence vanishes, namely $\partial^0\theta(z_3^2 - z_0^2) = 0$, where we have used the identity $\theta(z_3^2 - z_0^2) = \theta(z_0 + z_3)\theta(-z_o + z_3) + \theta(-z_0 - z_3)\theta(z_0 - z_3)$. Likewise, there is no contribution coming from the poles in the kernel, Eq. (5.14). Next, let us take the Dirac trace noting that

$$\begin{aligned}\mathrm{tr}\gamma^\mu \not{D} e^{-\frac{i}{2}eF\sigma s} = 4D_\nu\Big\{&\cos(eBs)\cosh(eEs)g^{\mu\nu} \\ &- \sin(eBs)\cosh(eEs)(-g^{\mu 1}g^{\nu 2} + g^{\mu 2}g^{\nu 1}) - \cos(eBs)\sinh(eEs)\epsilon^{\mu\nu 12}\Big\}\,. \end{aligned} \tag{6.6}$$

Only the first term with D_3 remains as the other terms do not posses any poles. Gathering all the terms we find consistency with Schwinger's formula, Eq. (2.23), using Eq. (5.25) and Eq. (5.21),

$$\begin{aligned} j^\mu &= \lim_{x\to y}\frac{e^2EB}{4\pi^2}\partial^3\theta(z_3)I_h(z_3,z_0)\delta_3^\mu \\ &= \frac{e^2EB\,t}{2\pi^2}\coth\Big(\frac{\pi B}{E}\Big)\exp\Big(-\frac{m^2\pi}{eE}\Big)\delta_3^\mu \\ &= 2\omega\,t\,. \end{aligned} \tag{6.7}$$

All the chirality (for a strong magnetic field) generated through the Schwinger mechanism is converted into an electromagnetic current parallel to the magnetic field: the CME. Indeed, it was inferred in Ref. [13] through a Lorentz transformation of Schwinger's formula a similar catalysis of the CME. The above, as are the real-time chiral density and pseudoscalar condensate, is one-loop exact and all Landau levels have been kept.

Here too, in addition to the chiral density, equilibrium observables of the CME vanish. As we found before in an Euclidean setting there can be no chirality generation and hence no CME. Indeed, the vanishing of the CME in equilibrium has been noted elsewhere, see e.g. Ref. [122], yet that the out-of-equilibrium CME can stem from the vacuum instability is new here. And we correctly see that to see the CME real-time physics is a necessity.

Then it is important to see why in some cases even in equilibrium the CME is observed, and this is due to a finite μ_5 inserted by hand. However, μ_5 is an inherently out-of-equilibrium quantity, and even though a contradiction may be present in some applications, the insertion of μ_5 is an indispensable theoretical tool.

Chapter 7

Chiral Density Fluctuations

Having elucidated the effects of chirality generation as well as the CME due to Schwinger pair production it is prudent that we confirm similar behavior in chiral density fluctuations, also referred to as a chiral susceptibility. A measure of the chiral fluctuations is important in systems in which a chirality imbalance may be present locally, however globally is conserved. An example setting is provided in the context of heavy-ion collisions. There for a single collision event or an average over many collision events it is thought local parity violation may occur [24, 25], giving way to an observable signal for the CME. Specifically, fluctuations in the topological charge are related to an electric charge separation in the direction of the magnetic field. What is observable is then fluctuations in the charge density; this is made possible by virtue of the CME relating topology to a measurable electric current. However, for our purposes of chirality generation via the Schwinger mechanism it is essential that we rather show chiral density fluctuations be non-vanishing, and then one may relate such a chiral imbalance to the CME as was put forth in Sec. 3.3.4. Also it is important that we confirm the role the Schwinger mechanism plays in the fluctuations as well as its real-time dependence.

The chiral density fluctuations in real-time and in equilibrium

$$\chi_5 := \langle\langle N_5^2 \rangle\rangle - \langle\langle N_5 \rangle\rangle^2 \,, \tag{7.1}$$

$$\bar{\chi}_5 := \langle N_5^2 \rangle - \langle N_5 \rangle^2 \,, \tag{7.2}$$

where $N_5 \coloneqq \int d^3x \bar{\psi}(x)\gamma^0\gamma_5\psi(x)$. In heavy-ion collisions while chirality is conserved globally local fluctuations in chirality may provide observable effects averaged over many events.

$$\chi_5 = \lim_{x_0 \to y_0} \int d^3x d^3y \ \mathrm{tr}[\gamma_0\gamma_5 S^{\mathrm{c}}_{\mathrm{in}}(x,y)\gamma_0\gamma_5 S^{\mathrm{c}}_{\mathrm{in}}(y,x)]$$

$$= \tag{7.3}$$

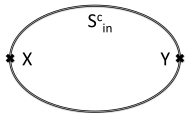

And we may also define here the equilibrium value as well,

$$\bar{\chi}_5 = \lim_{x_0 \to y_0} \int d^3x d^3y \, \mathrm{tr}[\gamma_0\gamma_5 S^{\mathrm{c}}(x,y)\gamma_0\gamma_5 S^{\mathrm{c}}(y,x)] \,. \tag{7.4}$$

Due to the presence of a finite spatial $\vec{z}$ in the propagators, calculations here are somewhat more involved, (but introduce no new methods than employed previously). The final form of the chiral density fluctuations both for the real-time and Euclidean equilibrium cases can be seen in Eq. (7.63).

Let us proceed with the calculation in equilibrium Eq. (7.4) and out-of-equilibrium Eq. (7.3), where the respective correlation functions can found from Eqs. (4.14) and (4.77). Taking note that the traces of an odd number of Dirac matrices vanishes we find for the real-time observable

$$\chi_5 = -\lim_{x_0\to y_0}\int d^3x d^3y\ \mathrm{tr}\Big[\gamma_0 \not{D}_x \int_{in} ds\, g(x,y,s)\gamma_0 \not{D}_y \int_{in} ds'\, g(y,x,s')\Big] - \lim_{x_0\to y_0} m^2 \int d^3x d^3y\, \mathrm{tr}\Big[\gamma_0 \int_{in} ds\, g(x,y,s)\gamma_0 \int_{in} ds'\, g(y,x,s')\Big]\,. \tag{7.5}$$

Unlike before when calculating expectation values, such as the chiral density and current, in which the $x_\mu \to y_\mu$ limit was taken, here $\not{D}_x g(x,y,s)$ provides a contribution (except for $x_0 \to y_0$). However, let us first look at the side which contains covariant derivative pieces and eliminate a few terms. Note that the derivative acting on $\int_{in} ds$ yields a delta function. Moreover, we find a term that contains $\mathrm{tr}[\gamma_0(\not{\partial}_x \int_{in} ds)g(x,y,s)\gamma_0 \int_{in} ds'(\not{D}_y g(y,x,s'))]$, and this term we can show vanishes. First notice that when the covariant derivative acts on the kernel we aquire a linear term in z_μ in the integrand; see Eq. (5.12). Then, for the term in question, there are integrals over z_1 and z_2

$$\int dx_1 dx_2 dy_1 dy_2 z^{1,2} e^{-\frac{i}{4}eB(z_1^2+z_2^2)[\cot(eBs)+\cot(eBs')]}\,.$$

The poles in the cotangent functions are not picked up, and these integrals are gaussian with a linear $z^{1,2}$ term and thus vanish. Likewise the z^0 term in the covariant derivative equation above will also vanish due to the $x_0 \to y_0$ limit. In a similar way, we will acquire a delta function from the $(\not{\partial}_x \int ds)$ term which will give us an $x_3 \to y_3$ limit upon acting on the integral, and then the $x_3 \to y_3$ limit acting on z^3 in the covariant derivative term will also vanish. We are left with for the real-time chiral density fluctuations

$$\chi_5 = \mathcal{I}_t + \mathcal{I}_D + \mathcal{I}_m \tag{7.6}$$

$$\mathcal{I}_t := -\lim_{x_0\to y_0}\int d^3x d^3y \Big\{\mathrm{tr}\Big[\gamma_0(\not{\partial}_x \int_{in} ds)g(x,y,s)\gamma_0(\not{\partial}_y \int_{in} ds')g(y,x,s')\Big]\Big\} \tag{7.7}$$

$$\mathcal{I}_D := -\lim_{x_0\to y_0}\int d^3x d^3y \Big\{\mathrm{tr}\Big[\gamma_0 \int_{in} ds(\not{D}_x g(x,y,s))\gamma_0 \int_{in} ds'(\not{D}_y g(y,x,s'))\Big]\Big\} \tag{7.8}$$

$$\mathcal{I}_m := -\lim_{x_0\to y_0}\int d^3x d^3y\, m^2 \Big\{\mathrm{tr}\Big[\gamma_0 \int_{in} ds\, g(x,y,s)\gamma_0 \int_{in} ds'\, g(y,x,s')\Big]\Big\}\,. \tag{7.9}$$

Also, we may perform a similar analysis on the equilibrium quantity:

$$\bar{\chi}_5 = \bar{\mathcal{I}}_D + \bar{\mathcal{I}}_m \tag{7.10}$$

$$\bar{\mathcal{I}}_D := -\lim_{x_0\to y_0}\int d^3x d^3y \Big\{\mathrm{tr}\Big[\gamma_0 \int_0^\infty ds(\not{D}_x g(x,y,s))\gamma_0 \int_0^\infty ds'(\not{D}_y g(y,x,s'))\Big]\Big\} \tag{7.11}$$

$$\bar{\mathcal{I}}_m := -\lim_{x_0\to y_0}\int d^3x d^3y\, m^2 \Big\{\mathrm{tr}\Big[\gamma_0 \int_0^\infty ds\, g(x,y,s)\gamma_0 \int_0^\infty ds'\, g(y,x,s')\Big]\Big\}\,. \tag{7.12}$$

Let us treat in the following each set of integrals separately.

7.1 Time Dependent Portion

Let us look at the piece which yields a time dependence, $\mathcal{I}_t$. All time dependence, as we found originated from a phase space factor, is in fact contained in this term. Moreover, no such term is present in the in-out equilibrium calculation. It is convenient here and throughout this section to adopt a closed form of the proper time contour. This is to ensure in the $z \to 0$ limit no contribution from the kernel about the full closed contour will contribution after being acted by the derivative. We find the time dependent piece becomes

$$\begin{aligned}\mathcal{I}_t &= -\lim_{x_0\to y_0}\int d^3x d^3y\,\mathrm{tr}\Big[\gamma_0(\not{\partial}_x\Theta(z))\int_{\gamma^f} ds\, g(x,y,s)\gamma_0(\not{\partial}_y\Theta(-z))\int_{\gamma^f} ds'\, g(y,x,s')\Big]\\ &= -\lim_{x_0\to y_0}\int d^3x d^3y\delta(z_3)^2\,\mathrm{tr}\Big[\gamma_0\gamma^3(2\theta(z_3)+1)\int_{\gamma^f} ds\\ &\quad\times g(x,y,s)\gamma_0\gamma^3(2\theta(-z_3)+1)\int_{\gamma^f} ds'\, g(y,x,s')\Big]\,. \end{aligned} \tag{7.13}$$

$\Theta(z) = \theta(z_3)\theta(z_3^2 - z_0^2)$. Let us examine the squared delta function for arbitrary function, f, as

$$\int d^3x d^3y\delta(z_3)^2 f(x-y) = \lim_{z_0,z_3\to 0}\frac{eEVt}{\pi}\int d^2z f(z)\,. \tag{7.14}$$

The above integrals become upon taking the Dirac trace

$$\begin{aligned}\mathcal{I}_t &= \lim_{z_0,z_3\to 0}\frac{eEVt}{2\pi}\Big(\frac{e^2EB}{4\pi^2}\Big)^2\int d^2z\\ &\times\Big\{\Big[\int_{\gamma^f} ds e^{-im^2s+i\varphi(z,s)}\cot(eBT)\coth(eET)\Big]^2 - \Big[\int_{\gamma^f} ds\, e^{-im^2s+i\varphi(z,s)}\coth(eET)\Big]^2\Big\}\,.\end{aligned} \tag{7.15}$$

The singularities here are similar to those before; please see the contours listed above. Now we only take the z_0 and z_3 limits, however that is sufficient to remove higher order pieces coming from the essential singularity. We ultimately find

$$\begin{aligned}\mathcal{I}_t &= -\frac{eEVt}{2\pi}\Big(\frac{e^2EB}{4\pi^2}\Big)^2\int d^2z\\ &\quad\times\Big\{-\Big[\frac{2\pi}{eE}e^{-\frac{m^2\pi}{eE}}\coth\Big(\frac{B\pi}{E}\Big)e^{-\frac{1}{4}(z_1^2+z_2^2)eB\coth(B\pi/E)}\Big]^2\\ &\quad-\Big[\frac{2\pi}{eE}e^{-\frac{m^2\pi}{eE}}e^{-\frac{1}{4}(z_1^2+z_2^2)eB\coth(B\pi/E)}\Big]^2\Big\}\\ &\approx \frac{e^2EBVt}{2\pi^2}\exp\Big(-\frac{2m^2\pi}{eE}\Big)\,,\end{aligned} \tag{7.16}$$

where the LLLA has been taken in the last step. Again we see that the characteristic exponential quadratic mass suppression and time dependence have appeared. That the time be linear is guaranteed from our construction, and even though we are performing a loop calculation linear time independence is to be expected.

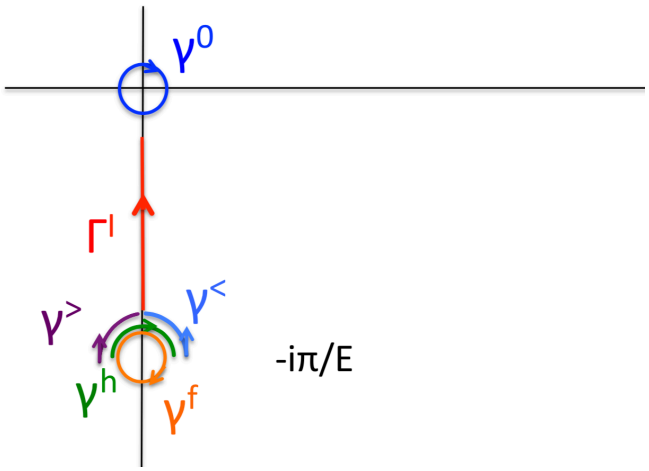

Figure 7.1: Various contours used to calculate chirality fluctuations. Vertical axis is imaginary s.

7.2 Quadratic Mass Portion

Let us now tackle the quadratic mass portion of the anomalous fluctuations, $\mathcal{I}_m$. Also, in this section and the next for compact expressions we take for the product of two similar expressions for arbitrary function, f, the following notation: $[f(z)][x \rightleftharpoons y] \coloneqq f(z,s)f(-z)$. Let us first take the Dirac trace and LLLA finding

$$\mathcal{I}_m \approx 2\left(\frac{me^2EB}{8\pi^2}\right)^2 \int d^3x d^3y \times \left\{\left[\int_{in} ds\, e^{-im^2 s + i\varphi(x,y,s)} \coth(eEs)\right]\left[x \rightleftharpoons y\right] - \left[\int_{in} ds\, e^{-im^2 s + i\varphi(y,x,s)}\right]\left[x \rightleftharpoons y\right]\right\}, \tag{7.17}$$

where we have used the fact that $\varphi(x,y,s)$ is quadratic in z. It proves convenient at this point to decompose the contours into two parts. For an arbitrary function f which may represent either of the integrands above we can see

$$\begin{aligned}
&[\int_{in} ds\, f(s)][x \rightleftharpoons y] \\
&= [\theta(z_3)\int_{\Gamma_>} ds + \theta(-z_3)\int_{\Gamma_<} ds][\theta(-z_3)\int_{\Gamma_>} ds' + \theta(z_3)\int_{\Gamma_<} ds']f(s)f(s') \\
&= [\int_{\Gamma^I} ds + \theta(z_3)\int_{\gamma_<} ds + \theta(-z_3)\int_{\gamma_>} ds] \\
&\quad \times [\int_{\Gamma^I} ds' + \theta(-z_3)\int_{\gamma_<} ds' + \theta(z_3)\int_{\gamma_>} ds']f(s)f(s')\,,
\end{aligned} \tag{7.18}$$

where the relevant contours can be found from Fig. 7.1. Had we dealt with a single operator point split or volume integral green's function only the Γ^I contour would remain. However, for the case of chiral density fluctuations the singularities also contribute. Then, using the property that $[\int_{\gamma_<} ds + \int_{\gamma_>} ds]f(s) = 0$, we can evaluate the above as

$$[\int_{in} ds\, f(s)][x \rightleftharpoons y] \approx [\int_{\Gamma^I} ds \int_{\Gamma^I} ds' + \int_{\gamma_<} ds \int_{\gamma_>} ds']\, f(s)f(s')\,. \tag{7.19}$$

The last step is valid upon considering that $([\int_{\gamma^<} ds + \int_{\gamma^>} ds]f(s))^2 = 0$ and therefore under the z_3 integral we can drop terms $\theta(z_3)\theta(-z_3) \ll 1$ acting on similar functions.

Gathering terms together we see that

$$\mathcal{I}_m \approx \frac{4\pi}{eB}\Big(\frac{me^2EB}{8\pi^2}\Big)^2 V\Big\{\Big(1-e^{-\frac{m^2\pi}{eE}}\Big)^2[C_1^m + C_2^m] + C_3^m + C_4^m\Big\}, \tag{7.20}$$

$$C_1^m := \int dz_3[Re\int_0^\infty ds\, v(z_3,s)\coth(eEs)]^2\,, \tag{7.21}$$

$$C_2^m := \int dz_3[\mathrm{Re}\int_0^\infty ds\, i\, v(z_3,s)]^2\,, \tag{7.22}$$

$$C_3^m := \int z_3 \int_{\gamma^<} ds \int_{\gamma^>} ds'\Big[v(z_3,s)\coth(eEs)\Big]\Big[v(z_3,s')\coth(eEs')\Big]\,, \tag{7.23}$$

$$C_4^m := -\int z_3 \int_{\gamma^<} ds \int_{\gamma^>} ds'\Big[v(z_3,s)\Big]\Big[v(z_3,s')\Big]\,, \tag{7.24}$$

$$v(z_3,s) := e^{-im^2 s + \frac{i}{4}z_3^2 eE\coth(eEs)} \tag{7.25}$$

Interestingly, in contrast to the point split single correlation function observables we find for the chirality fluctuation case there is no UV divergence in the quadratic mass portion, (however a divergence is found in the covariant derivative piece). Convergence of the integral is provided by the z_3^2 term in the exponential. Let us look at the integrals individually here. To treat a more manageable expression we approximate $\coth(eEs) \approx \frac{1}{eEs}$ within the integrand; this is equivalent to a weak electric field or large mass approximation. Let us analyze the following integrals under the approximation

$$\mathrm{Re}\int_0^\infty ds\, v(z_3,s)\coth(eEs) \approx \frac{2}{E}K_0(m\,|z_3|)\,, \tag{7.26}$$

$$\mathrm{Re}\int_0^\infty ds\, i\, v(z_3,s) \approx \sqrt{\frac{z_3^2}{m^2}}K_1(m\,|z_3|)\,. \tag{7.27}$$

Here K_n is the modified Bessel function of the nth kind. Then we can calculate the first two integrals above to find

$$C_1^m = \frac{2\pi^2}{e^2E^2m}\,, \quad C_2^m = \frac{3\pi^2}{16m^5}\,. \tag{7.28}$$

Evaluating the integrals with singularities requires a little more work. First, let us note that

$$[\int_{\gamma^<} ds - \int_{\gamma^>} ds]f(s) = \theta(z_3^2 - z_0^2)\int_{\gamma^f} ds\, f(s)\,. \tag{7.29}$$

Therefore upon using $[\int_{\gamma^<} ds + \int_{\gamma^>} ds]f(s) = 0$, we find

$$\int_{\gamma^<} ds \int_{\gamma^>} ds' f(s)f(s') = -\frac{1}{4}\theta(z_3^2 - z_0^2)\Big[\int_{\gamma^f} ds f(s)\Big]^2\,. \tag{7.30}$$

Next, let us focus our attention on the following integral which will display all the information needed for our integrals about the essential singularity.

$$I_{\gamma^f} := \int_{\gamma^f} ds\, v(z_3,s)\,. \tag{7.31}$$

Due to the essential singularity and no $z_3 \to 0$ limit a simple residue cannot be taken here. Rather we have an infinite number of higher-order poles whose higher-order residues must be taken. We cannot naively take the z_3 integration first either. We can immediately see in that case no pole about the annulus would be present and the above integral would vanish. We, in fact, find a nonzero contribution from the above integral and therefore the s and z_3 integrations are not interchangeable. We proceed with directly evaluating the essential singularity.

$$\begin{aligned} I_{\gamma f} &= e^{-\frac{m^2\pi}{eE}} \int_{\gamma^0} ds\, v(z_3, s) \\ &= -2\pi i\, e^{-\frac{m^2\pi}{eE}} \sum_{k=1}^{\infty} \Bigg\{ \frac{1}{(k-1)!} \lim_{s\to 0} \\ &\times \frac{d^{k-1}}{ds^{k-1}} \Big[s^k e^{-im^2 s + \frac{i}{4} z_3^2 eE(\coth(eEs) - \frac{1}{eEs})} \Big(\frac{(\frac{iz_3^2}{4s})^k}{k!} \Big) \Big] \Bigg\} \\ &= -2\pi i\, e^{-\frac{m^2\pi}{eE}} \sum_{k=0}^{\infty} \Bigg\{ \lim_{s\to 0} \frac{(\frac{iz_3^2}{4})^{k+1}}{k!(k+1)!} \frac{d^k}{ds^k} \Big[e^{-im^2 s + \frac{i}{4} z_3^2 eE(\coth(eEs) - \frac{1}{eEs})} \Big] \Bigg\}. \end{aligned} \tag{7.32}$$

Notice that we are ultimately taking the $s \to 0$ limit, so in the argument of the exponential let us take $\coth(eEs) - \frac{1}{eEs} \approx \frac{eEs}{3}$; this is also equivalent to a weak electric field approximation.

$$\begin{aligned} I_{\gamma f} &= -2\pi i\, e^{-\frac{m^2\pi}{eE}} \sum_{k=0}^{\infty} \Bigg\{ \frac{(\frac{iz_3^2}{4})^{k+1}}{k!(k+1)!} \Big[-i \Big(m^2 - \frac{z_3^2 eE^2}{12} \Big) \Big]^k \Bigg\} \\ &= e^{-\frac{m^2\pi}{eE}} \Big(\frac{|z_3|\pi}{eE\sqrt{(m/eE)^2 - z_3^2/12}} \Big) I_1(E|z_3|\sqrt{(m/eE)^2 - z_3^2/12})\,. \end{aligned} \tag{7.33}$$

I is a modified bessel function with a complex argument. Let us confine our attention to the case of $(m/E)^2 \ll z_3^2/12$, as is valid in the weak field approximation and considering that after the z_3 integral such for small z_3 the singularity contours will not contribute. See above. We are left with an imaginary argument in the Bessel function,

$$\begin{aligned} I_{\gamma f} &\approx e^{-\frac{m^2\pi}{eE}} \Big(\frac{|z_3|\pi}{\sqrt{-z_3^2 eE^2/12}} \Big) I_1(|z_3|\sqrt{-z_3^2 eE^2/12}) \\ &= e^{-\frac{m^2\pi}{eE}} \frac{\sqrt{12}\pi}{eE} J_1\Big(\frac{z_3^2 eE}{\sqrt{12}} \Big)\,. \end{aligned} \tag{7.34}$$

Applying the above to the last two sets of integrals in $\mathcal{I}_m$ we find

$$C_3^m = -\frac{1}{2} \int_0^\infty dz_3 \Big[\frac{4}{ieE} \frac{d}{dz_3^2} I_{\gamma f} \Big]^2 \approx e^{-\frac{2m^2\pi}{eE}} \frac{\pi^2}{2eE^2} \frac{12^{1/4}}{\sqrt{eE\pi}} \frac{\Gamma(\frac{1}{4})^2}{\Gamma(\frac{3}{4})^2}, \tag{7.35}$$

$$C_4^m = \frac{1}{2} \int_0^\infty dz_3 I_{\gamma f}^2 \approx e^{-\frac{2m^2\pi}{eE}} \frac{\pi^2}{2eE^2} \frac{12^{1/4}}{\sqrt{eE\pi}} \Big(\frac{92}{63} \Big) \frac{\Gamma(\frac{1}{4})^2}{\Gamma(\frac{3}{4})^2}\,. \tag{7.36}$$

We ultimately find for the in-in quadratic mass piece

$$\mathcal{I}_m = \frac{\pi}{eB}\left(\frac{me^2EB}{2\pi^2}\right)^2\left\{\left(1-e^{-\frac{m^2\pi}{eE}}\right)^2\left(\frac{2\pi^2}{e^2E^2m}+\frac{3\pi^2}{16m^5}\right) + e^{-\frac{2m^2\pi}{eE}}\frac{\pi^2}{e^2E^2}\frac{155}{126}\frac{12^{1/4}}{\sqrt{eE\pi}}\frac{\Gamma(\frac{1}{4})^2}{\Gamma(\frac{3}{4})^2}\right\}V\,. \tag{7.37}$$

Let us repeat similar arguments for the in-out equilibrium, $\bar{\mathcal{I}}_m$, term:

$$\bar{\mathcal{I}}_m = \frac{4\pi}{eB}\left(\frac{me^2EB}{8\pi^2}\right)^2 V\int dz_3\left\{\left[\int_0^\infty ds\, v(z_3,s)\coth(eEs)\right]^2+\left[\int_0^\infty dsi\, v(z_3,s)\right]^2\right\}. \tag{7.38}$$

We can see as before for the chiral condensate case there are imaginary pieces in the in-out correlation function. However, let us confine our attention to just the real part of the in-out correlation function to discern the most relevant physical properties. The real part is exactly the same as the in-in case without the exponential suppression, and we can immediately write down $\bar{\mathcal{I}}_m$ as

$$\bar{\mathcal{I}}_m = \frac{\pi}{eB}\left(\frac{me^2EB}{2\pi^2}\right)^2 V\left(\frac{2\pi^2}{e^2E^2m}+\frac{3\pi^2}{16m^5}\right). \tag{7.39}$$

7.3 Covariant Derivative Portion

We now proceed onto the last set of covariant derivative integrals. These sets of integrals proceed as before in the quadratic mass term evaluation. Upon examining the covariant derivative acting on the kernel, and using similar reasoning above we note that contributions to z_0 as well as integral sets with just one z_μ in the dz integral (after variable change) will disappear. We are left with the following:

$$\begin{aligned}\mathcal{I}_D = -\lim_{x_0\to y_0}\frac{eB}{4}\int d^3xd^3y\int_{in}ds\int_{in}ds'\Big\{&\mathrm{tr}\Big[\gamma_0 \\ &\times(-\gamma^2z^1+\gamma^1z^1\cot(eBs))g(x,y,s)\gamma_0(-\gamma^2z^1+\gamma^1z^1\cot(eBs'))g(y,x,s')\Big] \\ &+\mathrm{tr}\Big[\gamma_0(\gamma^1z^2+\gamma^2z^2\cot(eBs))g(x,y,s))\gamma_0(\gamma^1z^2+\gamma^2z^2\cot(eBs'))g(y,x,s')\Big] \\ &+\mathrm{tr}\,\frac{E}{B}\Big[\gamma_0(-\gamma^0z^3+\gamma^3z^3\coth(eEs))g(x,y,s))\gamma_0 \\ &\times(-\gamma^0z^3+\gamma^3z^3\coth(eEs'))g(y,x,s')\Big]\Big\}.\end{aligned} \tag{7.40}$$

Now we take the various Dirac traces and perform the LLLA. Note that integrations over z_1 and z_2 will give similar contributions and thus cross terms in the above will cancel. The above becomes

$$\mathcal{I}_D = \frac{e^5E^4B}{8\pi^3}V\left\{-2\Big[C_1^D+2C_2^D+2C_3^D+C_4^D\Big]\left(1-e^{-\frac{m^2\pi}{eE}}\right)^2+C_5^D+C_6^D+C_7^D+C_8^D\right\}, \tag{7.41}$$

$$C_1^D := \int dz_3z_3^2\Big[\mathrm{Re}\int_0^\infty ds\, i\, v(z_3,s)\Big]^2, \tag{7.42}$$

$$C_2^D := \int dz_3 z_3^2 \Big[\mathrm{Re} \int_0^\infty ds\, v(z_3,s) \coth(eEs) \Big]^2 , \tag{7.43}$$

$$C_3^D := \int dz_3 z_3^2 Re \int_0^\infty ds\, Re \int_0^\infty ds' v(z_3,s) v(z_3,s') \coth^2(eEs') , \tag{7.44}$$

$$C_4^D := -\int dz_3 z_3^2 \Big[\mathrm{Re} \int_0^\infty ds\, i\, v(z_3,s) \coth^2(eEs) \Big]^2 , \tag{7.45}$$

$$C_5^D := -2 \int dz_3 \int_{\gamma^<} ds \int_{\gamma^>} ds' z_3^2 \Big[iv(z_3,s) \Big] \Big[iv(z_3,s') \Big] , \tag{7.46}$$

$$C_6^D := -4 \int dz_3 \int_{\gamma^<} ds \int_{\gamma^>} ds' z_3^2 \Big[v(z_3,s) \coth(eEs) \Big] \Big[v(z_3,s') \coth(eEs') \Big] , \tag{7.47}$$

$$C_7^D := -2 \int dz_3 \int_{\gamma^<} ds \int_{\gamma^>} ds' z_3^2 \Big[v(z_3,s) \coth^2(eEs) \Big] \Big[v(z_3,s') \coth^2(eEs') \Big] , \tag{7.48}$$

$$C_8^D := -4 \int dz_3 \int_{\gamma^<} ds \int_{\gamma^>} ds' z_3^2 \Big[v(z_3,s) v(z_3,s') \coth^2(eEs') \Big] . \tag{7.49}$$

We can treat the various integrals as before. There is one additional integral in the mass piece however. Using a weak field approximation we find.

$$\mathrm{Re} \int_0^\infty ds\, i\, v(z_3,s) \coth^2(eEs) \approx -\frac{4}{e^2E^2} \sqrt{\frac{m^2}{z_3^2}} K_{-1}(m\,|z_3|) . \tag{7.50}$$

Then we can evaluate three of the integrals as before

$$C_1^D \approx 2 \int_0^\infty dz_3 z_3^2 \Big(\sqrt{\frac{z_3^2}{m^2}} K_1(m\,|z_3|) \Big)^2 = \frac{45\pi^2}{256\, m^7} , \tag{7.51}$$

$$C_2^D \approx 2 \int_0^\infty dz_3 z_3^2 \Big(\frac{2}{eE} K_0(m\,|z_3|) \Big)^2 = \frac{\pi^2}{4e^2E^2m^3} , \tag{7.52}$$

$$C_3^D = \frac{8}{e^2E^2} \int_0^\infty dz_3 z_3^2 K_1(m\,|z_3|) K_{-1}(m\,|z_3|) = \frac{3\pi^2}{4m^3e^2E^2} . \tag{7.53}$$

In contrast to the quadratic mass integrals, there is a divergence in the last integral as $z_3 \to 0$. This can be removed with a suitable UV cutoff in proper time:

$$\begin{aligned} C_4^D &\approx -\frac{2}{e^4E^4} \int_0^\infty dz_3 z_3^2 \Big(\int_{\frac{1}{\Lambda^2}}^\infty \frac{ds}{s^2} e^{-m^2 s - \frac{1}{4s} z_3^2} \Big)^2 \\ &= -\frac{\sqrt{\pi}}{2e^4E^4} \int_{\frac{1}{\Lambda^2}}^\infty \frac{ds}{s^2} \frac{ds'}{s'^2} e^{-m^2 s - m^2 s'} \Big(\frac{4ss'}{s+s'} \Big)^{\frac{3}{2}} \\ &\approx -\frac{\sqrt{\pi}}{2e^4E^4} 2^{\frac{3}{2}} \int_{\frac{1}{\Lambda^2}}^\infty \frac{ds}{s^2} \frac{ds'}{s'^2} e^{-m^2 s - m^2 s'} (ss')^{\frac{3}{4}} = -\frac{\sqrt{2\pi}}{e^4E^4} \Big(\int_{\frac{1}{\Lambda^2}}^\infty \frac{ds}{s^{\frac{5}{4}}} e^{-m^2 s} \Big)^2 \\ &= -\frac{\sqrt{2\pi} m}{e^4E^4} \Big(\Gamma[-\frac{1}{4}, \frac{m^2}{\Lambda^2}] \Big)^2 . \end{aligned} \tag{7.54}$$

We are left with an incomplete gamma function whose behavior for large Λ acts linear in Λ.

Next, we examine the essential singularity parts of I_D. Each integral can be handled as before however here we integrate numerically after a change of variables.

$$C_5^D = -\int_0^\infty dz_3 z_3^2 I_{\gamma^f}^2 = -e^{-\frac{2m^2\pi}{eE}} \frac{12^{\frac{7}{4}} \pi^2}{2\,(eE)^{\frac{7}{2}}} (79.5708) , \tag{7.55}$$

$$C_6^D = 2\int_0^\infty dz_3 z_3^2 \Big(\frac{4}{eEi}\frac{d}{dz_3^2} I_{\gamma^f}\Big)^2 = -e^{-\frac{2m^2\pi}{eE}}\Big(\frac{4\pi^2 12^{\frac{3}{4}}}{(eE)^{\frac{7}{2}}}\Big)(326.225)\,, \tag{7.56}$$

$$C_7^D = \int_0^\infty dz_3 z_3^2 \Big(\Big(\frac{4}{eEi}\Big)^2 \frac{d^2}{d(z_3^2)^2} I_{\gamma^f}\Big)^2 = e^{-\frac{2m^2\pi}{eE}}\Big(\frac{\pi^2}{2\cdot 12^{\frac{1}{4}}(eE)^{\frac{7}{2}}}\Big)(17.8975)\,, \tag{7.57}$$

$$C_8^D = 2\int_0^\infty dz_3 z_3^2 I_{\gamma^f}\Big(\Big(\frac{4}{eEi}\Big)^2 \frac{d^2}{d(z_3^2)^2} I_{\gamma^f}\Big) = e^{-\frac{2m^2\pi}{eE}}\Big(\frac{4\cdot 12^{\frac{3}{4}}\pi^2}{(eE)^{\frac{7}{2}}}\Big)(157.904)\,. \tag{7.58}$$

Let us also note here that all the essential singularity terms in $\mathcal{I}_D$ are of the same order in eE and thus

$$e^{-\frac{2m^2\pi}{eE}}(eE)^{-\frac{7}{2}} N^D := C_5^D + C_6^D + C_7^D + C_8^D\,. \tag{7.59}$$

N^D here is a numerical factor from the above integrals. Gathering all the terms for $\mathcal{I}_D$, we find

$$\begin{aligned}\mathcal{I}_D = \frac{2e^7E^6BV}{16^2\pi^3}\Bigg\{ & e^{-\frac{2m^2\pi}{eE}}(eE)^{-\frac{7}{2}}N^D \\ & + \Big(1-e^{-\frac{m^2\pi}{eE}}\Big)^2\Big[-\frac{45\pi^2}{128\,m^7} - \frac{\pi^2}{4(eE)^2m^3} + \frac{2\sqrt{2\pi}m}{(eE)^4}\Big(\Gamma[-\frac{1}{4},\frac{m^2}{\Lambda^2}]\Big)^2\Big]\Bigg\}\,.\end{aligned} \tag{7.60}$$

Repeating similar analyses, the equilibrium part follows as, where again we confine our attention to the real part of the in-out correlation function,

$$\begin{aligned}\bar{\mathcal{I}}_D &= -\Big(\frac{e^2EB}{(4\pi)^2}\Big)^2 V\frac{4\pi(eE)^2}{eB}\Big[C_1^D + 2C_2^D + 2C_3^D + C_4^D\Big] \\ &= \Big(\frac{e^2EB}{(4\pi)^2}\Big)^2 V\frac{2\pi(eE)^2}{eB}\Bigg\{-\frac{45\pi^2}{128\,m^7} - \frac{\pi^2}{4(eE)^2m^3} + \frac{2\sqrt{2\pi}m}{(eE)^4}\Big(\Gamma[-\frac{1}{4},\frac{m^2}{\Lambda^2}]\Big)^2\Bigg\}\,.\end{aligned} \tag{7.61}$$

Putting everything together we find for the real and equilibrium chirality fluctuations (N^D is given by Eq. (7.59))

$$\begin{aligned}\chi_5/V = \frac{e^2EB\,t}{2\pi^2}e^{-\frac{2m^2\pi}{eE}} + \frac{e^3E^2B}{\pi}\Bigg\{ & \frac{N^D}{2\cdot 4^3\pi^2}e^{-\frac{2m^2\pi}{eE}}(eE)^{-\frac{3}{2}} \\ & + \Big(1-e^{-\frac{m^2\pi}{eE}}\Big)^2\Big[-\frac{45\,e^2E^2}{128^2\,m^7} - \frac{1}{512m^3} + \frac{\sqrt{2\pi}m}{64e^2E^2\pi^2}\Big(\Gamma[-\frac{1}{4},\frac{m^2}{\Lambda^2}]\Big)^2\Big]\Bigg\} \\ & + \frac{e^3E^2B}{\pi}\Bigg\{(2.827)e^{-\frac{2m^2\pi}{eE}}m^2(eE)^{-\frac{7}{2}} + \Big(1-e^{-\frac{m^2\pi}{eE}}\Big)^2\Big(\frac{m}{2\,e^2E^2} + \frac{3}{64\,m^3}\Big)\Bigg\}\end{aligned} \tag{7.62}$$

$$\begin{aligned}\bar{\chi}_5/V = & \frac{e^3E^2B}{\pi}\Big(\frac{m}{2\,e^2E^2} + \frac{3}{64\,m^3}\Big) \\ & + \frac{e^3E^2B}{\pi}\Bigg\{-\frac{45\,e^2E^2}{128^2\,m^7} - \frac{1}{512m^3} + \frac{\sqrt{2\pi}m}{64e^2E^2\pi^2}\Big(\Gamma[-\frac{1}{4},\frac{m^2}{\Lambda^2}]\Big)^2\Bigg\}\,.\end{aligned} \tag{7.63}$$

To reiterate the LLLA and a weak electric field large mass, $m^2 \gg eE$, approximations have been taken in the above. The most significant difference between the two values is the presence of exponentially suppressed mass terms, (particularly with time dependence as well), in the real-time observable. Neither the suppression nor the real-time dependence are seen for the equilibrium chiral fluctuations. The real-time dependence is linear for the fluctuations and this is to be expected as a quadratic order real-time dependence was subtracted in $\langle\langle N_5 \rangle\rangle^2$. As for the remaining terms, considering the assumption of a weak electric field (small mass) we can quickly see which terms are dominant in the above. They reside in the $\mathcal{I}_D$ piece associated with the covariant derivative term, associated with a UV divergence. The divergence piece can be seen to go as linear in Λ in the chiral density fluctuation for both equilibrium and real-time cases. Curiously we also see terms that go like $1 - \exp(-\frac{m^2}{eE})$. While for chiral fluctuations, due to the weak field limit, such terms cannot vanish but we will see in the next section with a focused example, the chiral condensate, this term does vanish for strong fields. Furthermore the chiral condensate also possesses a similar UV divergence. Therefore it is instructive to examine the chiral condensate, which we do so next.

Chapter 8

Dynamical Chiral Condensate

We now shift our attention to the chiral condensate, as is commonly referred to in QCD applications–otherwise known as the scalar condensate. The condensate famously acquires a non-zero value in QCD due to the breaking of the chiral symmetry, which in turn imparts the bulk of mass to the hadrons. As we saw before in the chiral fluctuation calculation, properties not seen in the previous 2-point correlators were present: namely the presence of $1-\exp(-\frac{m^2}{eE})$ pieces and an ultraviolet divergence. The chiral condensate in fact, too, possesses such features and is more analytically tractable than is the chiral fluctuations. Furthermore, the chiral condensate, (much like the pseudoscalar condensate), is a quintessential observable in chiral phenomena and thus rounds out our analysis.

Perhaps one of the most prominent examples of the chiral condensate stems from its enhancement under a background magnetic field in what is known as magnetic catalysis [22, 123]. An intuitive extension would be to ask how the condensate behaves under an electric field in and out of equilibrium. Let us note here the equilibrium case has been explored in Ref. [124]; we expand on this by introducing real-time properties including effects stemming from the Schwinger mechanism.

The chiral condensates in and out-of-equilibrium respectively read

$$\bar{\Sigma} := \langle\bar{\psi}\psi\rangle = i\lim_{y\to x}\mathrm{tr}\Big[S^{\mathrm{c}}(x,y)\Big]\,, \tag{8.1}$$

$$\Sigma := \langle\!\langle\bar{\psi}\psi\rangle\!\rangle = i\lim_{y\to x}\mathrm{tr}\Big[S^{\mathrm{c}}_{\mathrm{in}}(x,y)\Big]\,. \tag{8.2}$$

To recover the magnetic catalysis case one only need to take the electric field to zero of either quantity above since the two are formally equivalent without the presence of an electric field. To analyze a simpler expression let us take the LLLA, then the chiral condensate then reads

$$\begin{aligned}\bar{\Sigma}\Big|_{E=0} &= -\frac{eB}{4\pi^2}\,m\int_0^\infty\frac{ds}{s}e^{-im^2s}\cot(eBs)\\ &= -\frac{eB}{4\pi^2}\,m\int_{m^2/\Lambda^2}^\infty\frac{ds}{s}e^{-m^2s}\coth(eBs)\\ &\simeq -\frac{eB}{4\pi^2}\,m\,\Gamma[0,m^2/\Lambda^2]\,.\end{aligned} \tag{8.3}$$

Here Γ is the incomplete gamma function. In the second step we have made a Wick rotation in $s\to -is$, and then introduced an ultraviolet cutoff. In so doing we may explicitly see the connection to familiar equations used for magnetic catalysis,

e.g. see Ref. [22, 123]. In the final step we have employed the LLLA. In the chiral condensate without an electric field a logarithmic divergence emerges,

$$\Gamma[0, m^2/\Lambda^2] \simeq -\gamma_{\rm E} + \ln(\Lambda^2/m^2)\,. \tag{8.4}$$

Applied to the effective potential this logarithmic singularity, with small m, yields an negative infinite curvature producing the magnetic catalysis. Here $\gamma_{\rm E}$ is the Euler-Mascheroni constant.

We introduced the magnetic catalysis in Sec. 2.3.3. There we found even under a massless limit a non-vanishing value persists for the dynamical mass, Eq. (2.31), (found from solving a gap equation), under a strong magnetic field. The physics behind this process is deducible from a LLLA effectively creating a dimensionally reduced system; there the magnetic field, in essence, could coalesce the–classically motivated–particle anti-particle pair through a spin alignment. It is then a fascinating extension to introduce an electric field; as one could gather much about the chiral condensate through a heuristic physical picture presumably one could also do the same with an electric field. Indeed this is the case we will show.

8.1 Euclidean Equilibrium

Then let us examine how the condensate behaves in and out-of-equilibrium with the addition of an electric field. First, we look at the equilibrium case. Following a similar procedure as employed in the sole magnetic field case, Eq. (8.3), we arrive at

$$\begin{aligned}
\bar{\Sigma} &= -\frac{e^2EB}{4\pi^2}\,m\int_0^\infty ds\, e^{-im^2 s}\cot(eBs)\coth(eEs)\\
&= -\frac{e^2EB}{4\pi^2}\,m\int_{m^2/\Lambda^2}^\infty ds\, e^{-m^2 s}\coth(eBs)\cot(eEs)\\
&\simeq -\frac{e^2EB}{4\pi^2}\,m\int_{m^2/\Lambda^2}^\infty ds\, e^{-m^2 s}\cot(eEs)\\
&\simeq -\frac{eB}{4\pi^2}\,m\left[\ln\frac{\Lambda^2\, e^{-\gamma_{\rm E}}}{2eE} - {\rm Re}\psi\left(\frac{im^2}{2eE}\right) - \frac{i\pi}{e^{\pi m^2/(eE)}-1}\right].
\end{aligned} \tag{8.5}$$

In the final step the approximation, $e^{-m^2/\Lambda^2} \sim 1$, has been used and then only leading order contributions for large Λ^2 are kept. From the cotangent function we see a digamma function, $\psi(x)$, emerges whose contributions include an augmentation of the chiral condensate as well as imaginary pieces. Using an asymptotic expansion, namely $\psi(x) \sim \ln x - 1/2x$ for large x in the digamma function, we can recover the magnetic catalysis case, Eq. (8.3) for $E \to 0$.

With the addition of a finite electric field we can see the logarithmic singularity with respect to m^2 disappears; see Ref. [124] for further investigation. What is more, here in the equilibrium case is the appearance of an imaginary part in the condensate. Analogous complex features were found in an examination of the condensate under a finite topological θ [125, 126]. A topological θ and parallel fields share a similar quantum number thus it is anticipated that complex values emerge. However, what is novel in our case is the formation of a bosonic-like distribution in the imaginary part of the condensate; here temperature is replaced with $\pi/(eE)$. Let us point

out also that the same structure is present in the matrix element predicting the probability of two pairs of particles emerging from the vacuum, i.e., Eq. (4.45). Let us emphasize here that the placement of the π/eE factor here is not indicative of a single pair as it includes the summation of all n factors of $n\pi/eE$ factors summed in a geometric series. Thus, with the above descriptions in terms of a Boson distribution, one can see that the π/eE factor present in the imaginary part should be associated with an out-of-equilibrium phenomena–one whose characteristic "temperature" is $\pi/(eE)$. Now, equipped with the in-out expectation value we can show the real-time chiral condensate does in fact contain such an exponential, $\exp(-\pi m^2/eE)$, factor. And moreover, the real-time expectation value is real.

8.2 Real-Time

The real-time or dynamical chiral condensate too displays interesting behavior under a parallel electric field. In the same way as in the equilibrium case above one may perform an imaginary rotation in s to find the real-time condensate is an augmentation of the equilibrium one:

$$\begin{aligned}\Sigma &:= -\frac{e^2EB}{4\pi^2}\, m \int_{in} ds\, e^{-im^2 s} \cot(eBs) \coth(eEs) \\ &= -\frac{e^2EB}{4\pi^2}\, m \int_{1/\Lambda^2}^{\pi/eE - 1/\Lambda^2} ds\, e^{-m^2 s} \coth(eBs) \cot(eEs) \\ &\simeq \left[1 - e^{-\pi m^2/(eE)}\right] \mathrm{Re}\, \bar{\Sigma}\,. \end{aligned} \tag{8.6}$$

We have only kept terms in leading order in the large Λ^2 limit. As in the equilibrium case we see UV divergences appear. Here (as in the same way for $s \to 0$ assuming LLLA) as $s \to -i\frac{\pi}{eE}$ we find an additional UV divergence. Therefore we regulate both divergences the same way with a $1/\Lambda^2$ prescription. Furthermore, as follows from the Hermiticity of in-in expectation values, there is no imaginary part as was observed in the equilibrium case. The real-time chiral condensate is plotted in Fig. 8.1 below.

What is interesting here is we see a diminishing effect on the constituent mass, or rather a "melting" of the chiral condensate in a parallel electric field. As $\exp(-\pi m^2/eE)$ grows large the real-time chiral condensate vanishes. Particles produced from the vacuum act to reduce the constituent mass. Furthermore, one can see that for any large electric field the chiral condensate vanishes, and in fact may even take on positive values, thus negating the catalyzing effect from the magnetic field. One can intuitively grasp this making use of the same classical picture of a condensed particle and anti-particle used in Sec. 2.3.3. A parallel to the background magnetic field electric field will act to pull apart the pair, weakening it. This stands in contrast to the magnetic field, which would act to strengthen the condensate from spin alignment, or a dimensional reduction in the LLLA.

In the context of spontaneous symmetry breaking, then it becomes an interesting question to ask: Under the effects of a dynamical mass, to which mass does the Schwinger mechanism apply–the constituent or bare mass? Eq. (8.6) provides some clarity. At the critical electric field strength, the chiral condensate should melt and no constituent mass would emerge (defined using an in-in formalism).

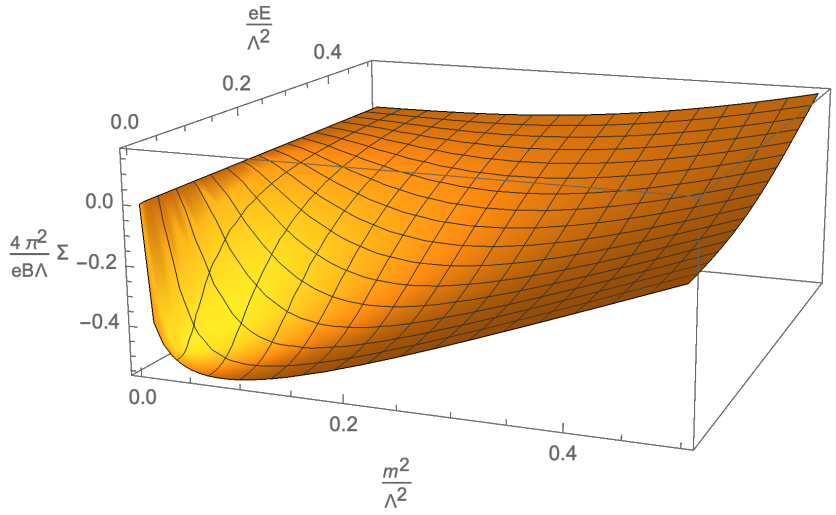

Figure 8.1: Real-time chiral condensate, Eq. (8.6), in background parallel electric and magnetic fields. The chiral condensate is multiplied by $\frac{4\pi^2}{eB\Lambda}$ and is plotted for electric field strength, eE (normalized by the scale Λ^2), and quadratic mass, m^2 (also normalized by the scale Λ^2). Notice the melting, $\Sigma \to 0$, of the condensate for larger values of E. This phenomenon can be attributed to the fact that an electric field acts to separate the condensate, in turn restoring the chiral symmetry. Note, this is an inverse magnetic catalysis behavior, in contrast to the behavior in a sole magnetic field. In effect, the Schwinger mechanism is acting to decrease the constituent mass.

With the advent of studies on the applicability of the Schwinger mechanism and magnetic catalysis in condensed matter systems, it too may be possible to verify (falsify) the melting of the chiral condensate. This may be particularly the case for a Weyl semimetal. In the semimetal, it is reasoned the Schwinger mechanism may be visible [127]. But not only the Schwinger mechanism, in fact, there might also be potential for the study of magnetic catalysis [128]. Let us also point out that the melting of the chiral condensate does not necessarily require the Schwinger mechanism and an out-of-equilibrium picture to verify. In fact, even in equilibrium a lessening of the condensate should be present according to Eq. (8.5) for strong magnetic fields.

Chapter 9

Conclusions

The interplay between the generation of chirality in strong electromagnetic background fields that are CP violating and the Schwinger mechanism has been examined. While it has been known at a cursory heuristic level that the Schwinger mechanism may give rise to a net chirality [13], we have clarified the importance of asymptotic vacuum states (in(out) states correspond to asymptotic times, $t \to -\infty(+\infty)$) in the realization of expectation values both in real-time and in an equilibrated Euclidean setting. Notably, the known heuristic picture of chirality production via the Schwinger mechanism corresponds to an in-in (or real-time) vacuum state expectation value, that describes a scenario out-of-equilibrium–where any number of pairs may be produced in the out state. Whereas the in-out state is a matrix element expectation value, and upon Wick rotation describes a scenario of Euclidean equilibrium–or a state in which no pairs of particles are produced in the out state. In-out and in-in expectation values were found utilizing the worldline formalism.

9.1 Summary of Results

Our primary new finding was the importance of asymptotic vacuum states, (whether in-out (Euclidean equilibrium) or in-in (out-of-equilibrium)), for the determination of expectation values related to the chiral anomaly. This was an essential finding in that not only does it paint a new picture of the chiral anomaly in and out-of equilibrium, but also it establishes the anomaly's dependence on the vacuum instability–the Schwinger mechanism. In turn, we also discovered the behavior of the anomaly in and out-of equilibrium with mass effects. Notably, there was no anomaly in equilibrium, regardless of the mass. Out-of-equilibrium mass effects are characteristic of an exponential mass suppression due to the Schwinger mechanism.

To achieve this understanding several quantities were calculated, and these are listed in Table 9.1. Before diving into the significance of each item, it is important to recapitulate which quantities were previously known and which were new. Here and throughout this chapter we refer to Table 9.1, and the notations for the various expectation values therein, for discussions. $\bar{P}$, $\bar{j}^\mu$, and j^μ were known expressions. P, $\partial_0 n_5$, j_5^μ, and $\bar{\Sigma}$ appeared in literature, however we provided significant new understandings and derivations of each. Last, to the best of our knowledge, $\partial_0 \bar{n}_5$, $\bar{j}_5^\mu$, $\bar{\chi}_5$, χ_5, and Σ were entirely new results, which could not be found elsewhere.

Let us review each known result first, and describe what we had done that was novel. The calculation of $\bar{P}$ was notably first achieved by Schwinger in Ref. [15] to

	Equilibrium (In-Out)	Real-Time (In-In)
Psuedo -scalar	$^{a}\,\bar{P} = -\dfrac{e^2EB}{4\pi^2 m}$	$^{b}\,P = -\dfrac{e^2EB}{4\pi^2 m}\Big[1-\exp\Big(-\dfrac{\pi m^2}{eE}\Big)\Big]$
Axial Ward Identity	$^{c}\,\partial_0\bar{n}_5 = 0$	$^{b}\,\partial_0 n_5 = \dfrac{e^2EB}{2\pi^2}\exp\Big(-\dfrac{\pi m^2}{eE}\Big)$
Chiral Current	$^{c}\,\bar{j}_5^{\mu} = 0$	$^{b}\,j_5^{\mu} = \dfrac{e^2EB\,t}{2\pi^2}\exp\Big(-\dfrac{\pi m^2}{eE}\Big)\delta_3^{\mu}$
Curent (CME)	$^{a}\,\bar{j}^{\mu} = 0$	$^{a}\,j^{\mu} = \dfrac{e^2EB\,t}{2\pi^2}\coth\Big(\dfrac{\pi B}{E}\Big)e^{-m^2\pi/eE}\delta_3^{\mu}$
Chiral Fluctuations	$^{c}\,\bar{\chi}_5/V \simeq \dfrac{\sqrt{2\pi}\,m}{(8eE\pi)^2}\Gamma[-\frac{1}{4},\frac{m^2}{\Lambda^2}]^2$	$^{c}\,\chi_5/V \simeq \dfrac{e^2EB\,t}{2\pi^2}e^{-\frac{2m^2\pi}{eE}} + \bar{\chi}_5/V$
Chiral Condensate	$^{b}\,\mathrm{Re}\,\bar{\Sigma} \simeq -\dfrac{eB\,m}{4\pi^2}\Big[\ln\dfrac{\Lambda^2\,e^{-\gamma_{\mathrm{E}}}}{2eE} - \mathrm{Re}\,\psi\Big(\dfrac{im^2}{2eE}\Big)\Big]$	$^{c}\,\Sigma \simeq \Big[1-e^{-\pi m^2/(eE)}\Big]\,\mathrm{Re}\,\bar{\Sigma}$

Table 9.1: Summary of results both previously known and new: ^{a} denotes known values, ^{b} denotes known values, but with significant new understandings and derivations, and ^{c} denotes entirely new results. Using both Euclidean equilibrium (in-out) representations and real-time (in-in) representation various expectation values were calculated pertaining to the spontaneous generation of chirality from the Schwinger mechanism. Calculations leading to the pseudoscalar condensates, the axial Ward identities, and chiral currents can be found in Ch. 5. Calculations for the chiral magnetic effect currents can be found in Ch. 6. Those for the chiral fluctuations are in Ch. 7, where the full expressions can be seen in Eq. (7.63); note here a truncated approximated expression is listed. And finally, calculations for the chiral condensate are located in Ch. 8.

characterize the decay of a neutral meson into two photons. However, that it cancels out in the axial Ward identity leading to $\partial_0\bar{n}_5$, and also $\bar{j}_5^{\mu}$, vanishing was a new and profound result, signaling a new understanding of the anomaly. As further evidence, it has been noted elsewhere [122] that $\bar{j}^{\mu}$, the CME, vanishes in equilibrium. And, it had been shown in Ref. [13] that j^{μ} may arise through the Schwinger mechanism. Through an identification of vacuum states, however, we had been able to provide a new perspective of the CME in and out-of-equilibrium stemming from the Schwinger mechanism. Moreover, $\partial_0 n_5$, and j_5^{μ} have indeed been known at a heuristic level in Ref. [13], and P was also conjectured from the Schwinger formula in Ref. [120]. However, it addition to our main finding of an identification of vacuum states, we had provided for the first time, using the worldline formalism, one-loop exact expressions for P, $\partial_0 n_5$, and j_5^{μ}. This was significant in that it supported our notions of the anomaly cancelling in equilibrium, yet reappearing out-of-equilibrium exactly. Last, while $\bar{\Sigma}$ has been discussed in equilibrium before [124], we had for the time shown its complex behavior, (i.e., imaginary pieces in the chiral condensate). Let us discuss the

ramifications of both known and new results in the context of Euclidean equilibrium and real-time pictures.

We found that P and hence the axial Ward identity took on finite values indicative with contributions to the Schwinger mechanism out-of-equilibrium in homogeneous parallel electric and magnetic fields. Prominent features of real-time out-of-equilibrium observables were both a characteristic exponentially suppressed quadratic mass term that was non-perturbative in the coupling and electric field, as well as a real-time linear time dependence. The former is seen in Schwinger's formula, Eq. (2.23), for the probability of a single particle anti-particle pair being produced in the out state. And the latter, the real-time dependence, is also characteristic of a space-time volume factor present in Schwinger's formula.

The real-time expectation values provided us with one-loop exact mass dependence of $\partial_0 n_5$ and the CME, j^μ. However, while an exponential mass dependence was seen for out-of-equilibrium expectation values, curiously there was no mass dependence for equilibrium quantities including $\bar{j}_5^\mu$ and $\bar{j}^\mu$. In fact, $\bar{j}_5^\mu$ and $\bar{j}^\mu$, which are associated with the anomaly, were seen to vanish in equilibrium or using an in-out formalism. Considering the quintessential cartoon of the anomaly, (see Sec. 2.3.1), one can see that to initiate the anomaly process two ingredients are required: an electric field to distort the Dirac eigenspectrum and a vacuum instability (or rather a source of infinite particles/holes by which the anomaly can initiate). The latter requirement is seen more clearly with an energy or mass gap, as in Fig. (1.3). We find that not only for homogeneous Abelian fields, but also in the massive Schwinger model as well as any case with weak field or large mass, the chiral anomaly indeed vanishes, and chirality is conserved according to the axial Ward identity.

We also found analogous in and out-of-equilibrium behavior in applications to the axial Ward identity including the CME, j^μ, and χ_5. The former, like the chiral density, possessed the characteristic Schwinger mass suppression along with linear time dependence. However, unlike the chiral density, j^μ, predictive of the CME, includes contributions from all Landau levels. However let us point out that strictly speaking only the lowest Landau level ought to be considered for a rigorous definition of the CME, and this is because only the lowest level can be associated with chirality production. Also, χ_5 was found to be finite and with linear time dependence for pieces associated with the production of particles. And, motivated by a melting behavior in the fluctuations we examined a theoretically interesting and supportive quantity known for its nonperturbative behavior in a magnetic field, that is the chiral condensate, Σ. Σ was found to weaken with the inclusion of an electric field, even vanishing for strong enough fields. We may heuristically understand this behavior as the electric field acting to tear the condensate (particle anti-particle) pair apart, whereas a magnetic field–responsible for magnetic catalysis of the condensate, serves to align the spins strengthening the condensate.

Let us discuss one limitation of our setup, that is that we are restricted to the use of homogeneous fields. The advantage is manifest in that we may obtain simple expressions unobscured by technicalities. However, the cost is that divergences appear due to infinite homogeneous fields; these divergences however were identifiable with real-time as was shown in Eq. (5.25). Additionally, one must assume for a realistic setup that our system is contained in some space-time volume box, i.e., Vt. To circumvent the problem of divergences, as well as a clear real-time dependence, inhomogeneous fields ought to be utilized, and this is a subject for future

work. Before discussing future projects, let us remark on some implications of our findings.

9.2 Implications

9.2.1 Weyl Semimetal Testing

Our findings are in principal testable both in QED in high-powered lasers and in QCD in heavy ion collisions, however both setups come with significant challenges. The Schwinger critical electric field is still beyond our technical limits in high-powered lasers–even though more exotic field configurations offer one solution. Also, ultra-peripheral collisions may offer a unique means to access non-linear QED effects, including the Schwinger mechanism, since the strong force is negated due to the large separation of colliding nuclei. However, how might one extract meaningful data on the Schwinger mechanism is still not at hand. Yet, testing of the Schwinger mechanism along with chirality generation in parity violating fields is eminently testable in semimetal environment; c.f. see Sec. 2.2.2.

The Schwinger mechanism is facilitated through a Landau Zener transition in condensed matter systems signaling a breakdown of an insulator. In the absence of a magnetic field, it has been reasoned, the mechanism may be observable in a Weyl semimetal [64]. While such a case is in theory gapless, a non-vanishing gap may be tunable [60]; in a direct analogy to mass let us call this Δ. Then using the CME to access the anomaly one may surmise a conduction current in the direction of parallel electric and magnetic fields to grow linear in time with an exponential gap suppression:

$$j_{CME} \propto e^2 EB\, t \coth\Big(\frac{\pi B}{E}\Big) \exp\Big(-\frac{\pi \Delta^2}{v_F \hbar e E}\Big)\,, \tag{9.1}$$

for large times following the switch-on of the electric field. However, let us point out that realistic effects in a semiconductor environment are not taken into account here. These, could include finite volume or temperature effects, or competing mechanisms which may conceal the above current. In any case, it would be a fruitful endeavor to more fully explore the generation of chirality by Landau Zener tunneling in semimetals, as this could serve as a tabletop experiment for the otherwise inaccessible physics of the anomaly and vacuum instability in QFTs.

9.2.2 Suppression of Anomaly

An immediate application of the work outlined in this thesis is apparent in that processes initiated through the anomaly that were once thought inhibited are now strongly exponentially suppressed. For example, the appearance (or rather lack there of) of anomaly fluctuations in colliders might be explainable due to a finite, though small, quark mass. A further example is provided in early universe applications; there, baryogenesis theories thought sourced through an anomalous term may now, too, be strongly suppressed. There may in fact be many affected theories built on an anomaly.

9.2.3 Strong CP Problem

One of the final unsolved problems for the Standard Model is the strong CP problem. Most proposed solutions lie beyond the Standard Model, the most popular of which is the addition of a new particle, the axion [129]. However, our Euclidean equilibrium calculation may shed some light on this famous problem not relying on beyond the Standard Model physics. In a nutshell, the problem is why is there no topological θ term in the QCD Lagrangian. While we have shown that the anomaly disappears in equilibrium, the more important point for this purpose is that the pseudoscalar condensate was found to be purely topological. Then upon a finite θ' chiral rotation of the QCD partition function, one could acquire a finite θ''[1] topological term in a mean field approximation, in effect cancelling any existing θ term. The cost of this procedure, however, is that the quark mass(es) would be lessened by $\cos(2\theta')$. Therefore, a finite theta QCD may in fact resemble a zero theta QCD but with reduced mass. However, this analogy relies on the hypothesis that the pseudoscalar condensate be purely topological. Proving this relationship we, however, leave for a future work.

9.3 Future Directions

We have established the connection between chirality generation and the Schwinger mechanism in this work, however, there are still future directions worth pursuit to both broaden our outlook and to deepen our understanding. Some future directions considered are an in-in formalism for generic field types, a closer examination of the anomaly cancellation also for generic field types, a non-perturbative worldline analysis beyond one loop, and a study of backreaction effects.

While we may indeed have a heuristic picture of chirality production via the Schwinger mechanism, as an extension to this work it is important to develop a general framework with which to calculate in-in real time propagators for general inhomogeneous fields.

Although we found for the equilibrium case the anomaly in homogeneous fields will vanish, it is a curious extension if this indeed exists for any field. Already preliminary calculations tell us that it should. To treat this problem justly a purely Euclidean metric should be used and the pseudoscalar should be calculated on the lattice, and moreover, the extension to non-Abelian fields with a topological winding number is most important in this analysis.

The Schwinger mechanism to all orders, including the effects of a dynamical gauge field, in a constant electric field has been established. However, a robust mathematical means which naturally includes the non-perturbative nature of the Schwinger mechanism while keeping all orders of a dynamical gauge field is needed. Worldline instantons provide a reliable non-perturbative method of handling inhomogeneous and other complicated background fields. And, encompassing worldline methods to include higher loop effects may prove indispensable. Already, interesting extensions to worldline instantons exist in homogeneous fields accompanied by dynamical photons [130]. Yet, a more thorough treatment valuable to high-intensity

[1] $\theta'' \neq \theta'$, since the axial Ward identity at finite chiral rotation is different from the one presented earlier, Eq. (2.26).

laser experiment environments is needed. Another needed extension lies with accurately treating an otherwise immutable background field or backreaction effects.

The background field method is illuminating and powerful for select QFT phenomena, however, there are instances in which the method breaks down. One such case lies with the Schwinger mechanism. Produced pairs affect the background field which produced them, and to treat the interplay judiciously is challenging. Yet, this is an important detail in for example high-intensity laser experiments causing beam depletion. In Ref. [131] a coherent state formalism under the Furry picture was used to treat backreaction effects. There, scattering between initial and final coherent states could be modeled through a complex background field. Further study in this direction would prove fruitful. Moreover, it would be an interesting extension to analyze backreaction effects modeled as a complex potential on worldline instantons as well as ramifications to known expectation values.

Bibliography

[1] K. Fujikawa, "Path Integral Measure for Gauge Invariant Fermion Theories," Phys. Rev. Lett. **42**, 1195 (1979).

[2] Y. Nambu and G. Jona-Lasinio, "Dynamical Model of Elementary Particles Based on an Analogy with Superconductivity I," Phys. Rev. **122**, 345 (1961).

[3] Y. Nambu and G. Jona-Lasinio, "Dynamical Model of Elementary Particles Based on an Analogy with Superconductivity II," Phys. Rev. **124**, 246 (1961).

[4] K. Fukushima, D. E. Kharzeev, and H. J. Warringa, "Chiral magnetic effect," Phys. Rev. D **78**, 074033 (2008).

[5] Q. Li, D. E. Kharzeev, C. Zhang, Y. Huang, I. Pletikosic, A. V. Fedorov, R. D. Zhong, J. A. Schneeloch, G. D. Gu, and T. Valla, "Observation of the chiral magnetic effect in $ZrTe_5$," Nat. Phys. **12**, 550 (2016).

[6] Z. Wang, Y. Sun, X.-Q. Chen, C. Franchini, G. Xu, H. Weng, X. Dai, and Z. Fang, "Dirac semimetal and topological phase transitions in A_3Bi (A = Na, K, Rb)," Phys. Rev. B **85**, 195320 (2012).

[7] Z. Wang, H. Weng, Q. Wu, X. Dai, and Z. Fang, "Three-dimensional Dirac semimetal and quantum transport in Cd_3As_2," Phys. Rev. B **88**, 125427 (2013).

[8] M. Neupane, S.-Y. Xu, R. Sankar, N. Alidoust, G. Bian, C. Liu, I. Belopolski, T.-R. Chang, H.-T. Jeng, H. Lin, A. Bansil, F. Chou, and M. Z. Hasan, "Observation of a three-dimensional topological Dirac semimetal phase in high-mobility Cd_3As_2," Nat. Commun. **5**, 3786 (2014).

[9] Z. K. Liu, J. Jiang, B. Zhou, Z. J. Wang, Y. Zhang, H. M. Weng, D. Prabhakaran, S.-K. Mo, H. Peng, P. Dudin, T. Kim, M. Hoesch, Z. Fang, X. Dai, Z. X. Shen, D. L. Feng, Z. Hussain, and Y. L. Chen, "A stable three-dimensional topological Dirac semimetal Cd_3As_2," Nat. Mater. **13**, 677 (2014).

[10] D. Kharzeev, K. Landsteiner, A. Schmitt, and H.-U. Yee, *Strongly Interacting Matter in Magnetic Fields* (Springer Berlin Heidelberg, 2013).

[11] D. Kharzeev, A. Krasnitz, and R. Venugopalan, "Anomalous chirality fluctuations in the initial stage of heavy ion collisions and parity odd bubbles," Phys. Lett. B **545**, 298 (2002).

[12] T. Lappi and L. McLerran, "Some features of the glasma," Nucl. Phys. A **772**, 200 (2006).

[13] K. Fukushima, D. E. Kharzeev, and H. J. Warringa, "Real-time dynamics of the Chiral Magnetic Effect," Phys. Rev. Lett. **104**, 212001 (2010).

[14] L. Barron, "True and false chirality and parity violation," Chem. Phys. Lett. **123**, 423 (1986).

[15] J. S. Schwinger, "On gauge invariance and vacuum polarization," Phys. Rev. **82**, 664 (1951).

[16] A. Casher, H. Neuberger, and S. Nussinov, "Chromoelectric-flux-tube model of particle production," Phys. Rev. D **20**, 179 (1979).

[17] S. L. Adler, "Axial-Vector Vertex in Spinor Electrodynamics," Phys. Rev. **177**, 2426 (1969).

[18] J. S. Bell and R. Jackiw, "A PCAC puzzle: $\pi^0 \to \gamma\gamma$ in the σ model," Nuovo Cim. **A60**, 47 (1969).

[19] P. Copinger, K. Fukushima, and S. Pu, "Axial Ward identity and the Schwinger mechanism – Applications to the real-time chiral magnetic effect and condensates," Phys. Rev. Lett. **121**, 261602 (2018).

[20] V. Domcke, Y. Ema, and K. Mukaida, "Chiral Anomaly, Schwinger Effect, Euler-Heisenberg Lagrangian, and application to axion inflation," (2019), arXiv:1910.01205 [hep-ph] .

[21] K. G. Klimenko, "Three-dimensional Gross-Neveu model at nonzero temperature and in an external magnetic field," Theor. Math. Phys. **90**, 1 (1992).

[22] V. P. Gusynin, V. A. Miransky, and I. A. Shovkovy, "Catalysis of dynamical flavor symmetry breaking by a magnetic field in (2+1)-dimensions," Phys. Rev. Lett. **73**, 3499 (1994), [Erratum: Phys. Rev. Lett.76,1005(1996)].

[23] I. A. Shovkovy, "Magnetic Catalysis: A Review," Lect. Notes Phys. **871**, 13 (2013).

[24] D. E. Kharzeev, L. D. McLerran, and H. J. Warringa, "The effects of topological charge change in heavy ion collisions: "Event by event $\mathcal{P}$ and $\mathcal{CP}$ violation"," Nucl. Phys. A **803**, 227 (2008).

[25] A. Bzdak and V. Skokov, "Event-by-event fluctuations of magnetic and electric fields in heavy ion collisions," Phys. Lett. B **710**, 171 (2012).

[26] A. D. Sakharov, "Violation of CP invariance, C asymmetry, and baryon asymmetry of the universe," JETP Lett. **5**, 24 (1967).

[27] C. A. Baker *et al.*, "An Improved Experimental Limit on the Electric Dipole Moment of the Neutron," Phys. Rev. Lett. **97**, 131801 (2006).

[28] D. E. Kharzeev, "Topologically induced local $\mathcal{P}$ and $\mathcal{CP}$ violation in QCD x QED," Annals Phys. **325**, 205 (2010).

[29] A. Belavin, A. Polyakov, A. Schwartz, and Y. Tyupkin, "Pseudoparticle solutions of the yang-mills equations," Phys. Lett. B **59**, 85 (1975).

[30] K. S. Novoselov, A. K. Geim, S. V. Morozov, D. Jiang, Y. Zhang, S. V. Dubonos, I. V. Grigorieva, and A. A. Firsov, "Electric Field Effect in Atomically Thin Carbon Films," Science **306**, 666 (2004).

[31] S. Borisenko, Q. Gibson, D. Evtushinsky, V. Zabolotnyy, B. Büchner, and R. J. Cava, "Experimental Realization of a Three-Dimensional Dirac Semimetal," Phys. Rev. Lett. **113**, 027603 (2014).

[32] Z. K. Liu, B. Zhou, Y. Zhang, Z. J. Wang, H. M. Weng, D. Prabhakaran, S.-K. Mo, Z. X. Shen, Z. Fang, X. Dai, Z. Hussain, and Y. L. Chen, "Discovery of a Three-Dimensional Topological Dirac Semimetal, Na_3Bi," Science **343**, 864 (2014).

[33] D. Xiao, M.-C. Chang, and Q. Niu, "Berry Phase Effects on Electronic Properties," Rev. Mod. Phys. **82**, 1959 (2010).

[34] M.-C. Chang and Q. Niu, "Berry curvature, orbital moment, and effective quantum theory of electrons in electromagnetic fields," J. of Phys.: Con. Matt. **20**, 193202 (2008).

[35] X. Huang, L. Zhao, Y. Long, P. Wang, D. Chen, Z. Yang, H. Liang, M. Xue, H. Weng, Z. Fang, X. Dai, and G. Chen, "Observation of the Chiral-Anomaly-Induced Negative Magnetoresistance in 3D Weyl Semimetal TaAs," Phys. Rev. X **5**, 031023 (2015).

[36] M. A. Stephanov and Y. Yin, "Chiral Kinetic Theory," Phys. Rev. Lett. **109**, 162001 (2012).

[37] D. T. Son and B. Z. Spivak, "Chiral Anomaly and Classical Negative Magnetoresistance of Weyl Metals," Phys. Rev. B **88**, 104412 (2013).

[38] Z.-T. Liang and X.-N. Wang, "Globally Polarized Quark-Gluon Plasma in Noncentral $A + A$ Collisions," Phys. Rev. Lett. **94**, 102301 (2005).

[39] X.-G. Huang, P. Huovinen, and X.-N. Wang, "Quark polarization in a viscous quark-gluon plasma," Phys. Rev. C **84**, 054910 (2011).

[40] D. Kharzeev, J. Liao, S. Voloshin, and G. Wang, "Chiral magnetic and vortical effects in high-energy nuclear collisions–a status report," Prog. Part. Nucl. Phys. **88**, 1 (2016).

[41] B. I. Abelev *et al.* (STAR Collaboration), "Azimuthal Charged-Particle Correlations and Possible Local Strong Parity Violation," Phys. Rev. Lett. **103**, 251601 (2009).

[42] B. Abelev *et al.* (ALICE Collaboration), "Charge separation relative to the reaction plane in pb-pb collisions at $\sqrt{s_{NN}}$=2.76 TeV," Phys. Rev. Lett. **110**, 012301 (2013).

[43] F. Sauter, "Über das Verhalten eines Elektrons im homogenen elektrischen Feld nach der relativistischen Theorie Diracs," Zeitschrift für Physik **69**, 742 (1931).

[44] W. Heisenberg and H. Euler, "Consequences of Dirac's theory of positrons," Z. Phys. **98**, 714 (1936).

[45] S. W. Hawking, "Particle creation by black holes," Commun. Math. Phys. **43**, 199 (1975).

[46] W. G. Unruh, "Notes on black-hole evaporation," Phys. Rev. D **14**, 870 (1976).

[47] P. W. Higgs, "Broken Symmetries and the Masses of Gauge Bosons," Phys. Rev. Lett. **13**, 508 (1964).

[48] O. Klein, "Die Reflexion von Elektronen an einem Potentialsprung nach der relativistischen Dynamik von Dirac," Z. Phys. **53**, 157 (1929).

[49] R. Schutzhold, H. Gies, and G. Dunne, "Dynamically assisted Schwinger mechanism," Phys. Rev. Lett. **101**, 130404 (2008).

[50] G. V. Dunne, "The search for the Schwinger effect: Nonperturbative vacuum pair production," Int. J. Mod. Phys. **A25**, 2373 (2010).

[51] A. Yildiz and P. H. Cox, "Vacuum behavior in quantum chromodynamics," Phys. Rev. D **21**, 1095 (1980).

[52] J. Ambjorn and R. J. Hughes, "Canonical quantisation in non-Abelian background fields," Annals Phys. **145**, 340 (1983).

[53] M. Gyulassy and A. Iwazaki, "Quark and gluon pair production in SU(N) covariant constant fields," Phys. Lett. B **165**, 157 (1985).

[54] C. Schubert, "Perturbative quantum field theory in the string-inspired formalism," Phys. Rept. **355**, 73 (2001).

[55] O. Corradini and C. Schubert, "Spinning Particles in Quantum Mechanics and Quantum Field Theory," (2015) arXiv:1512.08694 [hep-th] .

[56] D. Sauzin, "Resurgent functions and splitting problems," (2007), arXiv:0706.0137 [math.DS] .

[57] M. F. Linder, A. Lorke, and R. Schützhold, "Analog Sauter-Schwinger effect in semiconductors for spacetime-dependent fields," Phys. Rev. B **97**, 035203 (2018).

[58] L. D. Landau, "Zur Theorie der Energieubertragung II," Phys. Z. Sowjet. **2**, 46 (1932).

[59] C. Zener and R. H. Fowler, "Non-adiabatic crossing of energy levels," Proc. R. Soc. (London) A **137**, 696 (1932).

[60] J. Kim, S. S. Baik, S. H. Ryu, Y. Sohn, S. Park, B.-G. Park, J. Denlinger, Y. Yi, H. J. Choi, and K. S. Kim, "Observation of tunable band gap and anisotropic Dirac semimetal state in black phosphorus," Science **349**, 723 (2015).

[61] E. Kane, "Zener tunneling in semiconductors," J. Phys. Chem. Solids **12**, 181 (1960).

[62] D. Allor, T. D. Cohen, and D. A. McGady, "Schwinger mechanism and graphene," Phys. Rev. D **78**, 096009 (2008).

[63] B. Dóra and R. Moessner, "Nonlinear electric transport in graphene: Quantum quench dynamics and the Schwinger mechanism," Phys. Rev. B **81**, 165431 (2010).

[64] S. Vajna, B. Dóra, and R. Moessner, "Nonequilibrium transport and statistics of Schwinger pair production in Weyl semimetals," Phys. Rev. B **92**, 085122 (2015).

[65] M. Marklund and J. Lundin, "Quantum vacuum experiments using high intensity lasers," Eur. Phys. J. **D55**, 319 (2009).

[66] G. V. Dunne, "New Strong-Field QED Effects at ELI: Nonperturbative Vacuum Pair Production," Eur. Phys. J. **D55**, 327 (2009).

[67] A. Ringwald, "Boiling the Vacuum with An X-Ray Free Electron Laser," in *Quantum Aspects of Beam Physics 2003* (2004) pp. 149–163.

[68] T. Heinzl and A. Ilderton, "Exploring high-intensity QED at ELI," Eur. Phys. J. **D55**, 359 (2009).

[69] A. Gonoskov, S. Bastrakov, E. Efimenko, A. Ilderton, M. Marklund, I. Meyerov, A. Muraviev, A. Sergeev, I. Surmin, and E. Wallin, "Extended particle-in-cell schemes for physics in ultrastrong laser fields: Review and developments," Phys. Rev. E **92**, 023305 (2015).

[70] C. Bamber, S. J. Boege, T. Koffas, T. Kotseroglou, A. C. Melissinos, D. D. Meyerhofer, D. A. Reis, W. Ragg, C. Bula, K. T. McDonald, E. J. Prebys, D. L. Burke, R. C. Field, G. Horton-Smith, J. E. Spencer, D. Walz, S. C. Berridge, W. M. Bugg, K. Shmakov, and A. W. Weidemann, "Studies of nonlinear QED in collisions of 46.6 GeV electrons with intense laser pulses," Phys. Rev. D **60**, 092004 (1999).

[71] M. Ruf, G. R. Mocken, C. Muller, K. Z. Hatsagortsyan, and C. H. Keitel, "Pair Production in Laser Fields Oscillating in Space and Time," Phys. Rev. Lett. **102**, 080402 (2009).

[72] D. Kharzeev, E. Levin, and K. Tuchin, "Multi-particle production and thermalization in high-energy QCD," Phys. Rev. **C75**, 044903 (2007).

[73] N. Tanji, "Quark pair creation in color electric fields and effects of magnetic fields," Annals Phys. **325**, 2018 (2010).

[74] Y. Zhong, C.-B. Yang, X. Cai, and S.-Q. Feng, "Spatial distributions of magnetic field in the RHIC and LHC energy regions," Chin. Phys. C **39**, 104105 (2015).

[75] L. Keldysh, "IONIZATION IN THE FIELD OF A STRONG ELECTROMAGNETIC WAVE," Sov. Phys. JETP **20**, 1307 (1965).

[76] N. B. Narozhnyi and A. I. Nikishov, "The Simplist processes in the pair creating electric field," Yad. Fiz. **11**, 1072 (1970).

[77] H. Gies and K. Klingmuller, "Pair production in inhomogeneous fields," Phys. Rev. D **D72**, 065001 (2005).

[78] C. Schneider and R. Schutzhold, "Dynamically assisted Sauter-Schwinger effect in inhomogeneous electric fields," JHEP **02**, 164 (2016).

[79] C. Kohlfurst, M. Mitter, G. von Winckel, F. Hebenstreit, and R. Alkofer, "Optimizing the pulse shape for Schwinger pair production," Phys. Rev. D **88**, 045028 (2013).

[80] M. Orthaber, F. Hebenstreit, and R. Alkofer, "Momentum spectra for dynamically assisted Schwinger pair production," Phys. Lett. B **698**, 80 (2011).

[81] K. Enqvist, "Primordial Magnetic Fields," Int. J. Mod. Phys. D **7**, 331 (1998).

[82] K. Fukushima and C. Sasaki, "The phase diagram of nuclear and quark matter at high baryon density," Prog. Part. Nucl. Phys. **72**, 99 (2013).

[83] T. D. Cohen and D. A. McGady, "Schwinger mechanism revisited," Phys. Rev. D **78**, 036008 (2008).

[84] G. V. Dunne, "Heisenberg-Euler effective Lagrangians: Basics and extensions," in *From fields to strings: Circumnavigating theoretical physics* (2004) pp. 445–522.

[85] J. Ambjorn, J. Greensite, and C. Peterson, "The axial anomaly and the lattice Dirac sea," Nuclear Physics B **221**, 381 (1983).

[86] P. I. Fomin, V. A. Miransky, and Yu. A. Sitenko, "Infrared problem and boson suppression in massless Abelian gauge theory," Phys. Lett. B **64**, 444 (1976).

[87] J. Bardeen, L. N. Cooper, and J. R. Schrieffer, "Theory of Superconductivity," Phys. Rev. **108**, 1175 (1957).

[88] S. P. Klevansky, "The Nambu—Jona-Lasinio model of quantum chromodynamics," Rev. Mod. Phys. **64**, 649 (1992).

[89] E. Fradkin, D. Guitman, and S. Shvartsman, *Quantum electrodynamics: with unstable vacuum* (Springer-Verlag, 1991).

[90] K. Fukushima, F. Gelis, and L. McLerran, "Initial singularity of the little bang," Nucl. Phys. A **786**, 107 (2007).

[91] J. S. Schwinger, "Brownian motion of a quantum oscillator," J. Math. Phys. **2**, 407 (1961).

[92] L. V. Keldysh, "Diagram technique for nonequilibrium processes," Zh. Eksp. Teor. Fiz. **47**, 1515 (1964).

[93] E. A. Calzetta and B.-L. B. Hu, *Nonequilibrium Quantum Field Theory* (Cambridge University Press, 2008).

[94] A. K. Das, *Finite Temperature Field Theory* (World Scientific, New York, 1997).

[95] R. D. Jordan, "Effective field equations for expectation values," Phys. Rev. D **33**, 444 (1986).

[96] J. Berges, "Introduction to nonequilibrium quantum field theory," AIP Conf. Proc. **739**, 3 (2004).

[97] D. M. Gitman, "Processes of arbitrary order in quantum electrodynamics with a pair creating external field," J. Phys. A **10**, 2007 (1977).

[98] G. Baym and L. P. Kadanoff, "Conservation Laws and Correlation Functions," Phys. Rev. **124**, 287 (1961).

[99] F. Gelis and R. Venugopalan, "Particle production in field theories coupled to strong external sources, I: Formalism and main results," Nucl. Phys. A **776**, 135 (2006).

[100] F. Gelis and R. Venugopalan, "Particle production in field theories coupled to strong external sources, II: Generating functions," Nucl. Phys. A **779**, 177 (2006).

[101] R. P. Feynman, "Mathematical formulation of the quantum theory of electromagnetic interaction," Phys. Rev. **80**, 440 (1950).

[102] R. P. Feynman, "An Operator calculus having applications in quantum electrodynamics," Phys. Rev. **84**, 108 (1951).

[103] I. K. Affleck, O. Alvarez, and N. S. Manton, "Pair production at strong coupling in weak external fields," Nucl. Phys. B **197**, 509 (1982).

[104] G. V. Dunne and C. Schubert, "Worldline instantons and pair production in inhomogeneous fields," Phys. Rev. D **72**, 105004 (2005).

[105] P. Copinger and K. Fukushima, "Spatially Assisted Schwinger Mechanism and Magnetic Catalysis," Phys. Rev. Lett. **117**, 081603 (2016), [Erratum: Phys. Rev. Lett.118,099903(2017)].

[106] S. P. Kim and D. N. Page, "Schwinger pair production via instantons in a strong electric fields," Phys. Rev. D **65**, 105002 (2002).

[107] G. V. Dunne, Q.-h. Wang, H. Gies, and C. Schubert, "Worldline instantons and the fluctuation prefactor," Phys. Rev. D **73**, 065028 (2006).

[108] D. Cangemi, E. D'Hoker, and G. V. Dunne, "Effective energy for QED in (2+1)-dimensions with semilocalized magnetic fields: A solvable model," Phys. Rev. D **52**, R3163 (1995).

[109] G. V. Dunne and T. M. Hall, "An exact (3+1)-dimensional QED effective action," Phys. Lett. B **419**, 322 (1998).

[110] T. M. Tritt, N. D. Lowhorn, R. T. Littleton, A. Pope, C. R. Feger, and J. W. Kolis, "Large enhancement of the resistive anomaly in the pentatelluride materials $HfTe_5$ and $ZrTe_5$ with applied magnetic field," Phys. Rev. B **60**, 7816 (1999).

[111] G. N. Kamm, D. J. Gillespie, A. C. Ehrlich, T. J. Wieting, and F. Levy, "Fermi surface, effective masses, and Dingle temperatures of $ZrTe_5$ as derived from the Shubnikov–de Haas effect," Phys. Rev. B **31**, 7617 (1985).

[112] Y. L. Chen, J.-H. Chu, J. G. Analytis, Z. K. Liu, K. Igarashi, H.-H. Kuo, X. L. Qi, S. K. Mo, R. G. Moore, D. H. Lu, M. Hashimoto, T. Sasagawa, S. C. Zhang, I. R. Fisher, Z. Hussain, and Z. X. Shen, "Massive Dirac Fermion on the Surface of a Magnetically Doped Topological Insulator," Science **329**, 659 (2010).

[113] A. A. Burkov, "Chiral Anomaly and Diffusive Magnetotransport in Weyl Metals," Phys. Rev. Lett. **113**, 247203 (2014).

[114] M. D. Schwartz, *Quantum Field Theory and the Standard Model* (Cambridge University Press, 2014).

[115] D. Vasak, M. Gyulassy, and H.-T. Elze, "Quantum transport theory for abelian plasmas," Annals Phys. **173**, 462 (1987).

[116] H.-T. Elze and U. W. Heinz, "Quark-Gluon transport theory," Phys. Rept. **183**, 81 (1989).

[117] A. Yamamoto, "Lattice QCD with Strong External Electric Fields," Phys. Rev. Lett. **110**, 112001 (2013).

[118] G. V. Dunne, J. Hur, C. Lee, and H. Min, "Precise Quark Mass Dependence of Instanton Determinant," Phys. Rev. Lett. **94**, 072001 (2005).

[119] G. V. Dunne, J. Hur, C. Lee, and H. Min, "Calculation of QCD instanton determinant with arbitrary mass," Phys. Rev. D **71**, 085019 (2005).

[120] H. J. Warringa, "Dynamics of the chiral magnetic effect in a weak magnetic field," Phys. Rev. D **86**, 085029 (2012).

[121] A. I. Nikishov, "Pair production by a constant external field," Zh. Eksp. Teor. Fiz. **57**, 1210 (1969).

[122] N. Yamamoto, "Generalized Bloch theorem and chiral transport phenomena," Phys. Rev. D **92**, 085011 (2015).

[123] V. P. Gusynin, V. A. Miransky, and I. A. Shovkovy, "Dimensional reduction and dynamical chiral symmetry breaking by a magnetic field in (3+1)-dimensions," Phys. Lett. B **349**, 477 (1995).

[124] L. Wang, G. Cao, X.-G. Huang, and P. Zhuang, "Nambu-Jona-Lasinio model in a parallel electromagnetic field," Phys. Lett. B **780**, 273 (2018).

[125] D. Boer and J. K. Boomsma, "Spontaneous $\mathcal{CP}$-violation in the strong interaction at $\theta=\pi$," Phys. Rev. D **78**, 054027 (2008).

[126] K. Mameda, "QCD θ-vacua from the chiral limit to the quenched limit," Nucl. Phys. B **889**, 712 (2014).

[127] S. Vajna, B. Dora, and R. Moessner, "Nonequilibrium transport and statistics of Schwinger pair production in Weyl semimetals," Phys. Rev. B **92**, 085122 (2015).

[128] B. Roy and J. D. Sau, "Magnetic catalysis and axionic charge density wave in Weyl semimetals," Phys. Rev. B **92**, 125141 (2015).

[129] R. D. Peccei and H. R. Quinn, "CP Conservation in the Presence of Pseudoparticles," Phys. Rev. Lett. **38**, 1440 (1977).

[130] O. Gould, A. Rajantie, and C. Xie, "Worldline sphaleron for thermal Schwinger pair production," Phys. Rev. D **98**, 056022 (2018).

[131] A. Ilderton and D. Seipt, "Backreaction on background fields: A coherent state approach," Phys. Rev. D **97**, 016007 (2018).